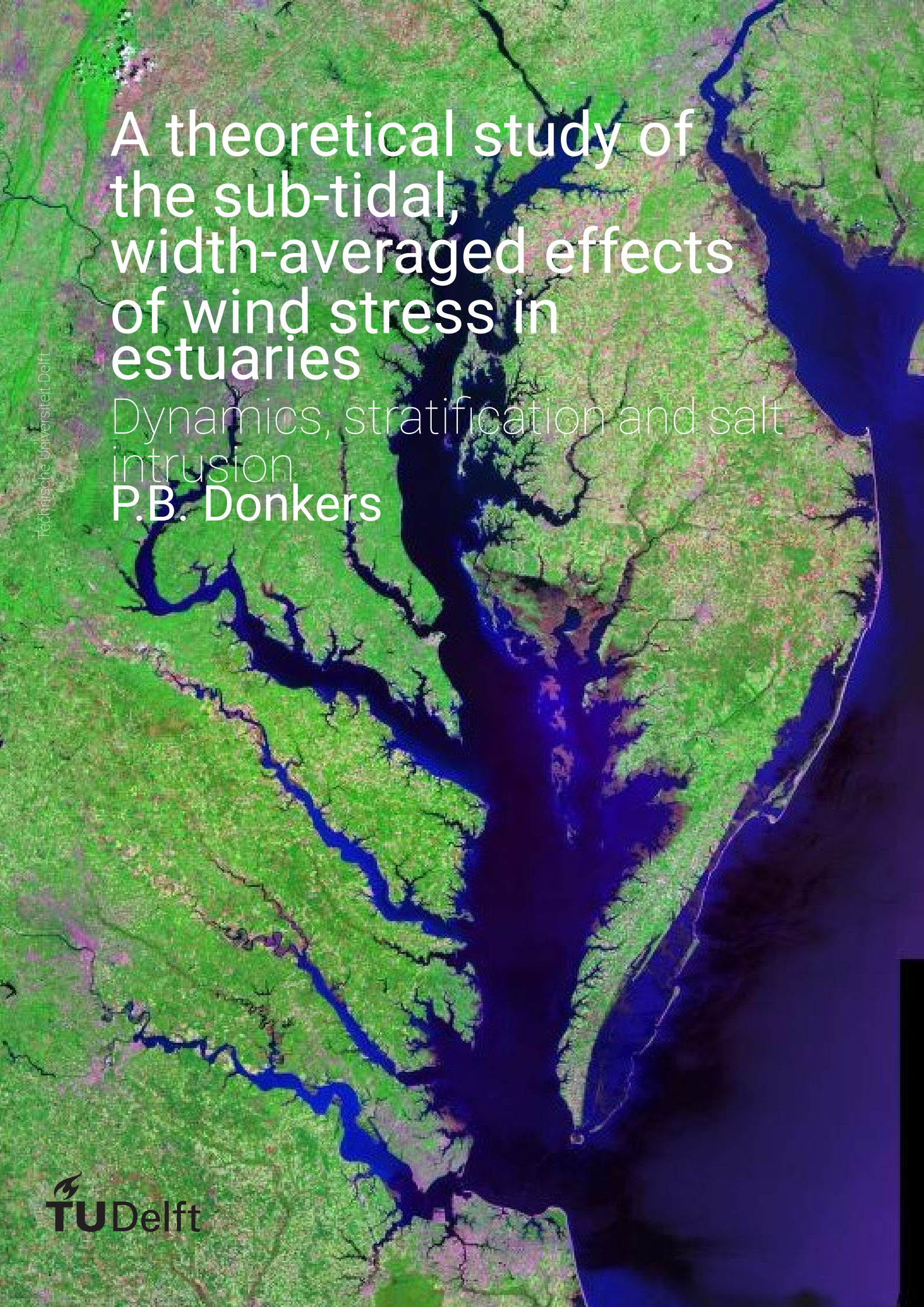

A theoretical study of the sub-tidal, width-averaged effects of wind stress in estuaries

Dynamics, stratification and salt intrusion

P.B. Donkers

Technische Universiteit Delft

TU Delft

A theoretical study of the sub-tidal, width-averaged effects of wind stress in estuaries

Dynamics, stratification and salt intrusion

by

P.B. Donkers

to obtain the degree of Master of Science
at the Delft University of Technology,
to be defended publicly on Tuesday July 7, 2020 at 9:30 AM.

Student number:	4366476	
Project duration:	December 1, 2019 – July 7, 2020	
Thesis committee:	dr. ir. Y. M. Dijkstra,	TU Delft, supervisor
	dr. H. M. Schuttelaars,	TU Delft, supervisor
	Prof. dr. ir. C. Vuik,	TU Delft

An electronic version of this thesis is available at `http://repository.tudelft.nl/`.

TU Delft

Contents

1 Introduction

This introduction serves to provide the reader with the necessary context for the work done in this thesis, explain the objective of the thesis and clarify the structure of the report. The goal of this thesis is to create a theoretical model that captures the influence of wind on the horizontal and vertical salinity distribution in an estuary, as well as the dynamics that arise within the estuary. A secondary, numerical model, that uses fewer assumptions, will be developed and analysed. This serves to determine whether the implications from the theoretical model hold only because of all the assumptions that are made, or whether the results are equally valid when some of these assumptions are relaxed. The focus of this thesis is on gaining conceptual insight in estuaries subject to wind, rather than on obtaining a high accuracy in describing a specific estuary.

This thesis is focused on steady-state solution in partially or well mixed estuaries. Moreover, the dynamics and salinity averaged over the width of the estuary are considered, such that only dynamics in the vertical and along channel direction are modelled. Estuaries are subject to periodical variations forced by tides. The variation within a tidal period is not studied in this thesis, but the dynamics and salinity averaged over a tidal period are considered. The effects of tides or variation along the width of the estuary are not neglected from this model, but are incorporated in the parametrisation of the model instead.

Section 1.1 will introduce estuaries, their role in society, the time scales found in estuarine dynamics and the categorisation of estuaries. Section 1.2 will give a short insight into the relevant dynamics. This is followed by section 1.3, which gives an overview of relevant literature for the problem studied. Subsequently, two models will be introduced in section 1.4 that will be modified and applied throughout this work. The objectives of this thesis are specified in section 1.5. Finally, an overview of the structure of this thesis will be given in section 1.6.

1.1. Estuaries

Estuaries are bodies of water where water from rivers and oceans mix. Examples of estuaries are the Scheldt and Mersey Rivers and the former Zuiderzee. Being connected to the ocean and the river, the salinity in an estuary varies over the length of the estuary, since the water from the river is fresh and the water from the ocean is saline. In figure 1.1, displaying the salt intrusion for the Scheldt estuary, it can, for example, be seen that the water near Antwerp is mostly fresh and that the salinity increases as one moves closer to the Noordzee.

Estuaries play a major role in irrigation and the supply of potable water [2–4]. Moreover, the specific dynamics of estuaries create pockets of water with a combination of micro-organisms and nutrients that gives rise to the unique biology of estuaries [5, 6]. Furthermore, Estuaries fulfil a nursery function for marine wildlife throughout the world [7–10].

Three major time scales can be identified for estuaries. The shortest time scale is the turbulent time scale, on which the chaotic dynamics that are found in fluids can be observed. Turbulent dynamics occur over a period of 1 second or less. The second time scale is the tidal time scale, associated with a period of approximately 12 hours. In this thesis, the sub-tidal velocity and salinity are considered, which are the velocity and salinity that are obtained by taking the average over a tidal period. This means that the forcing of water towards the estuary or towards the ocean is not taken into account, since this forcing has an average of zero over the tidal period. Mixing that occurs due to the tides is however taken into account. The third

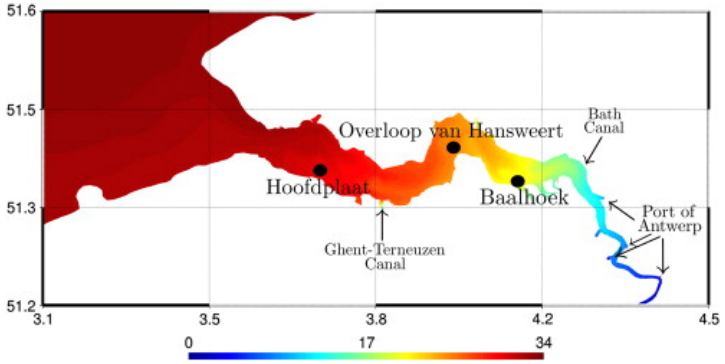

Figure 1.1: Numerically computed vertically averaged salinity (psu) for the Scheldt estuary [1].

time scale is the time scale at which sub-tidal velocity and salinity change. This thesis considers steady state solutions on this time scale.

Estuaries are commonly classified according to the vertical salinity distribution [11]. On one end of the spectrum, we find well-mixed estuaries, where the salinity is homogeneous over the vertical position within the estuary. On the other end of the spectrum is the salt-wedge estuary. In such estuaries, salt and fresh water are both present in the water column and are separated by a sharp interface. In between these extreme ends are partially mixed estuaries. These estuaries have significant differences in salinity between the top and bottom of the water column, separated by a smooth transition. Mixing is present between the upper and lower parts of the water column, but the mixing is not enough to fully counter all vertical salinity variation.

In typical estuaries, the salinity is larger near the bottom than near the surface, designated as stable stratification. Empirical examples are found where the salinity stratification is unstable [6]. In these cases, however, vertical variations in a different quantity than salt, such as temperature or sediment, ensure that the density of the water is still higher near the bottom than near the surface. As a result, the density stratification is stable. True unstable stratification is highly uncommon in nature.

1.2. Estuarine dynamics

As an introduction into the width-averaged sub-tidal dynamics of water in estuaries, three forcings will be identified in this paragraph: river flow, gravitational circulation and wind stress. It should be clear that this short overview of relevant forcings is not exhaustive, but aims to provide the essential background for understanding this thesis.

The effects these forcings have on the horizontal velocity and the salinity are sketched in figure 1.2. The sketches are generated using a model that will be described in section 2.3. The first panel plots the width-averaged sub-tidal contributions to velocity on the horizontal axis, versus the vertical position in the estuary on the vertical axis. Here the direction from the river towards the ocean is defined as positive. The second panel shows the width-averaged sub-tidal contribution each of the forcings has on the salinity. This figure plots the width-averaged sub-tidal salinity minus its vertical average, versus the vertical position on the vertical axis. The magnitudes of the contributions displayed in figure 1.2 are not to scale; the relative scaling depends on a host of factors, such as the wind speed, the dimensions of the estuary and the position within the estuary. The shown contributions are not specific to a certain point in the estuary.

Firstly, the river discharges a certain volume of water per unit of time, causing a net flow towards the ocean throughout the estuary. As seen in figure 1.2a, the velocity contribution is positive over the entire depth of the estuary, but due to friction at the bottom, the velocity is lower in the lower parts of the water column. Since salt is transported by advection, the velocity profile directly influences the salinity profile. As the salinity increases towards the ocean, which is the positive direction, and the velocity is highest near the surface, the advective supply of fresh water is largest near the surface. As a result, the salinity contribution from the river is positive at the bottom and negative at the surface, as seen in figure 1.2b.

Secondly, the presence of horizontal salinity gradients in the estuary causes a circulation of water [12]. Since salt water is heavier than fresh water, differences in salinity cause differences in the density of water. This creates local differences in the gravitationally induced pressure in the estuary, which force the circulation of water. Gravitational circulation causes water to flow towards the river at the bottom of the estuary, and towards the ocean at the surface [13], as seen in figure 1.2a, which is caused by the fact that the baroclinic

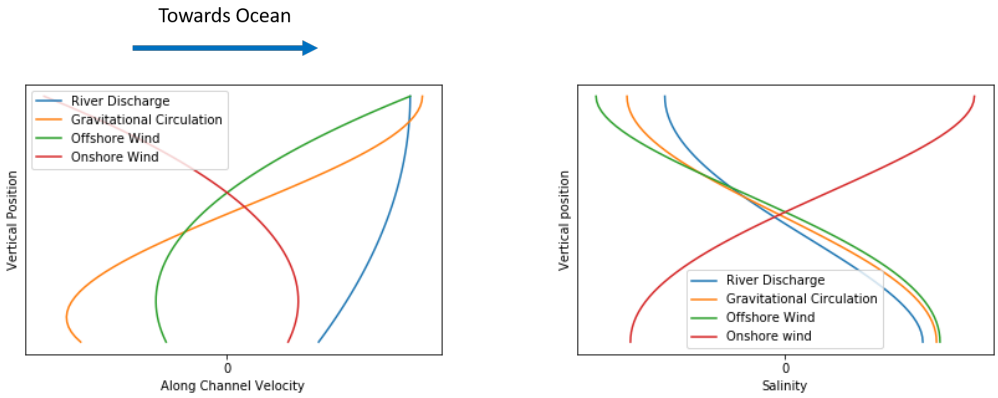

(a) Velocity

(b) Salinity

Figure 1.2: Sketch of the effects of river flow, gravitational circulation, offshore wind and onshore wind on velocity and salinity in an estuary

forcing, arising from salinity gradients, increases with depth. Gravitational circulation does not cause net horizontal transport of water, and so the vertical average of this contribution is zero. At the surface, gravitational circulation forces the advection of fresh water towards the ocean, while near the bottom saline water is forced towards the river. As a result, the contribution to the salinity profile is positive near the bottom and negative near the surface, as seen in figure 1.2b.

Finally, estuaries are subject to wind at the surface. This wind exerts a drag force on the water, which causes water to flow along the direction of the wind near the surface. Alike the case of gravitational circulation, the vertical average of the velocity contribution from wind is zero. This ensures that water flows in the opposite direction near the bottom of the estuary [14]. The contributions to velocity and salinity for wind in the direction from the river to the ocean (offshore) and wind directed from the ocean to the river (onshore) are both sketched in figure 1.2a. For offshore wind, the velocity contribution is positive at the surface and negative at the bottom. As a result, offshore wind supplies the estuary with fresh water near the surface and saline water near the bottom. Consequently, the contribution to the deviation from the vertically averaged salinity is positive near the bottom and negative near the surface. In case the wind blows in the opposite direction (onshore), the wind contributions to velocity and salinity flip sign. Onshore winds thus counter the velocity and salinity profiles caused by river flow and gravitational circulation.

1.3. Existing research

This section will cover the existing models on well mixed and partially mixed estuaries in a sub-tidal, width-averaged setting. Special is paid to whether the different models capture the influence of wind stress. Relevant models can be categorized into analytical and numerical models.

1.3.1. Analytical models

The first analytical model is a model by Hansen and Rattray [13] that describes how wind stress can either enhance gravitational circulation for offshore wind speeds, or reduce or possibly reverse the circulation for onshore wind speeds. This is done by breaking the water circulation down into contributions from different forcings, as done in section 1.2. Hansen and Rattray then proceed by deriving an expression for the horizontal salinity distribution in the "central regime" that is neither close to the ocean, nor to regions with zero salinity. To this end, it is assumed that the horizontal salinity gradient is constant. Moreover, wind is neglected from the part of the model that describes the horizontal salinity profile.

Secondly, an analytical model by Chatwin [15] is based on the assumption that no horizontal diffusion takes place. This model does not incorporate wind stress. While this model has historical value, it is not of value to this thesis.

The third analytical model is a model by MacCready [16, 17], based on the previously mentioned model by Hansen and Rattray. This model describes both the vertical and horizontal salinity and velocity profiles, but, similar to the first model, does not include wind in the model. Although a numerical solver has to be used to find the exact solution, the majority of the work done to obtain solutions is done analytically. As a

result, this model gives a large degree of insight into the solution and is categorized as an analytical model. This model will be further explored in section 1.4.

MacCready's model has been modified by Ralston [18] to, amongst others, incorporate wind stress. This adapted model is succesfully fitted to observations in the Hudson River and the San Francisco Bay. The focus of that paper is, however, on fitting this model to empirical data, rather than exploring the full implications of the model. As a result, the work does not provide the level of insight desired to obtain in this thesis.

1.3.2. Numerical models

Firstly, a numerical study on the effect of wind on stratification and horizontal transport has been carried out by Chen and Sanford [19]. Their findings agree with Hansen and Rattray on that onshore wind counters gravitational circulation, while offshore wind supports gravitational circulation. Moreover, it is stated that stratification is increased by offshore wind and decreased by onshore wind. Similar to the study discussed in the previous paragraph, the numerical nature of this model causes the model not to provide a sufficient level of intuitive insight.

The second numerical model is a model by Lange and Burchard that describes the effect wind stress has on circulation [20]. In their model, the horizontal salinity gradient is considered an independent parameter. Like the study of Chen and Sanford, the study finds that onshore wind speeds reduce or possibly reverse the circulation, while offshore wind increases gravitational circulation. Since this model assumes the horizontal salinity gradient not to be dependent on wind stress, this model does not capture the influence of wind on salt intrusion.

A recent numerical study by Lange et al. [21] has shown that wind stress can reverse circulation in the Warnow river estuary. This study does not consider equilibria, but looks at transient behaviour. As this model is numerical in nature, it does not provide the level of insight that is desired to obtain in this thesis.

Recently, Dijkstra has implemented a model for the salt intrusion in estuaries in the iFlow framework [22, 23]. This model can both be used to describe tidal and sub-tidal dynamics, but does not incorporate wind. This model is covered in more detail in section 1.4.

1.4. Used models and methods

In this thesis, two existing models that describe the vertical and horizontal salinity distribution will be extended to include wind at the surface of the estuary. The extension of the first model serves to provide a conceptual understanding of the width-averaged sub-tidal dynamics and salinity profiles found in estuaries. The model that is extended is the semi-analytical model by MacCready [16], described in the previous section. This model derives analytical expressions for the vertical velocity and salinity profile as a function of the vertically averaged salinity gradient. These analytical expressions are then used to derive a differential equation for the vertically averaged salinity that can be solved numerically. A large number of assumptions is made in the derivation of this model, such as assuming that momentum advection can be neglected. Since it is one of the few models that provide an analytical description of horizontal estuarine dynamics and describes different forcings using distinguishable length scales, it is commonly used as a means of gaining understanding of the dynamics of the system. The model is applicable to well mixed and partially mixed systems.

The second model is Dijkstra's model [22], which was quickly introduced in the previous section. Compared to the previous model, fewer assumptions concerning momentum advection and diffusion are made in the development of this model. As a consequence, it is valid for well mixed and partially mixed systems as well as salt wedge estuaries. This model is extended to include wind speed in order to verify the solutions obtained by the extended MacCready model.

1.5. Objective

As seen in section 1.3, no extensive theoretical study has yet been done on the influence of wind on the horizontal and vertical salinity structure in the desired type of estuary. The goal of this thesis is to create a model that captures the effects of wind on the dynamics and salinity structure of estuaries, covering both a vertical and along-channel distribution variations in the velocity and salinity. Moreover, it is desired that the model provides conceptual tools for the analysis of the results from the model itself, related numerical models or empirical studies. The desired theoretical model is obtained by extending MacCready's model to include wind at the surface. Moreover, Dijkstra's model is extended to include wind stress as well, in order to check whether the results from MacCready's model can be reproduced in this model. Six research questions are tackled in this thesis:

1. Can MacCready's model be extended to included wind stress, and what difficulties arise when doing this?
2. What steady-state solutions are found by this model, and how are these solutions physically constituted?
3. In what way are the solutions from this model analysed best?
4. Are the solutions for the extended MacCready model possible in the extended Dijkstra model, and how do these solutions differ between the two models?
5. Can solutions from the extended Dijkstra model be analysed using the extended MacCready model?
6. What are the stability properties of the solutions from the extended Dijkstra model?

The first three questions focus on the theoretical model itself, while the fourth and fifth question are concerned with assessing to what extent the concepts and results from the extended MacCready model are transferable to the extended Dijkstra model. This will give insight into the consequences of the assumptions that are made in the derivation the extended MacCready model, but not in the derivation of the extended Dijkstra model. Answering the final question makes sure that a full conclusion can be made on the implications of the extended Dijkstra model.

1.6. Structure

This thesis will start in chapter 2 with a detailed derivation of a width-averaged sub-tidal model for the dynamics and salinity of an estuary. It will then be described how the extended MacCready model follows from the sub-tidal model and how that model is solved. This is followed by a description of how the sub-tidal model is solved using Dijkstra's approach.

Chapter 3 will describe the solutions to the extended MacCready model for different ranges of wind speeds, and analyse how these solutions are physically constituted. Chapter 4 will deal with the results for the extended Dijkstra model, describing all solutions found and their domains and stability properties. This chapter will verify whether the results found from the analytically based model hold when fewer assumptions are made, as well as study the stability properties of the solutions. This chapter also determines to what degree the extended MacCready model can be used to analyse solutions from the extended Dijkstra model.

This report will finish with a concluding chapter that gives an overview of the obtained results and reflects on the goals formulated in section 1.5.

2

Model and method

This chapter explains how the sub-tidal problem is derived and describes the two models derived from the sub-tidal model. The chapter will start by discussing the geometry of the problem and the relevant forcings. Next, a width-averaged sub-tidal model is derived from the width-averaged Navier-Stokes equations. Subsequently, the analytical model based on MacCready's model is derived and the solution method is described. Finally, the second model, based on Dijkstra's model, is described as well as the method used to obtain solutions for this model.

2.1. Geometry and forcing

We consider an estuary with constant dimensions B and H for the width and depth of the estuary, respectively. The estuary is semi-infinite, such that the estuary runs from $x = -\infty$ to the seaward end at $x = 0$. The banks of the river are located at $y = 0$ and $y = B$. Finally, the vertical boundaries of the domain are $z = 0$ and $z = -H$. An overview of the geometry is given in figure 2.1. Three-dimensional equations will be developed on the semi-infinite cuboid with the boundaries just described first. Subsequently, the model will reduce to a width-averaged two-dimension model, which reduces the domain to a semi-infinite two dimensional rectangle. The estuary is forced by a river discharge of Q at $x = -\infty$. Moreover, the x-component of the wind speed at 10 m above the estuary is given by u_a. An overview of the geometry is given in figure 2.1.

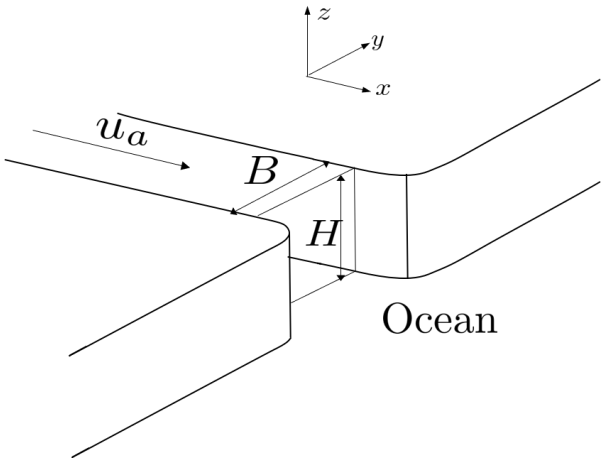

Figure 2.1: Sketch of the geometry of the model problem

2.2. Derivation of sub-tidal model

In this section, the sub-tidal model will be derived. First, the model assumptions are listed, followed by the derivation of the Navier-Stokes equations. From these equations, the sub-tidal equations for velocity are derived, followed by the salinity equation.

2.2.1. Overview of assumptions

Several assumptions will be made during the derivation of the equations. First, the density of salt water is assumed to be equal to $\rho_0(1+\beta s)$, where ρ_0 is the density of fresh water, s is the salinity in psu, and β is the haline contraction coefficient. This coefficient typically has a value of $7.6 \cdot 10^{-4}$ psu^{-1}. This density can be considered as a two-term expansion of the true density of salt water. Since seawater typically has a salinity of 30 psu, we find $\beta s \ll 1$.

Moreover, the Boussinesq approximation is applied, such that the variations in density of water are only taken into account when dealing with buoyancy force [24]. When buoyancy is considered, the density of water is assumed to be $\rho_0(1+\beta s)$, while in any other case the density is considered ρ_0. Thus, it is assumed that differences in inertia can be ignored, while differences in gravitational pull cannot. The Boussinesq approximation directly implies incompressibility of the fluid.

Furthermore, it is assumed that the depth H is small compared to the typical horizontal length scale. Therefore, the sub-tidal width-averaged vertical momentum equation is well-approximated by the hydrostatic balance [25]. Typically, the horizontal mixing of horizontal velocity is negligible compared to horizontal advection for the majority of the domain. Additionally, it is assumed that this can be extended for the whole domain, such that the horizontal mixing can be neglected for the entirety of the domain. Since the diffusion of salt can occur when the horizontal velocity is zero, saline diffusion is not assumed to be dominated by horizontal advection and is retained in the model.

In addition, the rigid-lid approximation [26] is used. This approximation says that the height of the surface of the estuary is constant, in this case 0, but that the pressure at the surface varies. It is assumed that water flows frictionlessly along the sides of the estuary, such that no energy is lost. Finally, it is assumed that the wind speed u_a is much larger than the velocity of the water at the surface. This allows the use of u_a when the wind speed relative to the surface is required.

In order to derive the width-averaged sub-tidal equations, the Navier-Stokes equations will be averaged over the two fast time scales, as well as over the width of the estuary. In the process of averaging over the width and the two fast time scales, advective contributions from these time scales and the variations along the width of the estuary will have to be parametrised. The specific parametrisations will be discussed as they are applied.

2.2.2. Navier-Stokes equations

The symbols $\tilde{u}$, $\tilde{v}$ and $\tilde{w}$ are used to denote the velocities in the x, y and z direction, respectively. The Navier-Stokes equation for this problem are:

$$\tilde{u}_t + \tilde{u}\tilde{u}_x + \tilde{v}\tilde{u}_y + \tilde{w}\tilde{u}_z = -\frac{1}{\rho_0}\tilde{p}_x + \tilde{f}^x + \nu(\tilde{u}_{yy} + \tilde{u}_{zz}), \tag{2.1}$$

$$\tilde{v}_t + \tilde{u}\tilde{v}_x + \tilde{v}\tilde{v}_y + \tilde{w}\tilde{v}_z = -\frac{1}{\rho_0}\tilde{p}_y + \tilde{f}^y + \nu(\tilde{v}_{xx} + \tilde{v}_{yy} + \tilde{v}_{zz}), \tag{2.2}$$

$$\tilde{w}_t + \tilde{u}\tilde{w}_x + \tilde{v}\tilde{w}_y + \tilde{w}\tilde{w}_z = -\frac{1}{\rho_0}\tilde{p}_z + \tilde{f}^z + \nu(\tilde{w}_{xx} + \tilde{w}_{yy} + \tilde{w}_{zz}), \tag{2.3}$$

$$\tilde{u}_x + \tilde{v}_y + \tilde{w}_z = 0. \tag{2.4}$$

Here, $\tilde{p}$ and $\tilde{f}$ are the pressure and body force respectively, where $\tilde{f}^x$ represents the x component of the body force. Lastly, ν is the kinematic viscosity. The first three equations are the momentum equations for the three different velocity components. Note that the Boussinesq assumption allows the use of ρ_0 as the density of water and that horizontal viscosity has been eliminated from equation 2.1 according to the assumptions in section 2.2.1. The final equation, the continuity equation, arises as the water is assumed incompressible, and so the divergence of velocity is 0.

The boundary conditions read:

$$\tilde{\tau}_{\text{visc}} = \tilde{\tau}_{\text{wind}} \quad \text{at } z = 0, \tag{2.5}$$
$$\tilde{v}_z = 0 \quad \text{at } z = 0, \tag{2.6}$$
$$\tilde{w} = 0 \quad \text{at } z = 0, \tag{2.7}$$
$$\tilde{p} = \tilde{p}_{\text{surf}} \quad \text{at } z = 0, \tag{2.8}$$
$$\tilde{u} = 0 \quad \text{at } z = -H, \tag{2.9}$$
$$\tilde{v} = 0 \quad \text{at } z = -H, \tag{2.10}$$
$$\tilde{w} = 0 \quad \text{at } z = -H, \tag{2.11}$$
$$\tilde{u}_y = 0 \quad \text{at } y = 0 \text{ and } y = B, \tag{2.12}$$
$$\tilde{v} = 0 \quad \text{at } y = 0 \text{ and } y = B, \tag{2.13}$$
$$\tilde{w}_y = 0 \quad \text{at } y = 0 \text{ and } y = B, \tag{2.14}$$
$$\tilde{v} = \tilde{v}_0 \quad \text{at } x = 0, \tag{2.15}$$
$$\tilde{w} = \tilde{w}_0 \quad \text{at } x = 0, \tag{2.16}$$
$$\tilde{u} \to u_0(z) \quad \text{as } x \to -\infty, \tag{2.17}$$
$$\tilde{v} \to 0 \quad \text{as } x \to -\infty, \tag{2.18}$$
$$\tilde{w} \to 0 \quad \text{as } x \to -\infty. \tag{2.19}$$

The first condition states that the viscous shear stress $\tilde{\tau}_{\text{visc}}$ at the surface is equal to the shear stress applied by wind at the surface. Since wind does not apply stress in the y direction, we find $\tilde{v}_z = 0$ at the surface. The third condition is the kinematic boundary condition that follows from the rigid-lid approximation [26]. Equation 2.8 states that the pressure at the surface is equal to $\tilde{p}_{\text{surf}}$, which is the pressure applied by the rigid lid to the water surface. This pressure is a variable, and its horizontal gradient needs to be solved for in unison with the velocity and the salinity in the sub-tidal width-averaged model. In line with MacCready and Dijkstra, the gradient of the pressure is denoted as $\tilde{p}_{\text{surf},x} = \rho_0 g \tilde{\zeta}_x$. Here $\tilde{\zeta}_x$ is a t, x and y dependent variable. Rather than solve for the pressure gradient at the surface, we now solve for the gradient of the water surface that would give rise to such as pressure gradient. This water level is purely fictional, since the modelled water level is constant with a value of 0. Note that this substitution does not change the properties of the model, but merely changes the presentation of the model.

At the bottom, a no-slip condition is prescribed for the x and y components by equations 2.9 and 2.10, such that the horizontal velocity is zero. The third condition at the bottom is the kinematic boundary condition that implies that the bottom of the estuary is non-permeable.

Boundary conditions 2.12 and 2.14for the horizontal and vertical velocity at the banks of the estuary is a free surface condition, in line with the assumption of the sides being frictionless. Condition 2.13 is the kinematic boundary condition that prescribes that the banks of the estuary are non-permeable. Equation 2.14 introduces a no-slip condition at the banks of the estuary for the vertical velocity component.

At $x = 0$, the velocity in the y and z directions is described by a Dirichlet boundary condition, as represented by equations 2.15 and 2.16 respectively. No condition for u is required at this end, since only the first derivative of u with respect to x is featured in these equations.

Finally, a horizontal velocity profile u_0 is prescribed as $x \to -\infty$. This profile satisfies $\int_{-H}^{0} u_0 dz = Q/B$, such that the water transport as $x \to -\infty$ is equal to the river discharge. Equations 2.18 and 2.19 state that as $x \to -\infty$, the velocity in the y and z directions goes to zero.

2.2.3. Width-averaged sub-tidal momentum equations

This section will use the Navier-Stokes equations to derive the width-averaged sub-tidal equations for the velocity. Three time scales were identified in chapter 1: the turbulent time scale, the tidal time scale and the time scale over which the solution changes to and from sub-tidal equilibria. The latter is the time scale of interest.

The horizontal velocity will be decomposed into contributions from the three different time scales as $\tilde{u} = \hat{u} + \hat{u}' + \hat{u}''$. All other variables will be decomposed similarly. In this decomposition, $\hat{u}$ represents the slow time scale contribution, $\hat{u}'$ represents the variations on the tidal time scale and $\hat{u}''$ captures the variations on the turbulent time scale. The averages of $\hat{u}'$ and $\hat{u}''$ over their respective time scales are zero.

This decomposition is substituted into the Navier-Stokes equations, and the equations are averaged over

the turbulent time scale, the width and the tidal time scale. These steps will be done per equation, and an overview of the full system of equations is given at the end of this section.

First, the decomposition into the different time scales is substituted in the horizontal momentum equation 2.1, which is then averaged over the turbulent time scale. The average of linear terms such as $\hat{u}''_t$ is zero, and these terms are hence dropped from the equation. This yields

$$\hat{u}_t + \hat{u}'_t + (\hat{u}+\hat{u}')(u+\hat{u}')_x + \overline{\hat{u}''\hat{u}''_x}^{\text{turb}} + (\hat{v}+\hat{v}')(u+\hat{u}')_y + \overline{\hat{v}''\hat{u}''_y}^{\text{turb}} + (\hat{w}+\hat{w}')(u+\hat{u}')_z + \overline{\hat{w}''\hat{u}''_z}^{\text{turb}} = -\frac{1}{\rho_0}(\hat{p}+\hat{p}')_x + (\hat{f}^x + \hat{f}'^x) + \nu((\hat{u}+\hat{u}')_{zz} + (\hat{u}+\hat{u}')_{yy}). \quad (2.20)$$

Here the $\overline{\cdot}^{\text{turb}}$ operator indicates averaging over the turbulent time scale. Equation 2.20 resembles a regular Navier-Stokes equation in $\hat{u}+\hat{u}'$, $\hat{v}+\hat{v}'$ and $\hat{w}+\hat{w}'$, with the addition of terms that represent the advective contributions from the turbulent time scale, e.g. $\overline{\hat{u}''\hat{u}''_x}^{\text{turb}}$. These need to be expressed in terms of the variables on slower time scales for the model to be solvable. The advective contributions are known as Reynolds stresses.

A common approach is to parametrise the Reynolds stress as $K_{\text{turb}}(\hat{u}+\hat{u}')_{zz} + K_{\text{turb},W}(\hat{u}+\hat{u}')_{yy} + K_{\text{turb},H}(\hat{u}+\hat{u}')_{xx}$, thus using eddy viscosities K_{turb}, $K_{\text{turb},W}$ and $K_{\text{turb},H}$ for the x, y and z direction, respectively. Since eddy viscosity is a parametrisation of turbulence, the value of the eddy viscosity that best represents the turbulence will vary depending on the dynamics of the estuary. In order to obtain a solvable model, eddy viscosity is, however, assumed constant in time and space. In addition, the eddy viscosity is not explicitly modelled to depend on the wind speed. Recalling the assumptions from section 2.2.1, the horizontal eddy viscosity $K_{\text{turb},H}$ is assumed zero. After substituting this parametrisation, equation 2.20 becomes

$$\hat{u}_t + \hat{u}'_t + (\hat{u}+\hat{u}')(u+\hat{u}')_x + (\hat{v}+\hat{v}')(u+\hat{u}')_y + (\hat{w}+\hat{w}')(u+\hat{u}')_z = -\frac{1}{\rho_0}(\hat{p}+\hat{p}')_x + (\hat{f}^x + \hat{f}'^x) + (\nu + K_{\text{turb}})(\hat{u}+\hat{u}')_{zz} + (\nu + K_{\text{turb},W})(\hat{u}+\hat{u}')_{xx}). \quad (2.21)$$

The next step is to average the equation over the width of the estuary. The width-average of $\hat{u}$ is denoted as u, and similar notation is applied to the other variables. Moreover, u^W is defined as the variation along the width of the estuary of the sum of the sub-tidal and tidal velocity, such that $u^W = (\hat{u}+\hat{u}') - (u+u')$. After averaging over the width of the estuary, the momentum equation becomes:

$$u_t + u'_t + (u+u')(u+u')_x + \overline{u^W u^W_x}^{\text{width}} + (w+w')(u+u')_z + \overline{w^W u^W_z}^{\text{width}} = -\frac{1}{\rho_0}(p+p')_x + (f^x + f'^x) + (\nu + K_{\text{turb}})(u+u')_{zz}, \quad (2.22)$$

where the $\overline{\cdot}^{\text{width}}$ operator indicates averaging over the width of the estuary. In a similar fashion to the advective terms from the turbulent time scale, the terms $\overline{u^W u^W_x}^{\text{width}}$ and $\overline{w^W u^W_z}^{\text{width}}$ are parametrised as an added viscosity. Like the eddy viscosity, this mixing coefficient is assumed constant in time and space. This added viscosity models the mixing that occurs due to the fact that the velocity and salinity are not homogeneous in the width of the estuary. In line with the assumptions, the horizontal mixing of the horizontal velocity is assumed negligible. The vertical mixing coefficient is denoted by K_{width}. The horizontal momentum equation averaged over the turbulent time scale and the width becomes

$$u_t + u'_t + (u+u')(u+u')_x + (w+w')(u+u')_z = -\frac{1}{\rho_0}(p+p')_x + (f^x + f'^x) + (\nu + K_{\text{turb}} + K_{\text{width}})(u+u')_{zz}. \quad (2.23)$$

Finally, this equation is averaged over the tidal time scale, resulting in the following equation:

$$u_t + uu_x + \overline{u'u'_x}^{\text{tidal}} + wu_z + \overline{w'u'_z}^{\text{tidal}} = -\frac{1}{\rho_0}p_x + f^x + (\nu + K_{\text{turb}} + K_{\text{width}})u_{zz}. \quad (2.24)$$

The average of the advective contributions from the tidal time scale are, similar to the contributions from the turbulent time scale, modelled as a vertical mixing coefficient K_{tidal} that is constant in time and space. This gives

$$u_t + uu_x + wu_z = -\frac{1}{\rho_0}p_x + f^x + A_v u_{zz}, \quad (2.25)$$

where A_v is the total effective mixing coefficient, consisting of molecular viscosity, turbulent eddy viscosity, mixing over the width over the estuary and tidal mixing. As a result of choosing the individual mixing coefficients constant in time and space, A_v is constant in time and space as well, and does not explicitly depend on the wind speed.

We will now proceed with averaging the other equations and boundary conditions from the system of equations presented in section 2.2.2. Equation 2.2, the momentum equation for the y direction, can be eliminated, since the corresponding velocity v is not part of the width-averaged equations.

Furthermore, equation 2.3, the vertical momentum equation, reduces to the hydrostatic balance after averaging over the turbulent time scale, the width of the estuary and the tidal time scale, as was assumed in section 2.2.1. This balance reads: $0 = -\frac{1}{\rho_0} p_z + f^z$. Equation 2.4 reduces to the two-dimensional continuity equation in the sub-tidal variables after taking the appropriate averages, as can be seen in equation 2.28.

Since the boundary conditions are linear, most are averaged by simply replacing the variables by their averages. Two boundary conditions are not averaged in a straightforward manner and will be discussed in the next paragraph. Moreover, boundary conditions 2.6, 2.10, 2.12, 2.13, 2.14, 2.18 and 2.19 are eliminated from the boundary conditions, since these have become superfluous after the changes made to the equations.

First, for the averaging of boundary condition 2.5, it is noted that the average sub-tidal shear stress τ_{visc} is given by $\rho_0 A_v u_z$, since A_v is the effective viscosity. The magnitude of wind-induced stress is modelled as the product of a drag coefficient, the density of air and the square of the wind velocity [27, 28], as seen in equation 2.29. Since it is assumed that $u_a \gg u(z=0)$, the absolute wind velocity can be used when determining the stress, rather than the wind speed relative to the velocity of the water. The draft coefficient C_D, amongst others, depends on the roughness of the water surface. This dependency will not be explicitly modelled, and a constant value will be assumed. Typical values for this constant are around 1×10^{-3} [29].

Secondly, averaging the boundary condition $\tilde{u}(z=-H)=0$ may seem trivial. However, the applied approach of modelling turbulence and tidal mixing by a fixed effective viscosity is not an accurate representation of the dynamical structure close to the bottom. Generally, turbulent flow contains eddies with a wide range of length scales. Close to the bottom of the estuary, however, only eddies of a length scale comparable to the distance to the bottom or smaller are featured. This means that the effective viscosity is small near the bottom of the estuary. Similarly, tidal velocities are small near the bottom, which causes tidal mixing to be small there. This reduced effective viscosity allows for large vertical gradients in u, such that u will obtain relatively large values just above the bottom. Such profiles are not supported by a model with a constant effective viscosity. In order to model the effect of diminishing mixing, the boundary condition at the bottom is replaced by a boundary condition that models the behaviour at a point just above the boundary layer, above which the assumption of constant viscosity is valid. This condition reads $A_v u_z = s_f u$, where s_f is the roughness parameter, which in line with Dijkstra is chosen as $s_f = \frac{2A_v}{H}$. This boundary condition is denoted as partial-slip.

Before the model can be used, the pressure and body forces have to be determined. The only external body force acting on the estuary is gravity, which has no horizontal component, such that f^x is zero. Recalling that the changes in density due to salinity are considered in the buoyancy force, we note that the width-averaged sub-tidal body force f^z is given by $-g(1+\beta s)$. Integrating the hydrostatic balance $\frac{1}{\rho_0} p_z = f^z$ from z to the top of the estuary gives

$$\frac{1}{\rho_0} p = g \int_z^0 (1+\beta s) dz' + \frac{1}{\rho_0} p_{\text{surf}}. \tag{2.26}$$

Taking the gradient with respect to x then gives $\frac{1}{\rho_0} p_x = g\beta \int_z^0 s_x dz' + g\zeta_x$. This introduces the variable ζ_x which is the sub-tidal width-averaged $\tilde{\zeta}_x$. This variable will be solved for as the solutions to s and u are obtained.

The width-averaged, sub-tidal momentum equations then become:

$$u_t + \underbrace{uu_x + wu_z}_{\text{Advection}} = \underbrace{-g\zeta_x}_{\text{Barotropic Pressure}} - \underbrace{g\beta \int_z^0 s_x dz'}_{\text{Baroclinic Pressure}} + \underbrace{A_v u_{zz}}_{\text{Viscosity}}, \tag{2.27}$$

$$u_x + w_z = 0. \tag{2.28}$$

The hydrostatic balance and boundary condition 2.8 for the surface pressure have been eliminated from the equations, since the pressure has already been solved for and has been substituted into the relevant equations. The pressure terms have been separated into a barotropic and a baroclinic pressure gradient, representing changes in surface pressure and salinity induced gravitational load, respectively. The boundary

conditions read:

$$\rho_0 A_v u_z = C_D \rho_a u_a^2 \mathrm{sgn}(u_a) \quad \text{at } z = 0, \tag{2.29}$$
$$w = 0 \quad \text{at } z = 0, \tag{2.30}$$
$$A_v u_z = s_f u \quad \text{at } z = -H, \tag{2.31}$$
$$w = 0 \quad \text{at } z = -H, \tag{2.32}$$
$$u \to u_0(z) \quad \text{as } x \to -\infty. \tag{2.33}$$

Finally, a choice has to be made for the velocity profile u_0 in equation 2.33. In line with Dijkstra's model, the velocity profile is required to satisfy

$$g\zeta_{x,0} = A_v u_{0,zz}, \tag{2.34}$$

for some $\zeta_{x,0}$ that is uniform in z. The velocity u_0 is subject to

$$\rho_0 A_v u_{0,z} = C_D \rho_a u_a^2 \mathrm{sgn}(u_a) \quad \text{at } z = 0, \tag{2.35}$$
$$A_v u_{0,z} = s_f u_0 \quad \text{at } z = -H, \tag{2.36}$$
$$\int_{-H}^{0} u_0 dz = Q/B. \tag{2.37}$$

This is the velocity profile that arises in steady-state solutions if the horizontal velocity and salinity gradients are assumed to be equal to zero.

2.2.4. Salinity equation

Salt is transported through the estuary by means of diffusion and advection. The salinity equation is given as

$$\tilde{s}_t + \tilde{u}\tilde{s}_x + \tilde{v}\tilde{s}_y + \tilde{w}\tilde{s}_z = D(\tilde{s}_{xx} + \tilde{s}_{yy} + \tilde{s}_{zz}), \tag{2.38}$$

where D is the molecular diffusivity. The boundary conditions are

$$\tilde{s}_z = 0 \quad \text{at } z = 0, \tag{2.39}$$
$$\tilde{s}_z = 0 \quad \text{at } z = -H, \tag{2.40}$$
$$\tilde{s}_y = 0 \quad \text{at } y = 0 \text{ and } y = B, \tag{2.41}$$
$$\tilde{s} = \tilde{s}_0(z) \quad \text{at } x = 0 \tag{2.42}$$
$$\tilde{s} \to 0 \quad \text{as } x \to -\infty. \tag{2.43}$$

Since no diffusive salinity flux is desired at the bottom and surface of the estuary, the vertical salinity gradient is considered zero at the extreme vertical ends of the water column. Similarly, the salinity gradient in the y direction is zero at the banks of the estuary. Moreover, a fixed salinity profile $\tilde{s}_0(z)$ is prescribed at the seaward end. The salinity goes to zero as $x \to -\infty$, since salt only penetrates the estuary over a limited length.

The three time scales from the previous section can also be identified in the context of salinity. Like for the momentum equation, we will take averages over the turbulent time scale, the width of the estuary and finally the tidal time scale of the salinity equation.

The process of averaging over the width of the estuary and over the turbulent and tidal time scales is similar to this process for the momentum equation. Hence, the process will not be fully specified in this section. Every time the average over a time scale or the width of the estuary is taken, the advective contributions introduce an added diffusivity term. These additional diffusivities are analogous to the viscosities introduced in the momentum equation.

The width-averaged sub-tidal salinity equation becomes

$$s_t + us_x + ws_z = K_v s_{zz} + K_H s_{xx}. \tag{2.44}$$

Here K_v is the vertical diffusion coefficient, which is the sum of molecular diffusion, eddy diffusion, mixing along the width of the estuary and tidal mixing. Similarly, K_H is the horizontal diffusion coefficient, encompassing contributions from the same mixing mechanisms. Both these coefficients are assumed constant in space and time, and independent of wind speed. Since the horizontal and vertical dynamics are different, K_H

and K_v are not equal. Typically $K_s s_{zz}$ is larger than $K_H s_{xx}$, due to the fact that the estuary is relatively shallow compared to the horizontal length scales. The boundary conditions become

$$s_z = 0 \qquad \text{at } z = 0, \tag{2.45}$$
$$s_z = 0 \qquad \text{at } z = -H, \tag{2.46}$$
$$s = s_0(z) \qquad \text{at } x = 0, \tag{2.47}$$
$$s \to 0 \qquad \text{as } x \to -\infty. \tag{2.48}$$

Boundary condition 2.41 has been dropped from the boundary conditions, since the equation has become two dimensional. The other boundary conditions are simply averaged. The salinity profile s_0 is not fixed at this stage. The choice of the salinity profile will be specified during the results chapters.

2.3. Extended MacCready model

Following MacCready [16], further assumptions will be made to the model described in section 2.2. Moreover, the method that is used to obtain solutions to the adjusted model is described. This information required to answer question 1 as formulated in section 1.5 will be obtained in this section. The section will commence with a short overview of the method used and the applied assumptions and follow with the derivation of the momentum and salinity equation. Next, the vertical profiles of the horizontal velocity and salinity are derived followed by the derivation of a differential equation for the vertically averaged salinity. Finally, the numerical method used to solve the problem is described.

2.3.1. Assumptions and methodology

This model solves for equilibrium solutions with velocity $u(x,z)$ and salinity $s(x,z)$. The horizontal velocity and salinity are decomposed into the vertical average and a vertically varying component:

$$u(x,z) = \bar{u}(x) + u'(x,z), \qquad s = \bar{s}(x) + s'(x,z). \tag{2.49}$$

Here u' and s' are defined to have a vertical average of zero. The notations of u' and $\bar{u}$ are redefined here, such that they denote variations and averages in depth rather than time.

A number of assumptions are made in this model, all in line with MacCready's assumptions. Since equilibrium solutions are considered, time derivatives can be eliminated from the equations. Moreover, it is assumed that $s'_x \ll \bar{s}_x$ and $s'_{xx} \ll \bar{s}_{xx}$. It is furthermore assumed that advection of horizontal velocity can be neglected and that $(ws')_z$, the vertical advection of s', is negligible. Furthermore, it is assumed that the vertically varying component of $(u's')_x$ is negligible in the salinity equation, but that the vertical average is significant. In order to simplify the resulting expressions, it is assumed that $A_v = K_v$. For the width-averaged sub-tidal model from section 2.2, $\lim_{x\to-\infty} \bar{s} = 0$ implies $\lim_{x\to-\infty} \bar{s}_x = 0$. It is assumed that this implication also holds for the reduced model.

In solving the resulting equations, u' is determined analytically as a function of $\bar{s}_x$ first. Subsequently, this expression is used to obtain an expression for the vertical salinity profile s' in terms of $\bar{s}_x$. Next, a horizontal transport balance is used to obtain a first order ordinary differential equation for $\bar{s}$, using the vertical profiles of the horizontal velocity and salinity. The differential equation is then integrated using a numerical method in order to obtain $\bar{s}(x)$. Finally, u and s are recovered using the analytical expressions for the velocity and salinity profiles and the numerically determined vertically averaged salinity.

2.3.2. Momentum and continuity equation

The assumptions from the previous section reduce the momentum and continuity equation to:

$$\underbrace{-g\zeta_x}_{\text{Barotropic Pressure}} + \underbrace{g\beta z\bar{s}_x}_{\text{Baroclinic Pressure}} + \underbrace{A_v u_{zz}}_{\text{Mixing}} = 0, \tag{2.50}$$

$$u_x + w_z = 0. \tag{2.51}$$

A boundary condition in the form of a full profile for u as $x \to -\infty$ is not required due to the fact that horizontal derivatives of u nor terms involving w are present in equation 2.50. However, it is required that the flux goes to the river discharge as x goes to $-\infty$. This is not conflicting with the original boundary condition,

since u_0 obeys this requirement. The boundary conditions then read:

$$\rho_0 A_v u_z = C_D \rho_a u_a^2 \mathrm{sgn}(u_a) \qquad \text{at } z = 0, \tag{2.52}$$

$$w = 0 \qquad \text{at } z = 0, \tag{2.53}$$

$$A_v u_z = s_f u \qquad \text{at } z = -H, \tag{2.54}$$

$$w = 0 \qquad \text{at } z = -H, \tag{2.55}$$

$$\int_{-H}^{0} u dz = Q/B \qquad \text{at } x = -\infty. \tag{2.56}$$

We see that in comparison with MacCready's original model, a partial slip boundary condition is applied at the bottom instead of the no slip boundary condition. Moreover, MacCready applies a homogeneous Neumann boundary condition for u at the water surface, whereas this model applies an inhomogeneous Neumann boundary condition to incorporate wind in the model.

2.3.3. Salinity Equation

After applying the assumptions from section 2.3.1, the salinity equation can be written as

$$(\bar{u}\bar{s})_x - \bar{u}_x \bar{s} + \bar{u}_x s' + u'\bar{s}_x + (\overline{u's'})_x = K_H \bar{s}_{xx} + A_v s'_{zz}, \tag{2.57}$$

with boundary conditions

$$s'_z = 0 \qquad \text{at } z = 0, \tag{2.58}$$

$$s'_z = 0 \qquad \text{at } z = -H, \tag{2.59}$$

$$\bar{s} + s' = s_{\mathrm{ocn}} \qquad \text{at } x = 0, z = -H, \tag{2.60}$$

$$\bar{s} \to 0 \qquad \text{as } x \to -\infty. \tag{2.61}$$

The derivation of equation 2.57 can be found in appendix A. The first two boundary conditions are obtained simply by substituting $s = \bar{s} + s'$ in equations 2.45 and 2.46. Instead of prescribing a full profile at the seaward end, only the value at the bottom of the estuary needs to be prescribed for the third boundary condition. The prescribed value is s_{ocn}, the oceanic salinity. Similarly, as $x \to -\infty$, only the average salinity is required to be zero, rather than the full profile. These simplifications of the boundary conditions are possible since no horizontal derivatives of s' are featured. This leads to conditions 2.60 and 2.61. According to the final assumption in section 2.3.1, condition 2.61 implies $\lim_{x\to-\infty} \bar{s}_x = 0$.

2.3.4. Vertical velocity profile

Using the reduced momentum equation, the vertical velocity profile will be determined. Before this can be done, the depth-averaged horizontal velocity $\bar{u}$ is determined. The continuity equation can be used to rewrite condition 2.53 to $-\int_{-H}^{0} u_x dz = 0$. The latter expression implies that $\bar{u}(x)$ is a constant. The condition $\lim_{x\to-\infty} \int_{-H}^{0} u dz = Q/B$ shows that this constant is given by $\bar{u} = Q/(BH)$.

Equation 2.50 is integrated twice to obtain an expression for u, introducing two unknown integration constants. In addition, the auxiliary variable ζ_x is unknown. The integration constants and ζ_x can be solved for using the top and bottom boundary condition for u and the fact that u' is defined to have a vertical average of zero. Performing the integration and solving for the integration constants gives

$$u' = \bar{u}\left(\frac{1}{5} - \frac{3}{5}\sigma^2\right) + u_E\left(\frac{8}{5} - \frac{54}{5}\sigma^2 - 8\sigma^3\right) + u_w\left(\frac{3}{10} + \sigma + \frac{3}{5}\sigma^2\right). \tag{2.62}$$

Here σ is the dimensionless coordinate z/H. The velocity profile is the superposition of contributions from river discharge, gravitational circulation and wind stress, characterised by $\bar{u}$, u_E and u_w, respectively. Here

$$\bar{u} = \frac{Q}{BH}, \tag{2.63}$$

$$u_E = \frac{g\beta\bar{s}_x H^3}{48 A_v}, \tag{2.64}$$

$$u_w = \frac{C_D \rho_a u_a^2 H}{\rho_0 A_v}\mathrm{sgn}(u_a). \tag{2.65}$$

Note that $\bar{u}$ and u_w only depend on given input parameters, while u_E is dependent on the average horizontal salinity gradient. The partial slip boundary causes the contributions belonging to $\bar{u}$ and u_E to be different from MacCready's model. Moreover, MacCready's profile does not feature the u_w term, since it does not include wind. We will proceed to derive the vertical salinity profile in the next subsection.

2.3.5. Vertical salinity profile

In this section, the vertical velocity profile will be used to determine the vertical salinity profile. Only considering the vertically varying terms from equation 2.57, we find $\bar{u}_x s' + u' \bar{s}_x = A_v s'_{zz}$. Since $\bar{u}$ is constant, this reduces to

$$u' \bar{s}_x = A_v s'_{zz}. \tag{2.66}$$

We see that the assumptions result in a balance between advection and vertical mixing. The depth-varying horizontal velocity u' is known as a function of $\bar{s}_x$ from the previous section, so s'_{zz} can be expressed as a function of the average salinity gradient. Integrating twice gives an expression for s', which includes two unknown integration constants. Two constraints are required in order to solve for these constants. The first constraint is boundary condition 2.59. Boundary condition 2.58 cannot be used as the second constraint, since it follows trivially from boundary condition 2.59 and equation 2.66. The second condition follows from the fact that the vertical average of s' is zero. Performing the integration gives:

$$s' = \frac{H^2 \bar{s}_x}{A_v}(\bar{u}(-\frac{7}{300} + \frac{1}{10}\sigma^2 - \frac{1}{20}\sigma^4) + u_E(-\frac{23}{150} + \frac{4}{5}\sigma^2 - \frac{9}{10}\sigma^4 - \frac{2}{5}\sigma^5) + u_w(-\frac{11}{600} + \frac{3}{20}\sigma^2 + \frac{1}{6}\sigma^3 + \frac{1}{20}\sigma^4). \tag{2.67}$$

Again, the salinity profile consists of distinct contributions from the river flow, gravitational circulation and wind. The first two contributions are different from MacCready's model due to the partial slip boundary, while the third contribution was not present in MacCready's model.

2.3.6. Horizontal salinity distribution

Using the previously derived vertical profiles, we will derive a differential equation for the vertically averaged salinity. Taking the vertical average of equation 2.57 gives $(\bar{u}\bar{s})_x - \bar{u}_x \bar{s} + (\overline{u's'})_x = K_H \bar{s}_{xx}$. The $-\bar{u}_x \bar{s}$ term is zero since $\bar{u}$ is a constant. Integrating the equation from $-\infty$ to x, we find, using the fact that both $\bar{s}$ and $\bar{s}_x$ go to zero as x goes to $-\infty$:

$$0 = -\bar{u}\bar{s} - \overline{u's'} + K_H \bar{s}_x. \tag{2.68}$$

Both u' and s' are known as a function of the gradient of the average salinity, and so $\overline{u's'}$ can be expressed in terms of this gradient as well.

A few quantities are introduced in order to rewrite this equation:

$$\Sigma = \frac{\bar{s}}{s_{\text{ocn}}}, \tag{2.69}$$

$$T_v = \frac{H^2}{A_v}, \tag{2.70}$$

$$c = (g\beta s_{\text{ocn}} H)^{1/2}. \tag{2.71}$$

Here, Σ is a dimensionless salinity, and will be the main variable of the differential equation. Furthermore, T_v is a time scale related to vertical mixing and c is a characteristic speed which describes how fast salinity fronts move through the estuary. Using these variables, equation 2.68 can be rewritten to

$$L^3_{gc-gc}\Sigma_x^3 + (L^2_{\text{gc-wind}} + L^2_{\text{gc-river}})\Sigma_x^2 + (L_{\text{river-river}} + L_{\text{river-wind}} + L_{\text{wind-wind}} + L_D)\Sigma_x - \Sigma = 0, \tag{2.72}$$

where 7 characteristic lengths are introduced, which will be clarified in due course. The characteristic lengths

are given as

$$L_{\text{river-river}} = 0.0030\bar{u}T_v, \tag{2.73}$$

$$L_{\text{river-wind}} = 0.0039u_w T_v, \tag{2.74}$$

$$L_{\text{wind-wind}} = 0.0014\frac{u_w^2}{\bar{u}}T_v, \tag{2.75}$$

$$L^2_{\text{gc-river}} = 0.028^2 c^2 T_v^2, \tag{2.76}$$

$$L^2_{\text{gc-wind}} = 0.023^2\frac{u_w}{\bar{u}}c^2 T_v^2, \tag{2.77}$$

$$L^3_{\text{gc-gc}} = 0.036^3\frac{c^4}{\bar{u}}T_v^3, \tag{2.78}$$

$$L_D = \frac{K_H}{\bar{u}}. \tag{2.79}$$

The first six length scales arise from the $\overline{u's'}$ term in equation 2.68. The vertical deviations in salinity and velocity are comprised of distinct contributions from river flow, gravitational circulation and wind. Each of the first six length scales features the interaction of two of these contributions in the $\overline{u's'}$ term. For example, the length scale $L_{\text{river-river}}$ covers the product of the velocity and salinity profile induced by river flow. The length scale $L_{\text{river-wind}}$ on the other hand covers the sum of the product of the river contribution to velocity and the wind contribution to salinity, and the product of the wind contribution to velocity and the river contribution to salinity. The numerical coefficients in the length scales all represent the integral of a product of velocity and salinity profiles. It should be noted that $L^2_{\text{gc-wind}}$ is negative if the wind speed u_w is negative. The diffusive length scale L_D arises from the $K_H\bar{s}_x$ term in equation 2.68. Finally, the Σ term in equation 2.72 stems from the $\bar{u}\bar{s}$ term, representing the advective transport in absence of vertical deviations.

Equation 2.72 only requires one boundary condition, since it only features first order derivatives. This boundary condition is obtained from boundary condition 2.48, which states that the salinity for $x = 0$ and $z = -H$ is equal to the oceanic salinity. Using equation 2.67, the vertical salinity deviation s' at $x = 0$ and $z = -H$ can be expressed in terms of the horizontal gradient of the vertically averaged salinity. After substituting this expression and dividing by s_{ocn}, this boundary condition reads:

$$\Sigma + \frac{11c^2T_v^2}{3600}\Sigma_x^2 + \frac{2\bar{u}T_v}{75}\Sigma_x + \frac{3u_wT_v}{200}\Sigma_x = 1. \tag{2.80}$$

Equation 2.72 is the main horizontal transport balance of this model. During the presentation of the results in chapter 3, this transport balance will be visualized by rewriting the equation to

$$\underbrace{\frac{L^3_{\text{gc-gc}}\Sigma_x^3}{\Sigma}}_{T_{\text{gc-gc}}} + \underbrace{\frac{L^2_{\text{gc-wind}}\Sigma_x^2}{\Sigma}}_{T_{\text{gc-wind}}} + \underbrace{\frac{L^2_{\text{gc-river}}\Sigma_x^2}{\Sigma}}_{T_{\text{gc-river}}} + \underbrace{\frac{L_{\text{river-river}}\Sigma_x}{\Sigma}}_{T_{\text{river-river}}} + \underbrace{\frac{L_{\text{river-wind}}\Sigma_x}{\Sigma}}_{T_{\text{river-wind}}} + \underbrace{\frac{L_{\text{wind-wind}}\Sigma_x}{\Sigma}}_{T_{\text{wind-wind}}} + \underbrace{\frac{L_D\Sigma_x}{\Sigma}}_{T_D} = 1. \tag{2.81}$$

Here the T terms are the transport contributions from the corresponding length scales. The term "1" corresponds to the contribution of the average river flow $\bar{u}\bar{s}$ in equation 2.68.

2.3.7. Numerical method

Using equation 2.72, Σ can be retrieved numerically. Given a value of Σ, equation 2.72 is solved for Σ_x. Next, $\Sigma(x-h)$ is approximated by $\Sigma(x)-\Sigma_x(x)h$ for a small h, from which $\Sigma_x(x-h)$ can be determined. The process of solving for Σ_x and using that value to compute the next Σ is repeated iteratively until the domain of interest has been fully computed. This domain can either be the domain that will be displayed, or one could continue the computations untill the salinity is below a certain threshold. The step-size h is kept constant, which means that the result is obtained on a uniform grid.

The integration is started at the seaward end. Boundary condition 2.80 is used to express $\Sigma(x = 0)$ in terms of $\Sigma_x(x = 0)$. This expression is substituted in equation 2.72, which is then solved for $\Sigma_x(x = 0)$. Equation 2.72 is then used to determine $\Sigma(x = 0)$, from which the integration can be started. After Σ has been determined for the desired domain, the full salinity and velocity profiles can be determined from equations 2.62 and 2.67.

The method used is the explicit forward Euler method, in the negative x-direction. This method is the most basic integration method available, but due to the simplicity of the problem, no issues with stability,

accuracy or computational speed are encountered in practice. Euler-forward has a first-order global error. It should be noted that this method is commonly applied to initial value problems where the method integrates in the time direction, whereas here it is used to integrate along the length of the estuary.

Since equation 2.72 is cubic in Σ_x, it may have two local extrema. Whenever Σ is in between these extrema, the equation has three solutions for Σ_x. In such a case, Σ_x cannot be determined uniquely from Σ. An example of a curve where this is the case can be found in figure 2.2.

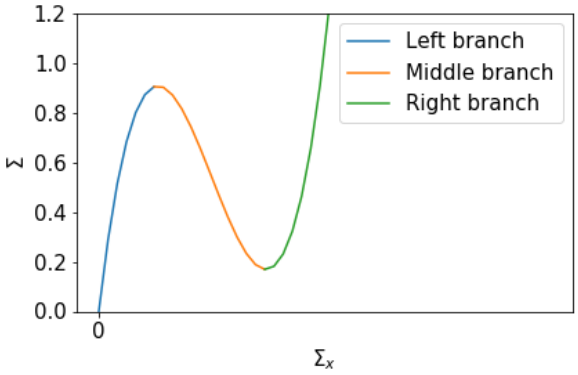

Figure 2.2: Σ vs Σ_x in a setting where equation 2.72 has two extrema

Three different branches can be found on this curve, seperated by the two extrema. The implications of being on one of these different branches and how these relate to physical regimes will be discussed in chapter 3. Whether such local extrema exist, and whether these are around the physical range of values for Σ depends on the seven length scales and thus on the parameters chosen.

In case Σ_x has multiple solutions, a choice has to be made on which Σ_x to use during the integration. It is unclear what strategy of choosing Σ_x would best describe the physical problem, if there even exists such a strategy. Two protocols will be applied to each problem in the results chapter. For the first protocol, the maximum possible value of Σ_x will be chosen, while for the other protocol the minimal possible value of Σ_x will be chosen at each Euler step. All other possible choices will result in solutions that lie in between these extreme solutions. These two protocols share the feature that they contain at most one point where Σ_x is discontinuous, whereas other protocols might have a multitude of such points. We do not expect physical solutions to have a large number of discontinuities in Σ_x, which advocates in favour of the two applied protocols.

2.4. Extended Dijkstra model

While the extended MacCready model applies a large number of assumptions to the sub-tidal model, the extended Dijkstra model does not require additional assumptions. As as consequence, vertical profiles cannot easily be determined upfront, and so a different approach is required. Compared to the extended MacCready model, this model will be more heavily reliant on numerical computations. This model will both be denoted as iFlow and as the extended Dijkstra model.

First, this section will provide an overview of the method applied and the model used. Subsequently, more detailed attention will be given to the different aspects of the applied method. Finally, this section will discuss how stability analysis is carried out and how solutions are decomposed into contributions from different physical mechanisms.

2.4.1. Assumptions and methodology

The assumptions required for the extended Dijkstra model are the same as the assumptions that were made in section 2.2. Since this model is solved numerically, it cannot be solved for $x \to -\infty$. Rather, all conditions that apply for $x \to -\infty$ are imposed at $x = -L$ for some computational length L. The length L is chosen sufficiently large, such that the displayed section of the estuary is not influenced by the finite length of the estuary. Besides this change, the governing equations are therefore identical to those presented in section 2.2.

In the approach used for this model, the horizontal velocity and salinity are vertically expanded into eigenfunctions. The problem is therefore reduced from a problem with two spatial dimensions, x and z, to a

problem with one spatial dimension, x. The number of variables is however increased, since the horizontal velocity and salinity are each replaced by a number of eigenfunctions. The equations for the corresponding eigenfunction coefficients are obtained through the Galerkin approach; the momentum and salinity equations are multiplied by a corresponding eigenfunction and integrated vertically in order to obtain an equation for each coefficient.

The equations for the coefficients are then discretised horizontally, such that the problem is transformed to a discrete problem. Roots to this discrete problem are found using Newton-Raphson iterations, while initial guesses are generated using parameter continuation. Using the solutions for the eigenfunctions at each grid point, the velocity and salinity can be constructed. While the fictional water level ζ has no meaning on its own and only ζ_x is relevant, iFlow explicitly solves for ζ to ensure compatibility with tidal models.

2.4.2. Eigenfunction expansion

In the process of solving the model just described, the vertical salinity and velocity profile are expanded into eigenfunctions first.

The horizontal velocity u is expanded according to:

$$u(x,\sigma) = \sum_{m=0}^{\infty} \beta_m(x) f_m(\sigma) + \beta_w f_w(\sigma). \tag{2.82}$$

Here the normalised height parameter $\sigma = \frac{z}{H}$ is introduced. Moreover, $\{f_m\}$ is a collection of functions that satisfy bottom boundary condition 2.31 and the homogeneous version of the top boundary condition 2.29. On the other hand, f_w is a function that satisfies condition 2.31 and does not satisfy the homogeneous version of boundary condition 2.29. The variable β_w is then tuned such that 2.29 is satisfied.

The homogeneous eigenfunctions $\{f_m\}$ are chosen as the eigenfunctions of the turbulent viscosity operator, and are given by $f_m = (-1)^m \cos(\lambda_m \sigma)$, where λ_m satisfies $\frac{1}{2}\lambda_m \tan(\lambda_m) = 1$. The latter requirement follows from the bottom boundary condition. The factor $(-1)^m$ is chosen in order to be able to apply upwind methods more easily during the discretisation. The term $\beta_w f_w$ ensures that the inhomogeneous boundary condition 2.29 is satisfied. Here β_w is a wind-dependent constant given as $\frac{HC_D\rho_a u_a^2 \mathrm{sgn}(u_a)}{A_v \rho_0}$, and f_w is chosen as $f_w = \sigma + \frac{3}{2}$.

For w, no eigenfunction expansion is required. Using equation 2.28, the continuity equation, and condition 2.32 for w, w can be expressed in the eigenfunction coefficients of u:

$$w(x,\sigma) = -H \sum_{m=0}^{\infty} \frac{1}{\lambda_m} \beta_{m,x}(x) \big(\sin(\lambda_m \sigma) + \sin(\lambda_m)\big). \tag{2.83}$$

The top boundary condition 2.30 for w is not automatically satisfied and so raises an additional constraint, written as

$$-H \sum_{m=0}^{\infty} \frac{1}{\lambda_m} \beta_{m,x}(x) \sin(\lambda_m) = 0. \tag{2.84}$$

This condition is satisfied by the correct value of the variable ζ_x.

The salinity s is expanded as

$$s(x,\sigma) = \sum_{m=0}^{\infty} \alpha_m(x) g_m(\sigma). \tag{2.85}$$

For this expansion, eigenfunctions of the vertical mixing operator are used. The boundary conditions are homogeneous Neumann boundary conditions, and so the eigenfunctions are given as $g_m(\sigma) = (-1)^m \cos(m\pi\sigma)$. Since ζ is a one-dimensional variable in x, a similar expansion is not applicable to, nor necessary for ζ

.

2.4.3. Galerkin equations

Using the eigenfunction expansions, the Galerkin equations can be formulated. We consider both the expansions of u and s to consist of M terms. This means that the expansions in equations 2.82 and 2.85 are truncated at $m = M-1$. This gives $2M+1$ unknowns: M velocity coefficients, M salinity coefficients and ζ. For each unknown, one equation is required. First, the equations for the fictional water level and the M unknowns of the expansion of the horizontal velocity are determined, followed by the equations for the M coefficients of the salinity expansion.

In order to obtain equations for the coefficients of the velocity profile, the expansions of u, w and s are substituted into the momentum equation. The resulting equation is then multiplied by an eigenfunction of the expansion of u and is integrated from $\sigma = -1$ to $\sigma = 0$. The equation corresponding to ζ is equation 2.84, stating that $w(z = 0) = 0$. This boundary condition can be represented as in equation 2.87. The Galerkin equations for momentum and fictional water level then become:

$$\underbrace{G^b_{1,k}\beta_{k,t}}_{\text{Inertia}} + \underbrace{\frac{A_v}{H^2}G_{1,km}\beta_m}_{\text{Viscosity}} + \underbrace{G_{2,kmn}\beta_n\beta_{m,x} + G^b_{2,km}\beta_{m,x}\beta_w + G_{3,kmn}\beta_{m,x}\beta_n - G^b_{3,km}\beta_{m,x}\beta_w}_{\text{Advection}} =$$

$$\underbrace{-g\zeta_x G_{4,k}}_{\text{Barotropic Pressure}} \quad \underbrace{+g\beta H G_{5,km}\alpha_{m,x}}_{\text{Baroclinic Pressure}}, \quad \forall k \in \{1,\dots,M\}, \tag{2.86}$$

$$G_{9,m}\beta_{m,x} = 0, \tag{2.87}$$

with boundary conditions

$$\frac{A_v}{H^2}G_{1,km}\beta_m = -g\zeta_x G_{4,k}, \qquad \forall k \in \{1,\dots,M\} \qquad \text{at } x = -L, \tag{2.88}$$

$$G_{9,m}\beta_m = \frac{Q}{BH} + G^b_9\beta_w \qquad \text{at } x = -L, \tag{2.89}$$

$$\zeta = 0 \qquad \text{at } x = -L. \tag{2.90}$$

In these equations, the Einstein summation convention is used. Terms such as $G_{1,km}$ and $G^b_{3,km}$ are coefficients involving integrals of products of eigenfunctions and eigenvalues, that will not be listed here, and can be found in appendix B. Each term can be related directly to a term from the momentum equation, as indicated by the horizontal braces in equations 2.27 and 2.86. Boundary condition 2.88 has been obtained by applying the Galerkin approach to equation 2.34. The second boundary condition (2.89) follows from equation 2.37 and specifies the river discharge. The final boundary condition, equation 2.90 is required since iFlow explicitly solves for ζ rather than just ζ_x. Since only the horizontal gradient of ζ is relevant, any Dirichlet boundary condition would yield the same salinity and velocity.

The same procedure is applied to the salinity equation, where the equation is multiplied by the eigenfunctions g_k of the expansion of the salinity profile and then integrated along the depth of the estuary. This provides an equation for the M time-derivatives of α_m, reading:

$$\underbrace{G_{6b,k}\alpha_{kt}}_{\text{Inertia}} + \underbrace{\frac{K_v}{H^2}G_{6,km}\alpha_m}_{\text{Vertical Diffusion}} + \underbrace{G_{7,kmn}\alpha_{m,x}\beta_n + G^b_{7,km}\alpha_{m,x}\beta_w + G_{8,kmn}\beta_{n,x}\alpha_m}_{\text{Advection}} = \underbrace{G_{6b,km}K_H\alpha_{m,xx}}_{\text{Horizontal Diffusion}}, \tag{2.91}$$

With boundary conditions

$$\alpha_k = (2-\delta_{1k})\int_{-1}^{0}\Big(\cos(k\pi\sigma)s_0(z=\sigma H)\Big)d\sigma \qquad \text{at } x = 0, \tag{2.92}$$

$$\alpha_k = 0 \qquad \text{at } x = -L. \tag{2.93}$$

Using the Galerkin approach, the partial differential equations in x, z and t have been transformed into a system of partial differential equations in x and t. For equilibria, the t dependency is removed and the problem becomes a boundary value problem.

2.4.4. Discretisation

Before the differential equations for the Galerkin coefficients and ζ can be solved numerically, the equations have to be discretised. This section will first describe the conceptual goal of discretising the equations, subsequently describe how the terms that were not present in Dijkstra's model are discretised and ultimately cover the grid chosen.

Before discretising, the problem can be seen as a 2 dimensional partial differential equation, in x and t, for a $2M+1$ dimensional state vector. This vector consists of M elements for the velocity coefficients, M for the salinity coefficients and 1 for ζ. This boundary value problem is transformed into an ordinary differential

equation for a $(2M+1)N$ dimensional vector y, where N is the number of grid points. Every element contains the value of one of the $2M+1$ variables at a certain grid point. The vector y is structured as

$$y_{k+(2M+1)j} = \beta_k(x_j) \qquad \text{for } j \in \{0,\dots,N-1\} \text{ and } k \in \{0,\dots,M-1\}, \tag{2.94}$$

$$y_{k+M+(2M+1)j} = \alpha_k(x_j) \qquad \text{for } j \in \{0,\dots,N-1\} \text{ and } k \in \{0,\dots,M-1\}, \tag{2.95}$$

$$y_{2M+(2M+1)j} = \zeta(x_j) \qquad \text{for } j \in \{0,\dots,N-1\}. \tag{2.96}$$

After discretising, the problem can be written as

$$\mathscr{M}\, y_t = M(y)\, y - f, \tag{2.97}$$

where $\mathscr{M}$ is a constant $(2M+1)N \times (2M+1)N$ matrix describing inertia and $M(y)$ is a matrix with the same dimensions, that is dependent on the state vector. The matrix M contains the discretisations of the different terms in the Galerkin equations. The dependency on the state vector arises through advection, which is not linear in the state vector. The right-hand side f is a constant vector, which is constituted of contributions from the non-homogeneous boundary conditions. First, the inertia matrix $\mathscr{M}$ is discussed, followed by the matrix $M(y)$.

The inertia matrix is a diagonal matrix that satisfies

$$\mathscr{M}_{ii} = G^b_{1,k} \qquad \text{if } i = k + (2M+1)\, j \qquad \text{for } j \in \{1,\dots,N-1\} \qquad \text{and } k \in \{0,\dots,M-1\}, \tag{2.98}$$

$$\mathscr{M}_{ii} = G^b_{6,k} \qquad \text{if } i = k + M + (2M+1)\, j \qquad \text{for } j \in \{1,\dots,N-2\} \qquad \text{and } k \in \{0,\dots,M-1\}, \tag{2.99}$$

$$\mathscr{M}_{ii} = 0 \qquad \text{else.} \tag{2.100}$$

The coefficients for the expansions of velocity and salinity have finite inertia on the interior of the domain. The velocity coefficients on the left boundary, the coefficients for salinity on both boundaries, and the fictional water level ζ on the entirety of the domain have zero inertia. An inertia of zero means that the time derivative of a variable is not present in the corresponding equation. This is true for coefficients at the boundary, where the profiles remain fixed, as well as for the rows that describe equation 2.87, which does not feature a ζ_t term. These equations are time independent. The equations that correspond to a zero mass term in $\mathscr{M}$ can, therefore, be seen as time independent constraints, rather than equations describing time evolution.

The matrix $M(y)$ contains the main discretisation of Galerkin equations. The full matrix is not specified here, due to the complexity of the matrix, and the fact that the discretisation used is highly similar to that used in the original model by Dijkstra. Three main discretisations are applied in the iFlow implementation of Dijkstra's model. These include a second-order central difference method for the Δ operator, a second-order central scheme for the ∇ operator and a second-order upwind scheme for the ∇ operator. All terms that were in the original iFlow model are discretised as in the original iFlow implementation. The reader is referred to Dijkstra's paper [22] for details of these discretisations.

The terms that are new to the Galerkin equations are the wind-induced terms. These are advective in nature, and therefore the same discretisation is applied that was used to discretise the other advective terms. This discretisation is based on flux vector splitting. Flux vector splitting is a method that enables the application of upwind methods in multi-dimensional settings. Assume that the operator is given as $A\nabla$. A is diagonalized as $K\Lambda K^{-1}$ and the operator is decomposed as $A\nabla = K\Lambda^+ K^{-1}\nabla^+ + K\Lambda^- K^{-1}\nabla^-$. Here Λ^+ and Λ^- are the diagonal matrices that only contain the positive or negative eigenvalues, respectively. By splitting Λ, A is effectively split according to the upwind direction. Operators ∇^+ and ∇^- are implementations of the ∇ operator with the corresponding upwind direction. A second order upwind scheme is used for the ∇^+ and ∇^- operators. The scheme is given as

$$\nabla^+ u = \frac{3u^j - 4u^{j-1} + u^{j-2}}{3x^j - 4x^{j-1} + x^{j-2}}. \tag{2.101}$$

The operator ∇^- is discretised analogously, where the indices $j-1$ and $j-2$ are replaced by $j+1$ and $j+2$, respectively.

While a uniform grid was used in the implementation of MacCready's model, a non-uniform grid is used for the numerical implementation of this model. Since changes in velocity and salinity occur on short length scales in boundary layers at the oceanic end, a non-uniform grid is used that is fine near the ocean and coarse in the interior of the estuary.

2.4.5. Root finding method

The previous section described how the continuous problem for the eigencoefficients and ζ is transformed into a discrete problem. This section will describe how the roots to this discrete problem are found. For roots, the time derivative of y is 0 and so equation 2.97 becomes

$$M(y)y = f. \tag{2.102}$$

Since the matrix M is dependent on the solution y, a linear solver cannot be used to recover y directly. Instead, an iterative Newton-Raphson solver is used. To this end, assume that an estimate y_n is given. The residual $r_n = f - M(y_n)y_n$ is determined, and the function $y \to M(y)y$ is linearized around y_n:

$$M(y)y \approx M(y_n)y_n + J(y_n)(y - y_n). \tag{2.103}$$

Here J is the Jacobian of the function $y \to M(y)y$. This linearized function is used to estimate a new point y_{n+1} by solving

$$J(y_n)\Delta y = r_n. \tag{2.104}$$

The new estimate used is then $y_{n+1} = y_n + \Delta y$. This procedure is repeated until $||\Delta y||$ is smaller than a prescribed tolerance.

The initial guess y_0 can be chosen in a variety of ways. For instance, y_0 can be chosen zero if no information is available. Alternatively, a simpler model such as MacCready's model can be used to generate an initial guess y_0. In addition, y_0 can be generated through the use of continuation procedures, which will be described in the next section.

2.4.6. Continuation

Every solution y has an area of convergence, which is the set of initial guesses y_0 that converge through the Newton algorithm to the solution y. Generally, if y_0 is close to y, y_0 converges to y. The guess $y_0 = 0$ is, however, not in the convergent set for most parameter regimes. Continuation is used to overcome this problem and generate solutions from $y_0 = 0$.

While $y_0 = 0$ is not in the convergent set for most parameter regimes, it is in that set for high values of the vertical viscosity parameter. Since viscosity is a linear phenomenon, the linearity of the problem increases with viscosity. As a result, the linearisation 2.103 becomes more accurate for larger viscosities, causing the estimates provided by the Newton-Raphson algorithm to become closer to the actual solution. Consequently, solutions can be found more efficiently for larger viscosities. The problem is solved for a high viscosity and the solution is used to estimate a suitable y_0 for a slightly lower viscosity. This process is repeated until the desired viscosity is obtained.

Other than in the setting previously described, continuation can also be used to see the effect of a parameter on a solution. If a solution is found, one could repeat the procedure that found that solution for slightly different parameters, and study the difference between the two solutions. However, it is quicker to use the previous solution to generate an estimate for the problem with altered parameters, and apply the root finder to this estimate. If the different parameter values differ significantly, the parameter has to be adjusted in steps to continuate from one solution to the next. This also assures that a solution on the same solution branch is found if multiple solutions exist.

2.4.7. Stability Analysis

A stability analysis of the equilibrium solutions, which was not performed by Dijkstra, will be carried out in this thesis. During stability analyses, the eigenvalues of the linearisation of equation 2.97 are determined, meaning that the following generalized eigenvalue problem is solved:

$$\lambda \mathscr{M} v = J(y)v, \tag{2.105}$$

where y is the equilibrium solution around which the analysis is carried out and v is an eigenvector with eigenvalue λ. The number of eigenvalues found is equal to the dimensionality of y, minus the amount of zeros along the diagonal of $\mathscr{M}$. Every zero along the diagonal of $\mathscr{M}$ is a linear constraint on the eigenvalues, which reduces the dimensionality of the linear subspace of eigenvectors by 1. The dimensionality of the subspace of eigenvectors is therefore $(2N-3)M$, since $N+3M$ linear constraints are applied to $(2M+1)N$ dimensional vectors.

The eigenvalues are calculated using the `eig` function within the `scipy.linalg` library in Python. This algorithm returns $(2M+1)N$ eigenvalues, of which $N+3M$ are either plus or minus infinity. These eigenvalues correspond to eigenvectors with zero inertia, which means that these eigenvectors do not satisfy the time independent constraints. The $N+3M$ infinite eigenvalues are removed from the set of eigenvalues, leaving the desired $(2N-3)M$ eigenvalues.

2.4.8. Decomposition

In order to facilitate an analysis of the contributions of different mechanisms to the solution, a technique is developed to separate the different contributions. Since advection introduces non-linearity, all different mechanisms interact with each other in some way. A true decomposition into independent contrbibutions is therefore not possible.

In the proposed decomposition, the velocity u and the auxiliary variable ζ are decomposed first. The terms are decomposed into u_i and ζ_i for $i \in \{1,\dots,4\}$. The decomposition for the horizontal velocity can be described as

$$g\zeta_{i,x} - (A_v u_{i,z})_z = -\underbrace{(uu_x + wu_z)}_{\text{Advection}}\delta_{i1} + \underbrace{g\beta\int_z^0 s_x dz'}_{\text{Baroclinic}}\delta_{i2}, \tag{2.106}$$

$$\int_{-H}^0 u_i dz = \underbrace{Q/B}_{\text{River}}\delta_{i3}, \tag{2.107}$$

$$\rho_0 A_v u_{i,z} = \underbrace{C_D\rho_a u_a^2 \operatorname{sgn}(u_a))}_{\text{Wind}}\delta_{i4} \qquad \text{at } z=0, \tag{2.108}$$

$$A_v u_{i,z} - s_f u_i = 0 \qquad \text{at } z=-H, \tag{2.109}$$

$$\zeta = 0 \qquad \text{at } x=0. \tag{2.110}$$

Here u, w and s are the full solutions from the model, and are assumed as given, while u_i and ζ_i for $i \in \{1,\dots,4\}$ are the different contributions that make up the decomposition. This means that $\sum_{i=1}^4 u_i = u$ and $\sum_{i=1}^4 \zeta_i = \zeta$. Only vertical derivatives of u_i are involved, such that no horizontal boundary conditions are required. Moreover, the equations are linear in u_i and ζ_i, such that the discretised problem can be solved using a linear solver, rather than an iterative root finder.

The velocity is decomposed into an advective contribution ($i=1$), a baroclinic contribution ($i=2$), a contribution from river flow ($i=3$) and a wind-induced contribution ($i=4$). All these contributions correspond to one of the braced terms on the right-hand side in the above representation.

Since the velocity and salinity used for the terms on the right-hand side are the full solutions for the velocity and salinity, the advective and baroclinic contributions are influenced by the other forcings. These forcings influence the terms in the right-hand sides, and thus the contributions of the decomposition. This type of interference is inevitable due to the non-linear nature of the problem, as discussed above.

Once the velocity and water level have been decomposed into different contributions, these can be used to decompose the salinity. The salinity is decomposed in the depth-averaged part $\bar{s}$ and the vertically varying s', which is further decomposed into various physical contributions. The four velocity contributions are used to generate corresponding salinity contributions according to:

$$-K_v s'_{i,zz} = -(u_i s_x + w_i s_z), \tag{2.111}$$

with boundary conditions

$$s'_{i,z} = 0 \text{ at } z=-H, \tag{2.112}$$

$$\int_{-H}^0 s'_i dz = 0. \tag{2.113}$$

, for $i \in \{1,\dots,4\}$. These contributions cover the vertical mixing forced by the various advective terms. The final contribution is the vertical mixing forced by horizontal dispersion, which reads

$$-(K_v s'_{K_H,z})_z = (K_H s_x)_x, \tag{2.114}$$

and obeys boundary conditions 2.112 and 2.113. The sum of these different s' contributions and $\bar{s}$ equals the total salinity.

3

Results for the extended MacCready model

In this chapter, the results for the extended MacCready model (EMM) will be presented, for an idealized case representing a typical estuary. This chapter answers research questions 2 and 3, which ask what equilibrium solutions are possible in this model and how these are constituted, as well as how these solutions are best analysed.

Section 3.1 analyses the relation between the salinity Σ and the salinity gradient Σ_x to define five ranges of wind speeds with different solutions. The next five sections each explore the solutions found for one of the five ranges of wind speeds. First, the results for offshore wind are presented in section 3.2. This is followed by sections 3.3 to 3.6, which each present the results for a set of onshore wind speeds, ranging from small to very large. The chapter will proceed with section 3.7, which shows the effects of changing vertical viscosity. Next, section 3.8 will reflect upon the choices made during the modelling stage. The chapter will end with a conclusion on the results for this chapter in section 3.9.

The parameters used during the computations are chosen to reflect the "general regime" in MacCready's 2004 paper [16]. An overview of these parameters can be found in table 3.1. All results are generated using these parameters, unless specified otherwise.

parameter	value
β	$7.6 \cdot 10^{-4}$ psu^{-1}
s_{ocn}	30 psu
h	500 m
H	11 m
B	250 m
Q	40 m^3/s
A_v	$4 \cdot 10^{-4}$ m^2/s
K_H	20 m^2/s
C_D	10^{-3}
ρ_a	1.225 kg/m^3
ρ_0	1000 kg/m^3

Table 3.1: List of parameters used during chapter 3

3.1. Overview

This section will study equation 2.72, the horizontal salinity balance, under the influence of changing wind speed in order to analyse the global structure of the solutions. First, two possible types of curves representing the relation between Σ and Σ_x are identified. Next, it is explored which types of solutions are possible for both curves. Finally, five different ranges of wind speeds are identified, for which different solutions exist.

3.1.1. Possible characteristics

Figure 3.1 plots Σ on the vertical axis vs Σ_x on the horizontal axis as determined by equation 2.72. This curve is referred to as the $\Sigma_x - \Sigma$ characteristic. There are two fundamental types of curves, which are displayed in

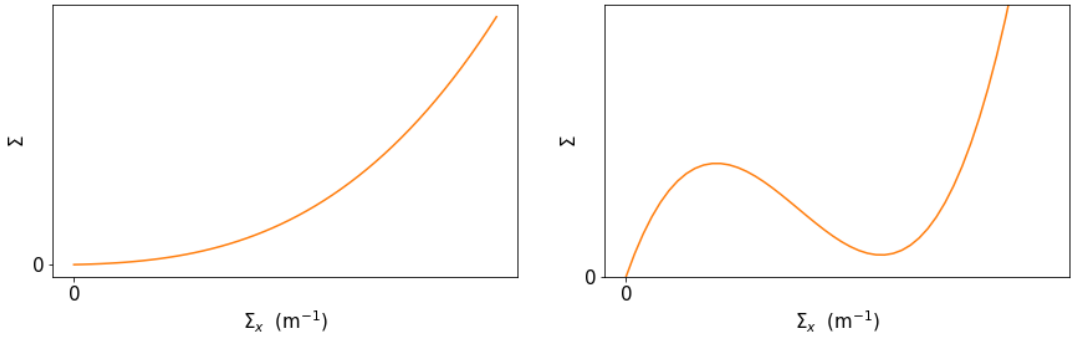

(a) No local extrema

(b) Two local extrema

Figure 3.1: Two plots of Σ vs Σ_x for different parameters

the two panels of this figure.

The first panel shows the curve for a wind speed for which the curve does not have local extrema. The curve in the second panel has two local extrema, connected by a section where Σ decreases as a function of Σ_x, resembling the curve in figure 2.2.

The section in the curve in the second panel where Σ decreases as a function of Σ_x is caused by the fact that $L^2_{\text{gc-wind}}$ is negative for negative wind speeds. If the other contributions are sufficiently small, this will result in a section where Σ decreases as a function of Σ_x. For smaller Σ_x, the linear terms $L_{\text{river-river}}\Sigma_x$, $L_{\text{river-wind}}\Sigma_x$, $L_{\text{wind-wind}}\Sigma_x$ and $L_D\Sigma_x$ are relatively larger, while for larger Σ_x the cubic term $L^3_{\text{gc-gc}}\Sigma_x^3$ dominates, such that the Σ increases as a function of Σ_x for those values of Σ_x.

For negative wind speeds, a decreasing section only arises if the wind speed is large enough in magnitude. Otherwise, the contribution $L^2_{\text{gc-wind}}\Sigma_x^2$ will not be large enough to create a decreasing section in the curve. For positive wind speeds, this contribution is increasing and so no decreasing section will occur in the $\Sigma_x - \Sigma$ characteristic. Whether a decreasing section occurs depends on the dimensionless quantities $\frac{u_w}{\bar{u}}$ and $\frac{K_H A_v}{\bar{u}^2 H^2}$. The first quantity is equivalent to the non-dimensional wind stress Ts, as defined by Lange and Burchard [20, 30] and covers the ratio between wind and average river flow. The second number covers the ratio between diffusion and average river flow and is given by $F_r^{-2}Ra^{-1}$, where Fr is the estuarine Froude number [31, 32] and Ra the estuarine Rayleigh number [13]. The existence of local extrema is therefore independent of gravitational circulation.

3.1.2. Possible solutions

The possible solutions for both shapes of the $\Sigma_x - \Sigma$ characteristic will now be analysed. The solutions are plotted in figure 3.2. The orange solid lines plot Σ vs Σ_x using equation 2.72. The blue scatter plot indicates the $\Sigma_x - \Sigma$ pairs that are obtained in each solution, and in this way highlights which branches of the characteristic are used. For the first type, where the characteristic does not have local extrema, only one type of solution is possible, since there are no points in the domain where multiple salinity gradients Σ_x are possible. This solution is indicated in figure 3.2a.

For a characteristic of the second type, which has two local extrema, two types of solutions are identified. The first type of solution uses the left branch at the oceanic end. An example of such a solution is depicted in figure 3.2b. Such a solution is only possible if the Σ value corresponding to the local maximum is higher than the Σ value at the boundary. The Σ value at the boundary depends on the specific solution, but is typically close to 1. If the Σ value of the local maximum is lower, the left branch cannot be selected at the oceanic end, which means that multiple branches have to be used.

The second type of solution does not use the left branch at the oceanic end. Two examples of such solutions are plotted in figures 3.2c and 3.2d. These are only two examples of the infinitely many solutions of this type which are possible. These types of solutions are only possible if the Σ value of the local minimum is lower than the Σ value at the oceanic boundary. If the Σ value of this minimum is higher, the right and middle branches are not feasible for any of the Σ values that are encountered in the estuary. As a result, only the left branch can be used.

The Σ values of the two local extrema determine which types of solutions are possible. The Σ values of these extrema are dependent on three dimensionless numbers: $\frac{u_w}{\bar{u}}$, $\frac{K_H A_v}{\bar{u}^2 H^2}$ and $\frac{\bar{u}}{c}$. The first two numbers were

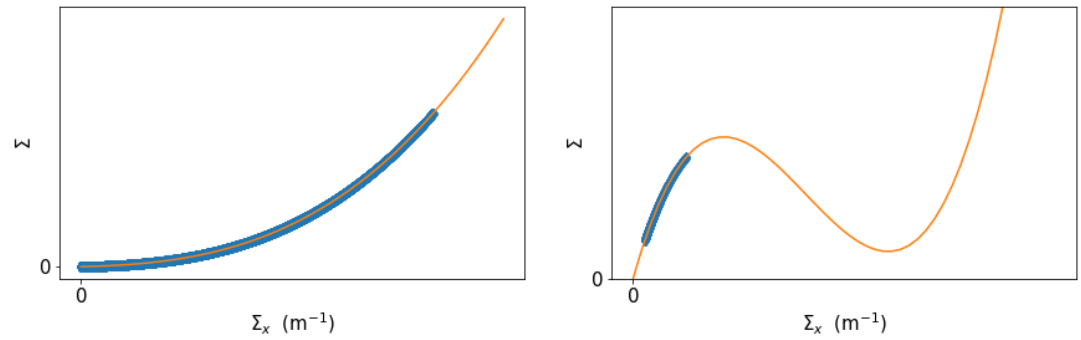

(a) Vertically averaged salinity

(b) Boundary stratification

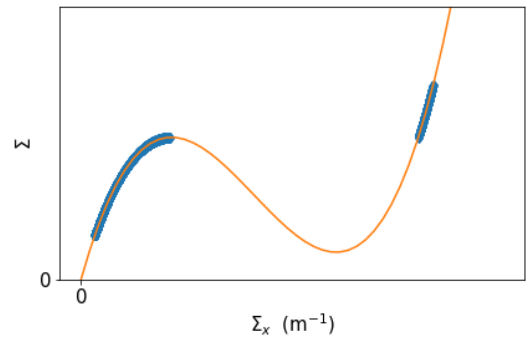

(c) Vertically averaged salinity

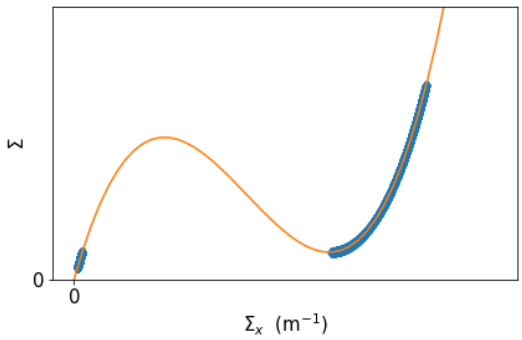

(d) Boundary stratification

Figure 3.2: The $\Sigma_x - \Sigma$ characteristics for four different solutions.

introduced in the previous section. The estuarine Froude number $\frac{\bar{u}}{c}$ compares the average river discharge to gravitational circulation. The values of the extrema scale quadratically with the estuarine Froude, the horizontal salinity balance, number, the scaling with the other two numbers is more intricate.

3.1.3. Wind speed ranges

This section will identify five different ranges of wind speeds. The first range is the range of offshore wind speeds. For this range of wind speeds, the $\Sigma_x - \Sigma$ characteristic has no local extrema, since the wind speed is positive.

The second range of wind speeds is the range of small onshore wind speeds. For this range the $\Sigma_x - \Sigma$ characteristic has no local extrema either. This is caused by the fact that the wind speed is too small in relation to horizontal diffusion and river discharge for local extrema to occur. For this range of wind speeds, only one solution is possible.

The third range of wind speeds is the range of medium onshore wind speeds. For these wind speeds, the $\Sigma - \Sigma_x$ characteristic has two local extrema. Both the local maximum and the local minimum have a Σ value below the Σ value at the oceanic end. As a consequence, only solutions which do not start on the left branch are possible, such as those in figures 3.2c and 3.2d. This gives an infinite amount of solutions.

Fourth, for the range of large wind speeds, the local maximum has a value above the value of Σ at the boundary, while the local minimum is below the value of Σ at the boundary. For this range of wind speeds, both solutions which start at the left branch of the $\Sigma_x - \Sigma$ characteristic and solutions which start at a different branch are possible. As a result, there are infinitely many solutions that start on the left branch, and infinitely many solutions that start on a different branch. The amount of solutions is therefore referred to as "2∞".

The fifth range of wind speeds is the range of very large wind speeds. For these wind speeds, the local minimum has a Σ value that is above the Σ value at the oceanic end. As a result, only the solution that exclusively uses the left branch is possible.

Since the values of Σ for the local extrema depend on three dimensionless quantities, the largest and smallest wind speed for each wind speed range cannot easily be described in terms of dimensionless quantities. Moreover, for different parameters, different structures will be found. For example, if the horizontal diffusion coefficient is increased from 20 m^2/s to 1000 m^2/s, it is seen that local extrema have salinities larger

than the vertically averaged salinity at the boundary, whenever such extrema exist. In that case, the range of medium wind speeds and the range of large wind speeds as defined in this section are not present. Since the different ranges of wind speeds cannot easily be identified in terms of dimensionless quantities, and not all ranges exist for all parameter choices, this thesis will refer to actual wind speeds, rather than dimensionless numbers. However, it should be kept in mind that different parameters alter the limits of the ranges of wind speeds.

3.2. Offshore wind

The first range of wind speeds considered is the regime of offshore winds. An overview of the salinity structure for a selection of wind speeds within this range is found in figure 3.3. For solutions within this range of

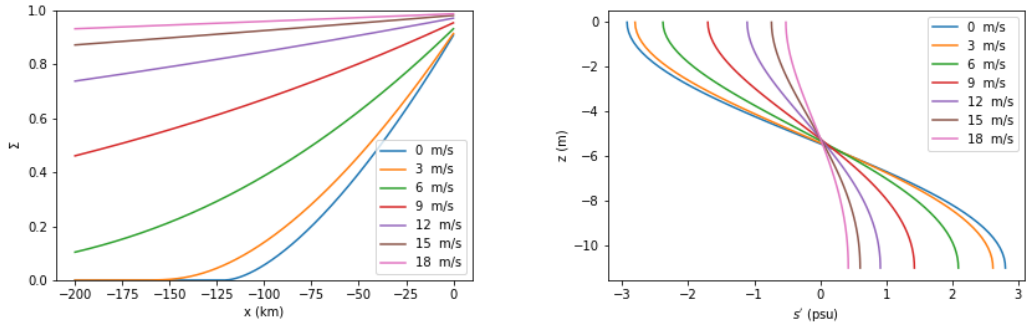

(a) Vertically averaged salinity

(b) Boundary stratification

Figure 3.3: Salinity structure for a range of offshore wind speeds. The first panel displays the vertically averaged salinity along first 200 km of the estuary. The second panel displays the vertical variation in salinity at the ocean.

wind speeds, one solution is found for each wind speed. Looking at the first panel, displaying the vertically averaged salinity along the channel for different offshore wind speeds, it can be noted that the penetration length increases as the offshore wind speed increases. This might seem counterintuitive, since one might expect wind directed towards the ocean to inhibit the transport of salt from the ocean to the estuary. This phenomenon will be explained later in this section.

Figure 3.3b displays the salinity shear s' at $x = 0$. It can be seen that the stratification is stable, and that the stratification becomes smaller for larger wind speeds. This follows directly from equation 2.67, which shows that stratification scales with the salinity gradient, which is smaller for larger wind speeds. As the offshore wind speed increases, the salt penetration length increases and the stratification decreases. Large offshore wind speeds thus cause the estuary to become better mixed, both vertically and horizontally.

The solutions for two different wind speeds will be studied in further detail. Firstly, we will look at the small wind speed of 3 m/s. An overview of the results can be found in figure 3.4. The top-left figure shows a heat map of the vertical variation in salinity s'. It can be seen that the estuary is stably stratified in the salinity and that the degree of stratification decreases as x decreases. This is in line with equation 2.67, which shows that the stratification scales with the salinity gradient, which decreases with decreasing x.

The top-right panel is a heat map of the horizontal velocity u. The panel for the horizontal velocity shows that water flows towards the river at the bottom of the estuary, and flows towards the ocean at the surface. Both offshore wind stress and gravitational circulation contribute to this type of circulation, as seen in section 1.1. An increase in offshore wind speed means an increase in the magnitude of the clockwise circulation seen in this figure. Since the water is most saline at the bottom of the estuary, an increase in offshore wind speed stimulates the transport of salt in the up-estuary direction. This explains how the salt penetration length increases as the offshore wind speed increases, as was seen in figure 3.3a.

The bottom-left panel displays the $\Sigma_x - \Sigma$ characteristic, which consists of an orange solid line plot and a blue scatter plot. The solid line plots Σ as a function of Σ_x, based on the analytical expression provided by equation 2.72. This analytical curve is overlaid by a blue plot of Σ vs Σ_x at all grid points of the numerical solution. Since the numerical implementation is based on the analytical expression, the points of the scatter plot are all positioned on the curve. In this figure, we see that Σ_x gradually decreases towards zero as Σ goes to zero.

The fourth panel shows the transport contributions as defined in equation 2.81. Contributions which

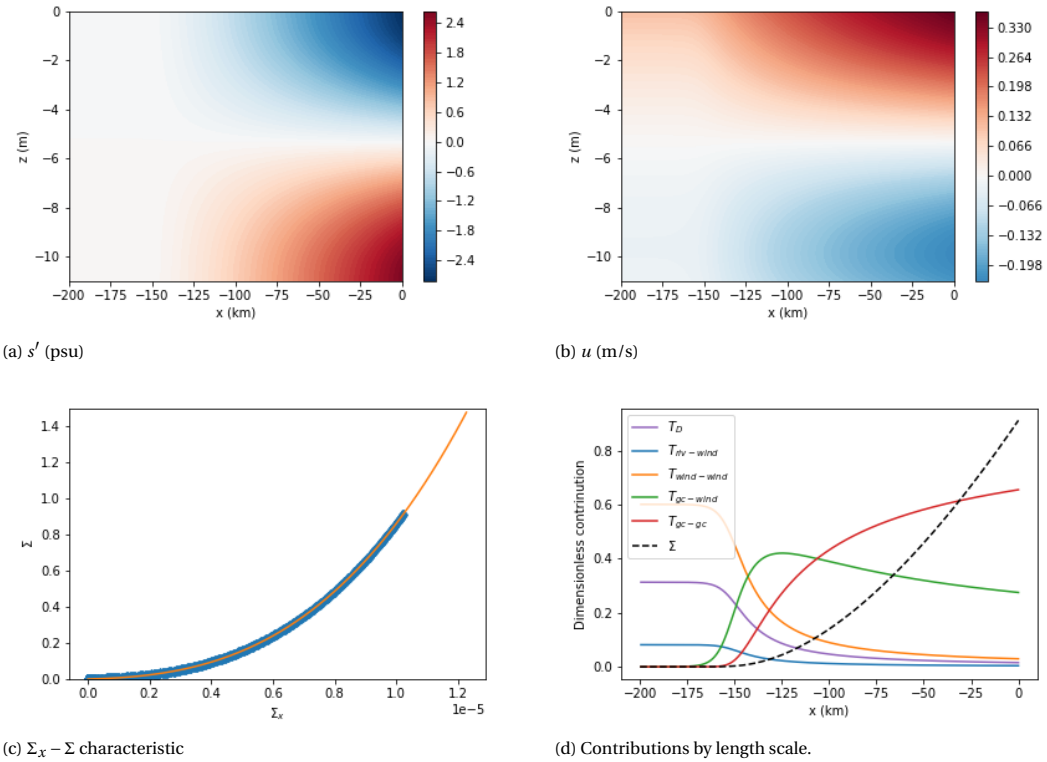

(a) s' (psu)

(b) u (m/s)

(c) $\Sigma_x - \Sigma$ characteristic

(d) Contributions by length scale.

Figure 3.4: Overview of the solution for $u = 3$ m/s. The figure for the $\Sigma_x - \Sigma$ characteristic features the analytical characteristic as a solid orange line, as well as a blue plot of the realized characteristic. The fourth plot displays the transport contribution as defined in equation 2.81 along the length of the estuary..

are negligible over the entire domain are not displayed. The sum of the terms equals 1, such that the terms balance the transport induced by the average river flow. A dashed line of the salinity Σ is included for visual reference. In the figure, we see two different regimes. In the seaward regime ($x > -135$ km), where the salinity is high, gravity-gravity interaction and gravity-wind interaction feature most prominently. The vertical profiles of the horizontal velocity and salinity are therefore determined by a combination of gravitational circulation and wind, and wind and gravitational circulation jointly counter the salt transport induced by the average river flow. The landward regime ($x < -135$ km), where salinity is low, shows that diffusion, wind-wind interaction and to a lesser extent wind-river interaction are dominant. These terms form a balance with the average river flow in equation 2.81. Since horizontal diffusion does not influence vertical profiles in this model, wind dominates the vertical salinity and velocity profiles. The shift between the two regions happens as Σ approaches zero. Since this approach is smooth, the transition is smooth as well, allowing for a region where gravitational circulation, wind and horizontal diffusion are all relevant in the transport balance. Since the influence of gravitational circulation gets smaller as the distance to the sea increases, the magnitude of the horizontal velocity decreases to the minimum magnitude determined by wind and river discharge driven circulation.

The second wind speed is the large offshore wind speed of 18 m/s. The results for this wind speed are found in figure 3.5 and show resemblance to the previous case. Again, the first panel, displaying a heat map of the vertical variation in salinity s', shows that the entire estuary is stably stratified. In contrast to the top left panel of figure 3.4, the magnitude of the stratification does not visibly decrease. This is caused by the fact that the salinity gradient does not significantly change in the visualized section of the estuary. The velocity profile in the second panel is constant along the visualized length of the estuary, and shows a profile similar to that in the top right panel of figure 3.4.

The bottom-left panel displays the $\Sigma_x - \Sigma$ characteristic. Compared to the case for a wind speed of 3 m/s, a smaller portion of the characteristic is covered by the solution, since only large salinities are present in the computed domain. The fourth panel, displaying the various transport contributions, shows that the wind-wind contribution dominates the entire estuary. Whereas for a wind speed of 3 m/s, wind and gravitational

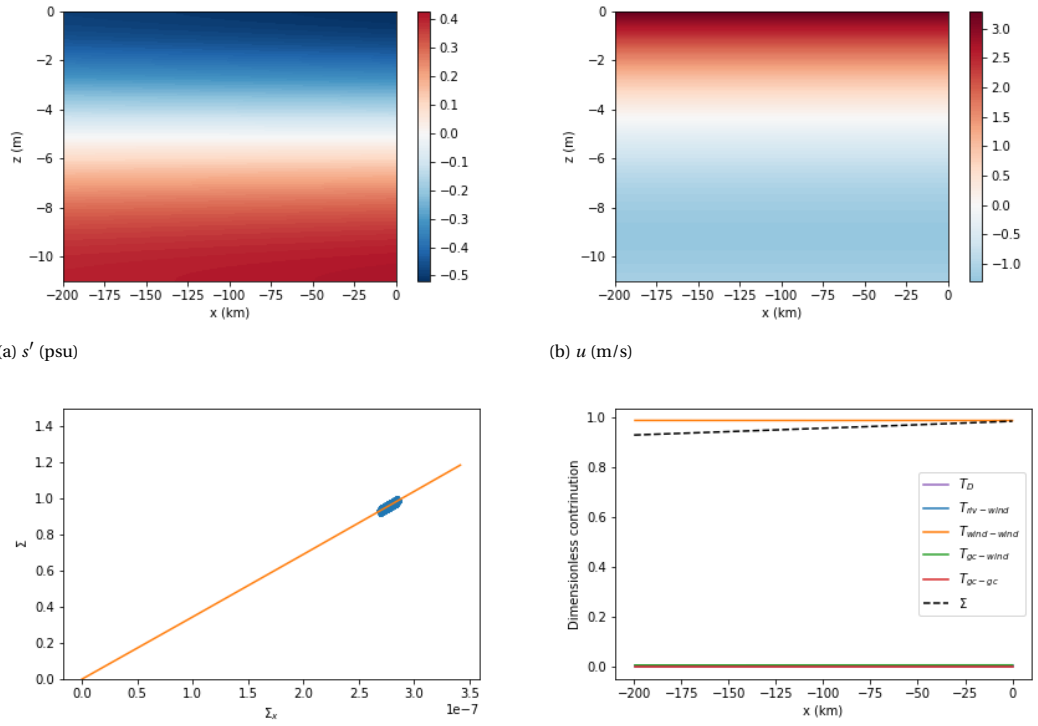

(a) s' (psu)

(b) u (m/s)

(c) $\Sigma_x - \Sigma$ characteristic

(d) Contributions by length scale.

Figure 3.5: Overview of the solution for $u = 18$ m/s. The figure for the $\Sigma_x - \Sigma$ characteristic features the analytical characteristic as a solid orange line, as well as a blue plot of the realized characteristic. The fourth plot displays the transport contribution as defined in equation 2.81 along the length of the estuary.

circulation both have significant contributions near the ocean, the contribution from gravitational circulation is negligible for wind speeds as large as 18 m/s.

We bring our attention back to the observations made about figure 3.3b. Here it was seen that stratification is decreased by offshore wind speeds. This is in contrast to the results from Chen and Sanford and Lange and Burchard, which conclude the exact opposite relation [19, 20].

In the problem studied by Lange and Burchard, the horizontal salinity gradient was considered an independent variable. If this assumption is applied to the EMM, the model agrees with the findings from Lange and Burchard. The contribution from offshore wind to the salinity profile in equation 2.67 is stably stratified. Hence, offshore wind speeds enhance the stratification brought about by gravitational circulation.

In the model by Chen and Sanford, the salinity gradient is not an input parameter, but is determined by the system, as is also the case for the models studied in this thesis. It is hypothesized that the mixing induced by tidal variations in the model by Chen and Sanford is significantly stronger than the mixing in the case studied in figure 3.3. In cases of large horizontal mixing, for example due to strong tides, the leading horizontal transport balance is between the average river flow and horizontal diffusion. Since contributions from wind stress are not part of the dominant balance, changes in the wind speed do not significantly alter the horizontal salinity gradient. The horizontal salinity gradient can therefore be considered fixed with respect to the wind speed. As a result, if figure 3.3 is reproduced using a larger horizontal diffusivity, the relation between wind and stratification is similar to that found by Chen and Sanford.

The effect of offshore wind speed on stratification is a competition between a reduction in salinity gradient, and an increase in stratification for a given salinity gradient. Which of these effects is stronger, depends on the concerned parameter regime. As a result, offshore wind can both increase or reduce the salinity stratification, depending on the parameters used. This advocates for a careful study of the relevant parameter regime before conclusions are copied from literature, since conclusions about the effect of wind stress on stratification can be polar opposites when considered for different parameter regimes.

3.3. Small onshore wind speeds

This section will cover the results for the EMM for small onshore wind speeds, denoted by negative wind speeds. Figure 3.6 gives an overview of the salinity structure for four small wind speeds. For this range of

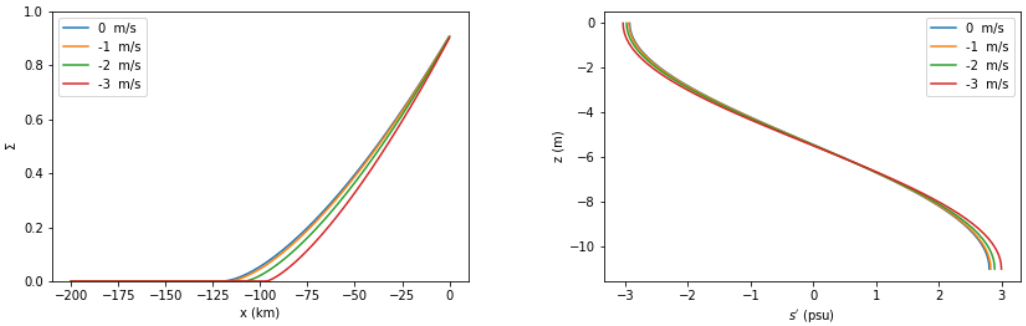

(a) Vertically averaged salinity

(b) Boundary stratification

Figure 3.6: Salinity structure for a range of small wind speeds. The first panel displays the vertically averaged salinity along first 200 km of the estuary. The second panel displays the vertical variation in salinity at the ocean.

wind speeds, one solution is found. This solution is on the same solution branch as the solution found for offshore wind speeds. The first panel displays the average salinity along the length of the channel for four small wind speeds. Looking at the first panel, we notice two things. First, onshore wind decreases the salt penetration length. This is in line with the results from section 3.2, where it was shown that offshore winds increase salt penetration.

Secondly, for offshore wind, we saw that the salinity decreases smoothly as x decreases. On the contrary, in case of onshore wind, a sharp kink is visible in the salinity profile. For a wind speed of -3 m/s, this kink occurs between $x = -95$ km and $x = -90$ km, when the vertically averaged salinity is near zero. The reason onshore winds feature such sudden changes in gradient will be explained further in this section.

Figure 3.6b displays the salinity shear s' relative to the mean salinity $\bar{s}$ at $x = 0$. It can be seen that negative wind speeds tend to increase the stratification. Equation 2.67 for s' shows that s' scales with the salinity gradient. The increased stratification is therefore directly related to the steeper horizontal salinity profile. Similar to the case of offshore wind speeds, the conclusion that onshore wind speeds promote stratification is the opposite of the conclusion that is obtained in various pieces of academic literature [19, 20]. The reader is referred to the end of section 3.2 for a detailed explanation of how this difference arises.

An overview of the solution for a wind speed of -3 m/s is given in figure 3.7. The heat map for s' on the top-left shows stable stratification for ($x > -90$ km). For ($x < -90$ km), no visible stratification is visible, but close inspection reveals that the stratification in this region is unstable. The location of this transition between stable and small unstable stratification transition is the same as that of the transition in the salinity gradient in figure 3.6a. This is explained by the fact that the stratification is directly linked to the salinity gradient by equation 2.67.

The horizontal velocity in figure 3.7b is significantly different from the horizontal velocity for a wind speed of 3 m/s, as displayed in figure 3.4b. Rather than the usual anti-clockwise motion for the entire domain, where water moves from the ocean at the bottom and towards the ocean at the top, the circulation suddenly switches to clockwise circulation for the part of the estuary further than 90 km from the right-hand boundary. In order to explain this, the bottom panels are studied first.

We will quickly look at figure 3.7d, before studying figure 3.7c. Here it can be noted that the contribution from gravity-wind interaction is negative, caused by the fact that the wind speed is negative. This contribution becoming negative causes the $\Sigma_x - \Sigma$ characteristic in figure 3.7c to flatten, as can be seen in the bottom left panel, where the section of the curve near $\Sigma = 0$ is decidedly flatter than the curve for small offshore wind. As a result, large salinity gradients can be maintained for low salinities. When the flat part of the curve is reached, small changes in the salinity lead to large changes in the salinity gradient. This explains the sharp transition between large and small salinity gradients discussed seen in figure 3.6a.

Since the gradient rapidly changes from large to small values around $x = -90$ km and all transport contributions depend on the salinity gradient Σ_x, the contributions plotted in the fourth panel suddenly change as well. At distances smaller than 90 km from the right boundary, we see a balance between gravity-gravity,

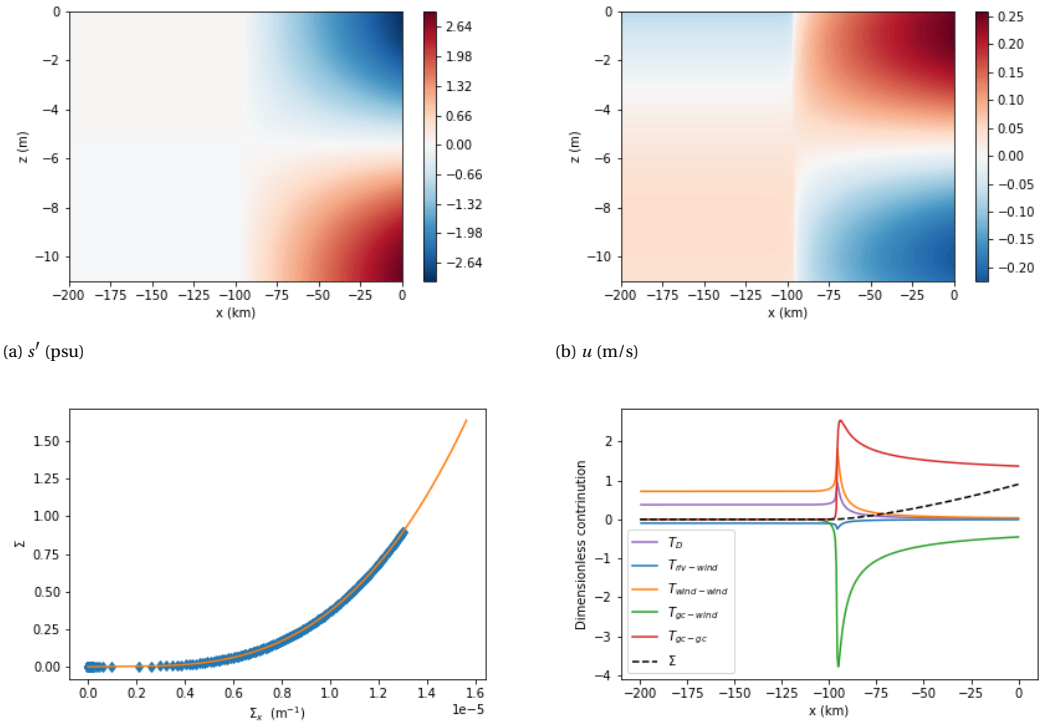

(a) s' (psu)

(b) u (m/s)

(c) $\Sigma_x - \Sigma$ characteristic

(d) Contributions by length scale.

Figure 3.7: Overview of the solution for $u = -3$ m/s. The figure for the $\Sigma_x - \Sigma$ characteristic features the analytical characteristic as a solid orange line, as well as a blue plot of the realized characteristic. The fourth plot displays the transport contribution as defined in equation 2.81 along the length of the estuary.

gravity-wind interaction and average river flow. Horizontal salinity gradients are large, and so gravitational circulation is large in this part of the estuary. For distances further from the right boundary, a balance is seen between wind-wind interaction, river-wind interaction, horizontal diffusion and the average river flow. Gravitational circulation is negligible, since the horizontal salinity gradients are small.

Looking back at the top right figure for the horizontal velocity, we note that the circulation changes direction at the point where the transport balance rapidly changes. For points less than 90 km from the right boundary, gravitational circulation is significant, which induce clockwise circulation. For points further from the right boundary, gravitational circulation is negligible and so wind is dominant in determining the vertical salinity and velocity profiles. Onshore wind promotes counterclockwise motion, and so this type of circulation is present in all points left of 90 km. The transition between these types of circulation is swift, since the flat part of the $\Sigma_x - \Sigma$ curve promotes rapid changes from large to small salinity gradients.

3.4. Medium onshore wind

For medium onshore wind speeds, multiple solutions can be found within the model. For these wind speeds, the $\Sigma_x - \Sigma$ characteristic has regions where one value of the average salinity Σ has three solutions for the horizontal gradient of the average salinity Σ_x, as illustrated in figure 2.2. There is no apparent reason to choose any Σ_x over the other two. As a result, infinitely many solutions are possible. In this section two extreme solutions will be displayed. One solution is obtained by choosing the smallest possible gradient at each point in the estuary. This solution is referred to as the maximum salinity solution, as it has the highest salinity at each point in the estuary of all possible solutions. This solution is plotted using a solid line for the remainder of this report. The minimum salinity solution, on the other hand, chooses the largest possible salinity gradient, resulting in the lowest salinity of all possible solutions at any point in the estuary. This solution is plotted using a dashed line. The reader is reminded that there are infinitely many solutions, which are all positioned in between the maximum and minimum salinity solution. The first panel displays the average salinity along the estuary and the second panel displays the relative stratification $s'/\bar{s}$ at $x = 0$.

An overview of the solutions for different medium onshore wind speeds is depicted in figure 3.8. In figure

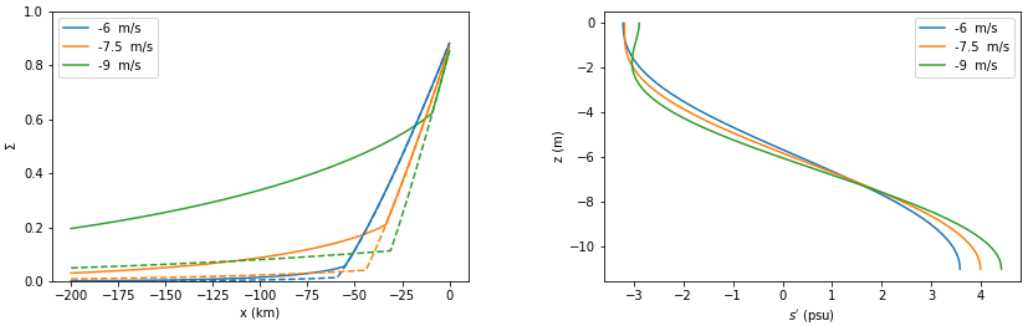

(a) Vertically averaged salinity

(b) Boundary stratification

Figure 3.8: Salinity structure for a range of medium onshore wind speeds. The first panel displays the vertically averaged salinity along first 200 km of the estuary. The second panel displays the vertical variation in salinity at the ocean. The maximum and minimum salinity solutions are depicted by a solid and dashed line, respectively

3.8a, we see that each solution features two sections of the domain with distinctly different gradients. The maximum and minimum salinity solution overlap near the right boundary. The difference between the two solutions is the point at which they switch from a large to a small gradient. This switch can be made at any point in between these two extremes. Theoretically, a solution could switch between the gradients an arbitrary number of times as long as the salinity is in the range that allows these changes. Alike figure 3.6a, salinity gradients near the mouth become larger for negative wind speeds.

The second panel shows that the stratification at $x = 0$ for the minimum and maximum solution are equal, since the dashed and solid lines overlap. This is caused by the fact that the salinity gradient is equal at the boundary for the two different solutions, and that stratification is determined by the salinity gradient. The stratification at the boundary is predominantly stable, with a small section of unstable stratification near the surface for a wind speed of -9 m/s ($z > -2$ m). The onshore wind causes saline water to flow towards the estuary at the surface, thus increasing the salinity near the surface. For a wind speed of -9 m/s, this results in an unstable stratification near the surface of the estuary. Moreover, we see that stratification increases as the onshore wind speed increases. This in line with the observation made in section 3.3, that onshore wind speeds promote large salinity gradients and therefore increase stratification.

Two solutions will be studied in further detail: the maximum and minimum salinity solutions for a wind speed of -9 m/s, the largest wind speed in figure 3.6. The maximum salinity solution is depicted in figure 3.9. Looking at the vertical variation of salinity s' in the top-left plot, the domain can be divided into two sections according to the salinity profile. Predominantly stable stratification is found near the ocean ($x > -10$ km), while the estuary is unstably stratified further away from the ocean ($x < -10$ km). The top-to-bottom stratification at $x = -200$ km is 0.026 psu. This same division is also present in figure 3.9b. Near the ocean ($x > -10$ km), velocity is positive between $z = -6$ m and $z = -1$ m of the estuary, while the velocity is negative below $z = -6$ m and above $z = -1$ m, resulting in mostly clockwise circulation. For points further than 10 km away from the ocean, the velocity is negative at the surface and positive near the bottom. This bears resemblance to the case of the small onshore wind speed displayed in figure 3.7, where different velocity profiles were visible at different locations in the estuary.

The transition between the two salinity profiles takes place at the same point along the estuary as the transition between the two velocity profiles. Moreover, this is the same point as where average salinity gradient (solid red line) switched from a large to a small gradient in figure 3.8a. A similar transition was found for the case of the small onshore wind speed of -3 m/s in figure 3.7. For a wind speed of -3 m/s, this transition was swift yet continuous, whereas the transition for the solution discussed in this section is discontinuous. This discontinuous transition can be explained by studying the $\Sigma_x - \Sigma$ characteristic.

Figure 3.9c shows the $\Sigma_x - \Sigma$ characteristic for this solution. The analytical curve differs significantly from the curves seen for the previous cases, seen in figures 3.4c, 3.5c and 3.7c. The curve has two local extrema and so resembles that of figure 2.2. The high salinity solution is obtained by choosing the smallest gradient possible and so the switch between the right and left branch is made at the highest possible salinity. The switch is indicated by a cyan arrow. This switch in the characteristic explains the abrupt switch between the large and small salinity gradient in figure 3.8a around x =-10 km. The point where the switch between the branches is made coincides with the point where the salinity and velocity profiles change.

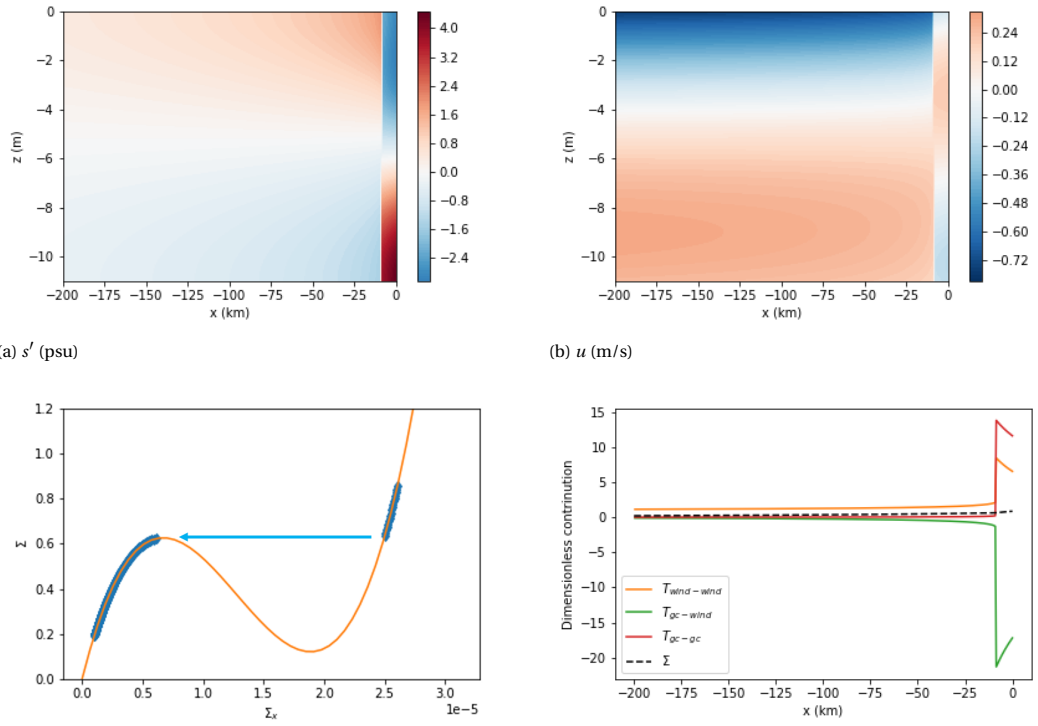

(a) s' (psu)

(b) u (m/s)

(c) $\Sigma_x - \Sigma$ characteristic

(d) Contributions by length scale.

Figure 3.9: Overview of the maximum solution for $u = -9$ m/s. The figure for the $\Sigma_x - \Sigma$ characteristic features the analytical characteristic as a solid orange line, as well as a blue plot of the realized characteristic. The fourth plot displays the transport contribution as defined in equation 2.81 along the length of the estuary.

A change in behaviour around -10 km can also be found in the contributions of the different length scales shown in figure 3.9d. In the seaward regime ($x > -10$ km), the contributions from wind-wind and gravity-gravity interaction are positive while gravity-wind interaction has a negative contribution. Gravitational circulation and wind on themselves bring about transport in the negative direction, whereas the interaction between the two causes transport in the positive direction. This is caused by the fact that both mechanisms induce similar velocity and salinity profiles, but with a different sign. The sign cancels in case of gravity-gravity or wind-wind interaction, but is retained for gravity-wind interaction. All three contributions are significantly larger than 1. The average river contribution is therefore negligible. Thus, this regime features a balance between gravitational circulation and wind.

In the landward regime ($x < -10$ km), however, wind-wind interaction is the only significant contribution to counter the transport from the average river flow. The transport balance is therefore between the average river flow and wind-wind interaction. Moreover, the vertical salinity and velocity profile are determined solely by wind. Since the horizontal salinity gradient is small, gravitational circulation is negligible. A sharp interface can be found between these two regimes, which like the sharp interfaces for s' and u', is caused by the discontinuity in Σ_x at $x = -10$ km. To the left of this discontinuity, gradients are small, thus causing gravitational circulation to be small as well. To the right, the gradients are larger, and so gravitational circulation is relevant.

The vertical profiles observed in 3.9a and 3.9b can be explained using these observations. For points far from the ocean ($x < -$ 10 km), wind dominates the vertical profiles, resulting in unstable stratification and counterclockwise circulation. For smaller distances to the ocean ($x >$ 10 km), a mixture of gravitational circulation and wind determines the profiles. This results in stable stratification, and circulation that is counterclockwise for a small layer near the surface and clockwise for the rest of the domain.

Figure 3.10 shows the minimum salinity solution. The two top panels show that the same regimes that have been identified for the maximum salinity solution are present for this solution as well. The transition between them occurs further from the ocean ($x \approx$-28 km). Moreover, s' is near zero in the landward regime ($x <$ -28 km). A close look at the data reveals that in this regime stratification is unstable, albeit with a small

magnitude. The top-to-bottom stratification at $x = -200$ km is $6.6 \cdot 10^{-3}$ psu, compared to 0.026 psu for the maximum salinity solution.

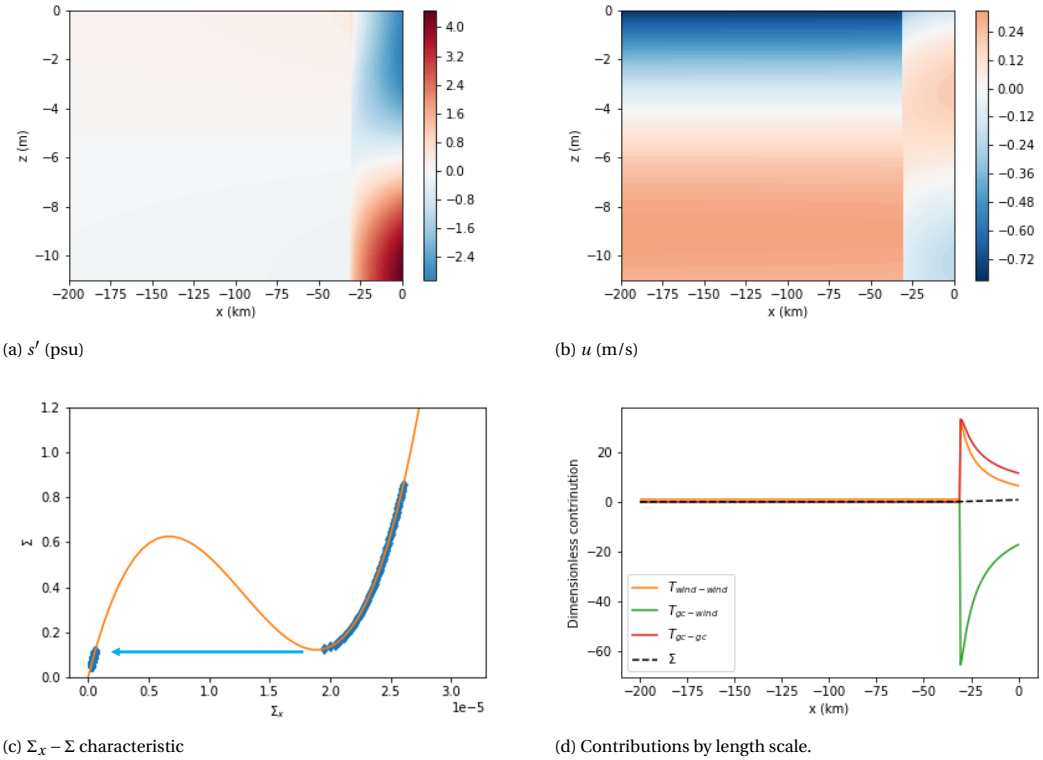

(a) s' (psu)

(b) u (m/s)

(c) $\Sigma_x - \Sigma$ characteristic

(d) Contributions by length scale.

Figure 3.10: Overview of the minimum solution for $u = -9$ m/s. The figure for the $\Sigma_x - \Sigma$ characteristic features the analytical characteristic as a solid orange line, as well as a blue plot of the realized characteristic. The fourth plot displays the transport contribution as defined in equation 2.81 along the length of the estuary.

The $\Sigma_x - \Sigma$ characteristic in figure 3.10c confirms that the minimum salinity solution switches between the left and right branch at the lowest possible salinity. This causes the solution to remain on the right branch for a larger part of the domain, thus ensuring that the transition between the regimes occurs further from the ocean than for the maximum salinity solution.

The plot of the contribution of length scales on the bottom-right confirms that the only major difference between this solution and the maximum salinity solution is the position where the switch between the different regimes happens. For $x > -28$ km, the previously seen balance between gravity-gravity, wind-wind and gravity-wind terms is found. Close inspection reveals that for $x < -28$ km the wind-wind length scale dominates the other length scales and is the only term to balance the average river flow. It can furthermore be noted that the wind-wind contribution and wind-gravity contributions become larger relative to $L_{\text{gc-gc}}$ as one moves closer to the point where the regimes switch. This is due to the fact that the salinity gradient gradually decreases, which limits the effect of gravitational circulation. The wind-wind contribution almost equals the gravity-gravity contribution at the point where the switch is made. This indicates that the switch has to be made, because gravitational circulation becomes too weak relative to the wind speed, in order to maintain clockwise circulation and stable stratification.

It has become clear that the branches of the $\Sigma_x - \Sigma$ characteristic reflect different physical regimes. The right branch is a regime where wind and gravitational circulation both have significant contributions that partially counter each other, but where gravitational circulation has a slightly stronger contribution than wind stress. The left branch corresponds to a regime where wind dominates vertical profiles of salinity and velocity and where wind is balanced by averaged river flow in horizontal transport. For medium onshore winds these branches are separated, and so the transition between the two regimes is non-continuous. In figure 3.7, we saw the same two regimes for small wind speed, with the main difference that the transition was continuous as opposed to discontinuous. The transition was still relatively swift. In this case, the wind speed was such that the two branches were not separated by a decreasing section (the middle branch) but by a region of

near-zero increase.

3.5. Large onshore wind

This section will look at large onshore winds, which are wind speeds between -10 and -12 m/s. Figure 3.11 depicts a number of solutions for large wind speeds. The first panel, displaying the average salinity, shows

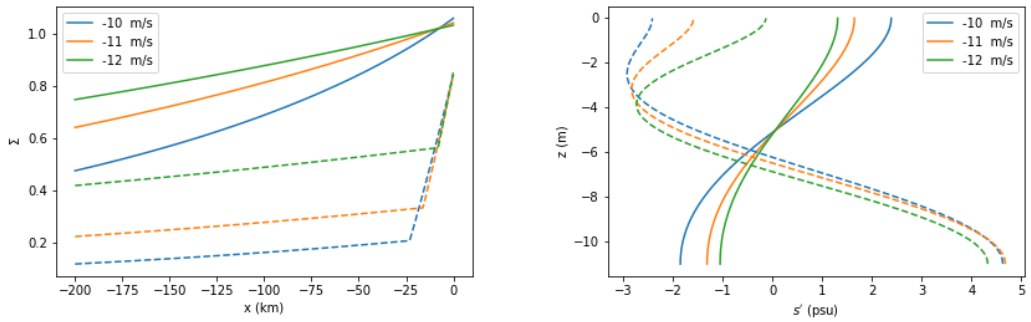

(a) Vertically averaged salinity

(b) Boundary stratification

Figure 3.11: Salinity structure for a range of large onshore wind speeds. The first panel displays the vertically averaged salinity along first 200 km of the estuary. The second panel displays the vertical variation in salinity at the ocean. The maximum and minimum salinity solutions are depicted by a solid and dashed line, respectively

that also for these wind speeds, multiple solutions exist. The solutions for the medium wind speeds from the previous section overlapped near the ocean, whereas the maximum and minimum salinity solutions for these wind speeds are entirely distinct. Each wind speed has an infinite number of solutions that resemble the solutions from the previous section, with a discontinuous salinity gradient at some point in the interior and stable stratification at the boundary. Every wind speed depicted in figure 3.11 also has an infinite amount of solutions with unstable stratification at the boundary. The minimum salinity solution and the maximum salinity solution have been depicted in this figure.

Figure 3.11b shows that the maximum salinity solution has low salinity gradients throughout the estuary, indicated by solid lines, are unstably stratified at the boundary. This suggests that for large wind speeds, solutions are possible that are in the wind dominated regime at the boundary, which is characterised by small salinity gradients and unstable stratification. For these solutions, the unstable stratification is smaller in magnitude for larger wind speeds. This is in line with the fact that the gradients are smaller for larger wind speeds, since equation 2.67 shows that stratification scales with the horizontal gradient of the average salinity. For the dashed solutions, we predominantly see stable stratification, with a section of unstable stratification near the surface. This effect was observed to a more limited extent in figure 3.8b. The reader is referred to the description of that figure for an explanation of this profile.

The maximum salinity solution will be studied in further detail. The minimum salinity solution is analogous to the minimum salinity solutions for medium wind speeds, and the reader is referred to section 3.4 for details of these solutions. The maximum salinity solution for a wind speed of -11 m/s is displayed in figure 3.12.

The top-left figure shows the vertical variation in salinity. It is clear that the estuary is unstably stratified over its whole length. The degree of stratification reduces as x decreases, though it remains of the same order of magnitude throughout the visualized domain. This is caused by the fact that the average salinity, and as a consequence its gradient, never approach zero within the visualized part of the estuary, as seen in figure 3.11.

The velocity profile in the second panel shows counterclockwise motion over the entire visualized estuary. No visual changes in the velocity profile are observed. This velocity profile is typical of the regime that was obtained far from the ocean in the previous figures on onshore wind.

The $\Sigma_x - \Sigma$ characteristic in figure 3.12c shows that the solution is located entirely on the left branch. For lower wind speeds, this branch was not feasible for the average salinities typically found at the boundary. Because the wind speed is larger, the maximum salinity of the left branch is raised beyond $\Sigma = 1$, such that the left branch can be used at the ocean. In addition, it can be seen that the right branch in this case is feasible for the salinities typically found at the boundary. This is in agreement with the fact that this wind speed also featured solutions with stable stratification at the boundary.

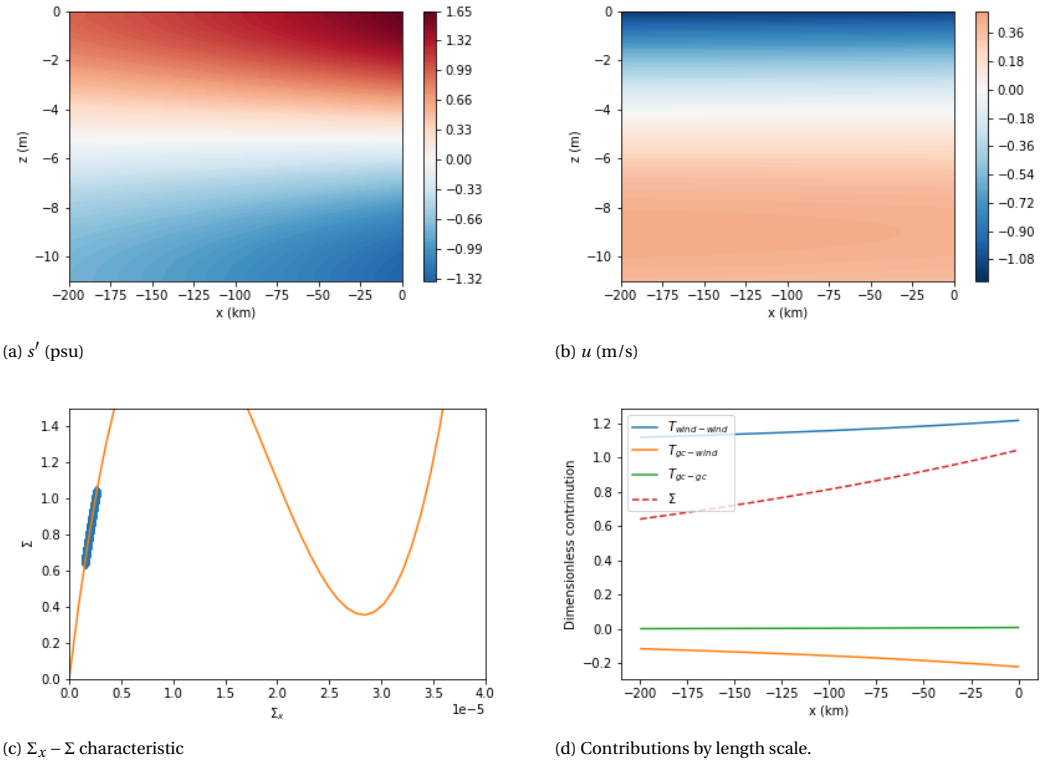

(a) s' (psu)

(b) u (m/s)

(c) $\Sigma_x - \Sigma$ characteristic

(d) Contributions by length scale.

Figure 3.12: Overview of the maximum solution for $u = -11$ m/s. The figure for the $\Sigma_x - \Sigma$ characteristic features the analytical characteristic as a solid orange line, as well as a blue plot of the realized characteristic. The fourth plot displays the transport contribution as defined in equation 2.81 along the length of the estuary.

The fourth panel shows that the major balance is formed between wind-wind interaction and average river flow, with a small negative gravity-wind contribution. Thus, wind fully determines the salinity and velocity profiles.

We can conclude that for large onshore winds, solutions are possible where the estuary comes in a state where fast counterclockwise circulation ensures that the estuary is well-mixed, both vertically and horizontally. Fresh water flows along the bottom of the estuary to the ocean, whereas salt water is carried by the wind from the ocean towards the estuary. Although gravitational circulation forces the estuary towards the opposite type of circulation, this effect is small compared to the fast circulation in the estuary. The entire estuary is in the regime that was found at points far from the ocean for medium wind speeds, characterized by the left branch of the $\Sigma_x - \Sigma$ characteristic.

3.6. Very large onshore wind

The final set of wind speeds discussed in this chapter is the set of the very large wind speeds. An overview of the salinity structure for these wind speeds is found in figure 3.13.

The first panel shows that for these wind speeds, only one solution is found. This solution is characterized by a small salinity gradient, which decreases as the onshore wind speed increases. Looking at the stratification at the boundary in figure 3.13, we see that all solutions are unstably stratified at the boundary. Again, the degree of stratification is small for larger onshore wind speeds, since the salinity gradients are smaller for these wind speeds.

The solution that is found for this range of wind speeds is the same type of solution as the maximum salinity solution for the range of large onshore wind speeds, discussed in the previous section. The reader is referred to that section for details of this solution.

Solutions with stable stratification at the oceanic boundary, such as the minimum salinity solution that was featured for large onshore winds, are not feasible for this range of wind speeds, since the minimum value of Σ for the right branch of the $\Sigma_x - \Sigma$ characteristic is larger than 1. As a consequence, only the left branch is feasible for these wind speeds, and so only solutions with stable stratification throughout the estuary are

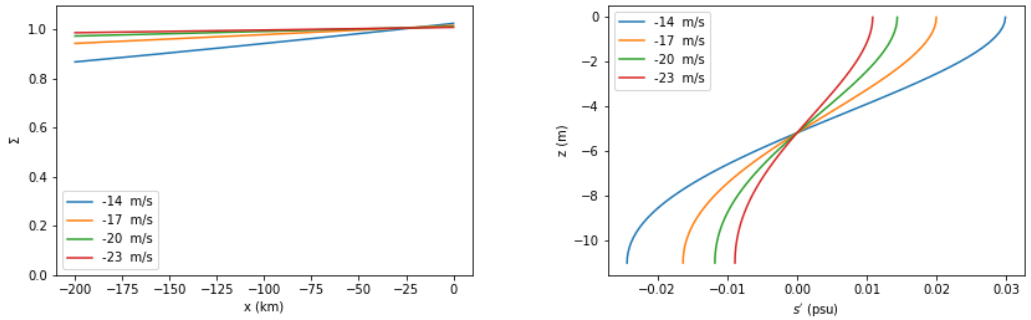

(a) Vertically averaged salinity

(b) Boundary stratification

Figure 3.13: Salinity structure for a range of large onshore wind speeds. The first panel displays the vertically averaged salinity along first 200 km of the estuary. The second panel displays the vertical variation in salinity at the ocean.

possible.

3.7. Effect of Vertical Eddy Viscosity

This section will give an overview of the consequences of increased vertical mixing. First, an overview of the salinity structure for different viscosities will be given. Subsequently, an analysis will be made of stratification for large viscosities.

An overview of the solutions for the large onshore wind speed of -12 m/s is given for different viscosities in figure 3.14. From the first panel for the average salinity, it can be seen that an increase in viscosity decreases

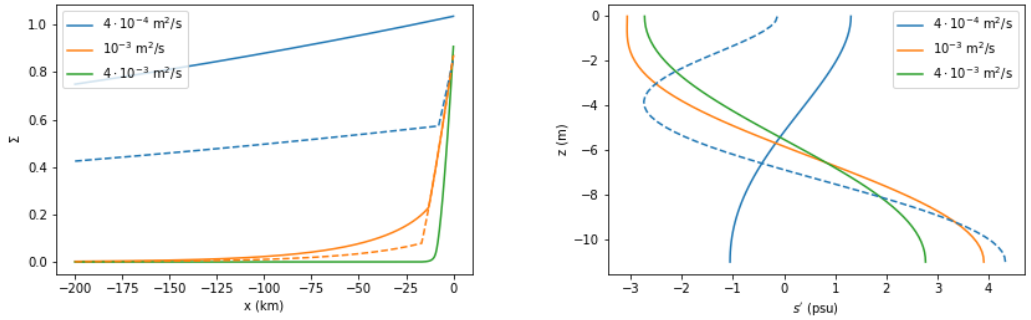

(a) Vertically averaged salinity

(b) Boundary stratification

Figure 3.14: Salinity structure for a range of small wind speeds. The first panel displays the vertically averaged salinity along first 200 km of the estuary. The second panel displays the vertical variation in salinity at the ocean.

salt penetration. Moreover, analogues of different wind speed regimes are retrieved. For a viscosity of $4 \cdot 10^{-4}$ m^2/s, 12 m/s acts as a large wind speed, as was already seen in figure 3.11. For a viscosity of $1 \cdot 10^{-3}$ m^2/s, 12 m/s acts as a medium wind speed, since it has multiple solutions which all have a discontinuity in the gradient. Finally, 12 m/s becomes a low wind speed for a viscosity of $4 \cdot 10^{-3}$ m^2/s. For this viscosity, no discontinuities in the gradient are present, since the $\Sigma_x - \Sigma$ characteristic does not have local extrema. The second panel for the stratification at the boundary confirms this classification. The solutions with large gradients at the boundary are stably stratified, while the maximum salinity solution for a viscosity of $4 \cdot 10^{-4}$ m^2/s is unstably stratified.

The fact that increasing the viscosity can cause the wind speed to behave like a lower wind speed is the result of the fact that the definition of the wind speed ranges, as defined in section 3.1.3, depends on the wind speed through $u_w/\bar{u}$. This dimensionless number scales as the ratio between the wind speed and the viscosity, if all other parameters are considered fixed

Since all solutions just presented resemble a solution from one of the previous sections, these solutions will not be studied in further detail. Conclusions that are made for a solution are generally valid for analogue

solutions with different viscosities.

One thing that does change for large viscosities is the stratification in cases of low salinity gradients for onshore wind speeds. For the effective vertical viscosity used in the previous section, stratification becomes unstable if the salinity gradient becomes sufficiently small. This implies that parts of the estuary far from the sea are unstably stratified. For large viscosities, however, this changes.

Equation 2.67 can be used to obtain an expression for the vertical derivative of the vertical deviation of salinity:

$$s'_z(\sigma) = \bar{u}s'_{\bar{u},z}(\sigma) + u_E s'_{u_E,z}(\sigma) + u_w s'_{u_w,z}(\sigma). \tag{3.1}$$

All of the s' contributions $s'_{\bar{u}}$, s'_{u_E} and s'_{u_w} are stably stratified, such that all their vertical derivatives are negative. Characteristic speeds $\bar{u}$ and u_E are always positive, while u_w is negative for negative wind speeds. In the case of negative wind speeds, the stratification is the result of a competition between wind, which causes unstable stratification, and gravitational circulation and river flow, which cause stable stratification. The estuary is thus unstably stratified if the magnitude of u_w is large enough compared to $\bar{u}$ and u_E.

In the regime of small salinity gradients, u_E is negligible, since it scales with Σ_x. We thus expect stable stratification if u_w is sufficiently smaller than $\bar{u}$, and unstable stratification if u_w is sufficiently large. Characteristic speed u_w is inversely proportional to A_v, while $\bar{u}$ is not dependent on the viscosity parameter. Increasing A_v will thus reduce the magnitude of u_w relative to $\bar{u}$. Stable stratification is therefore obtained if A_v is sufficiently large. We thus expect the stratification in the low salinity gradient regime to switch from unstable to stable as A_v passes the point where u_w and $\bar{u}$ are similar in magnitude.

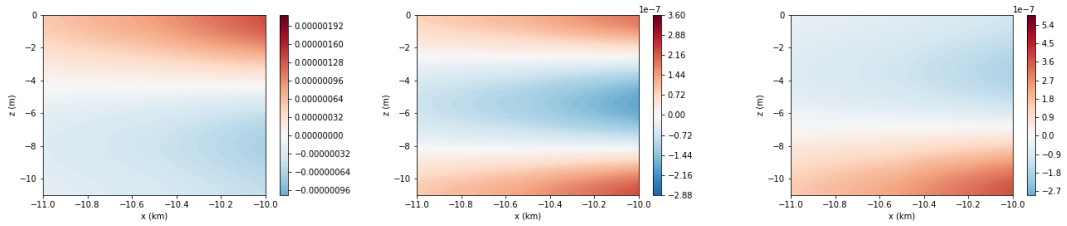

(a) s' (psu) for $A_v = 6 \cdot 10^{-2}$ m^2/s (b) s' (psu) for $A_v = 9 \cdot 10^{-2}$ m^2/s (c) s' (psu) for $A_v = 1.2 \cdot 10^{-1}$ m^2/s

Figure 3.15: Vertical deviation of salinity in the low salinity gradient regime, for a range of high viscosities

Figure 3.15 displays the vertical salinity profile for a small part of the estuary for a range of large viscosities. For the first panel, the estuary is unstably stratified, as was the case for the viscosity of $4 \cdot 10^{-4}$ m^2/s in section 3.5. For a slightly higher viscosity, presented in the second panel, salinity is higher than the vertical average at the surface and at the bottom of the estuary, whereas for an even higher viscosity, displayed in the third panel, the estuary is stably stratified. The viscosity for which $u_w = \bar{u}$ is $A_v = 1.3 \cdot 10^{-1}$ m^2/s. The point where the stratification changes to stable stratification is close to this point, which confirms the theoretical derivation.

3.8. Model Reflection

This section will reflect on the model used to obtain the results in this chapter. This section will also mention some predictions done by the model of which it is questioned whether they hold in physical cases.

The boundary condition at $x = 0$ in this model prescribes the salinity at the bottom of the estuary at $x = 0$ to be equal to the oceanic salinity. Since a number of solutions have unstable stratification at the oceanic boundary, the average salinity becomes larger than the oceanic salinity at the point where the estuary meets the ocean. This is not a physically reasonable result. The imposed boundary condition is only valid if it is assumed that the estuary is stably stratified at the boundary, which is not the case for a number of solutions for large or very large onshore wind speeds. A physically reasonable boundary condition would be to assume that the maximum salinity is equal to the oceanic salinity. This boundary condition is not expected to change the results qualitatively. The same solutions will still be valid, although the sets of wind speeds for which the different solutions are valid will change slightly, as the salinity at the boundary will be lower for an altered boundary condition in case of (partially) unstable stratification.

In deriving the EMM from the sub-tidal model, it is assumed that s'_x is negligible compared to $\bar{s}_x$. Looking at figures 3.9 and 3.10, we see that s' is not continuous and so s'_x is infinitely large at the interface. The assumption is therefore violated. Moreover, the EMM neglects the advection of momentum. Since the horizontal derivative of velocity is infinitely large at the interface, this transport mechanism is negligible either.

Due to momentum advection, salinity advection and horizontal diffusion of salinity, sharp interfaces as found in figures 3.9 and 3.10 will not occur in physical situations. Either, solutions similar to those in figures 3.9 and 3.10 are featured, with the presence of an interior layer in between the two regimes, or the solutions are not feasible at all. Chapter 4 will check which of the two outcomes is correct, by solving a similar model that does not make the assumption of neglecting momentum advection and the term s'_x.

For any onshore wind speed, the results presented have unstable stratification at points far from the ocean. As pointed out in the introduction, such stratification is not found in nature. Results containing unstable stratification are therefore expected not to be true for physical cases.

In the derivation of the sub-tidal model, it was shown that the viscous and diffusive coefficients that feature in the model discussed in this chapter are the combination of molecular viscosity/diffusivity, mixing along the width of the channel, turbulent mixing and tidal mixing. While molecular viscosity and diffusivity are constants, the other mixing terms depend on the dynamics of the water in the channel. Wind is known to increase turbulent mixing [19, 33]. Not modelling this wind dependency in the effective viscosity is a disadvantage of this model.

Section 3.7 shows that increased effective viscosity eliminates unstable stratification. Since unstable stratification is highly uncommon in nature, it is hypothesized that in true situations, effective viscosity and mixing could become large enough to eliminate unstable stratification.

3.9. Conclusion

The conclusion to this chapter will start by giving an overview of the solutions for the different wind speeds. Table 3.2 lists, for different sets of wind speeds: the relevant range of wind speeds, the type of salinity stratification typically found per solution, the dominant transport terms per solution, the number of solutions and a sketch of the $\Sigma_x - \Sigma$ characteristic.

While studying the results of the EMM, six major conclusions can be drawn. Firstly, the $\Sigma_x - \Sigma$ characteristic is a valuable tool in analyzing solutions. The different branches can be interpreted as different regimes and the feasibility of certain regimes can be read from the characteristic. Moreover, the length over which transitions between regimes occur is prescribed by this characteristic. The effect of changing parameters can be understood by studying the effects these parameters have on the curve. The next chapter will show whether the $\Sigma_x - \Sigma$ can also be used to analyse results from the extended MacCready model. In light of the third research question formulated in section 1.5, it can be said that the solutions to the EMM are best analysed using the $\Sigma_x - \Sigma$ characteristic.

Secondly, multiple equilibrium solutions are possible for onshore winds. This is because values of Σ arise for which equation 2.72 has multiple solutions. What is more striking is that there is not a finite number of solutions, but an uncountably infinite number of solutions. The problem is not necessarily unique to wind related extensions, as other extensions of MacCready's model could see situations where the characteristic curve has sections with multiple solution. The upcoming chapter will research which of these infinitely many solutions are expected to hold in a less restrictive model.

Third, large or very large onshore and equally large offshore winds produce similar penetration lengths. In these cases, the vertical salinity and velocity profiles are fully determined by wind. The estuary sees rapid circulation of water, and so the estuary becomes both vertically and horizontally well mixed. The only difference between the two cases, is that the circulation is clockwise for offshore wind, and counterclockwise for onshore wind. Since saline water flows towards the estuary at the surface in case of onshore winds, the salinity is highest near the surface and the estuary is stably stratified for these winds. For offshore winds, saline water flows towards the estuary at the bottom of the estuary and so the salinity is highest near the bottom and the estuary is stably stratified. Wind and gravitational circulation work in concert for offshore winds, while they compete in case of onshore winds. For wind speeds large enough, the entire contribution from gravitational circulation is however negligible.

Fourth, discontinuous transitions between regimes are possible in MacCready's framework. This phenomenon is also the consequence of the fact that equation 2.72 has multiple solution branches. Consequences of these discontinuous transitions are discontinuities in the average salinity gradient as well as discontinuous local salinity and horizontal velocity. The next chapter will study whether such transitions, albeit in a continuous way, are possible in the extended Dijkstra model.

Moreover, in the parameter regime studied, stratification is decreased by offshore wind speeds, and increased by small or medium onshore wind speeds. This is in contrast to the results from Chen and Sanford and Lange and Burchard, which concluded the exact opposite [19, 20]. For Lange and Burchard this is caused

Wind speed	Wind speed (m/s)	Stratification	Transport	# of solutions	$\Sigma_x - \Sigma$ characteristic
Large Offshore	$u_a > 10$	Stable throughout	$L_{\text{wind-wind}}$	1	
Small Offshore	$0 < u_a < 10$	Stable throughout	Near sea: $L_{\text{gc-gc}}, L_{\text{gc-wind}}$ Far from sea: $L_{\text{wind-wind}}, L_D, L_{\text{riv-wind}}$	1	
Small Onshore	$-4.5 < u_a < 0$	Near sea: stable Far from sea: unstable	Near sea: $L_{\text{gc-gc}}, L_{\text{gc-wind}}$ Far from sea: $L_{\text{wind-wind}}, L_D (, L_{\text{riv-wind}})$	1	
Medium Onshore	$-9.5 < u_a < -4.5$	Near sea: stable Far from sea: unstable	Near sea: $L_{\text{gc-gc}}, L_{\text{gc-wind}}, L_{\text{wind-wind}}$ Far from sea: $L_{\text{wind-wind}} (, L_{\text{gc-wind}})$	∞	
Large Onshore	$-13 < u_a < -9.5$	Maximum salinity solution: unstable throughout Minimum salinity solution: Near sea: stable Far from sea: unstable	Maximum salinity solution: $L_{\text{wind-wind}} (, L_{\text{gc-wind}})$ Minimum salinity solution: Near sea: $L_{\text{gc-gc}}, L_{\text{gc-wind}}, L_{\text{wind-wind}}$ Far from sea: $L_{\text{wind-wind}} (, L_{\text{gc-wind}})$	"2∞"	
Very Large Onshore	$u_a < -13$	Unstable throughout	$L_{\text{wind-wind}} (, L_{\text{gc-wind}})$	1	

Table 3.2: Overview of the solutions for the different wind speeds, including the relevant range of wind speeds, the type of salinity stratification typically found per solution, the dominant transport terms per solution, the number of solutions and a sketch of the $\Sigma_x - \Sigma$ characteristic. The amount of solutions for large wind speeds is indicated as "2∞", since the model has an infinite amount of solutions with stable stratification and an infinite amount of solutions with unstable stratification at the boundary.

by the fact that Lange and Burchard make the assumption that the horizontal salinity gradient is fixed, while this is not done in the EMM. The relation obtained by Chen and Sanford can be reproduced in the EMM if a large diffusivity is used. It is unknown whether the relation found in this chapter can also be reproduced in the model of Chen and Sanford if weak tides are used in that model.

The final conclusion is that unstable stratification is possible within the framework formulated by MacCready. It is expected that this is the result of the insufficient modelling of mixing, and that in physical applications unstable stratification will not occur.

The next chapter will study the results obtained by the extended Dijkstra model, and verify whether these conclusions can also be found for the extended of Dijkstra model, or whether these results were only possible due to the assumptions made in the EMM.

4

Results for the extended Dijkstra model

In this chapter, the results for the extended Dijkstra model (EDM) will be presented. The goal of this chapter is to verify whether the conclusions for the EMM also hold for the EDM. It will be explored which of the solutions from the EMM are feasible in this model and in what way these solutions differ between the two models. Moreover, it will be tested to what extent the $\Sigma_x - \Sigma$ characteristic from the EMM can be used to analyse the results from the EDM. Finally, a bifurcation diagram encompassing the different solutions will be created. This chapter thus answers research questions 4, 5 and 6 formulated in section 1.5.

In section 4.1, a brief overview of the found solutions will be featured for four ranges of wind speeds. Across the four ranges of wind speeds, three distinct types of solutions are found. Since in this chapter an elaborate analysis is carried out for each solution type, these analyses will be presented in separate sections, rather than in section 4.1. The three solution types are described in sections 4.2-4.4. In each of these three sections, a solution is analysed and decomposed into contributions from different transport mechanisms. It is analysed to what extent the solution is similar to a solution from the EMM, and how the estuary behaves in sections of the solution that do not correspond to the EMM. This is followed by an overview of the full dynamic structure in section 4.5. The chapter will end with a conclusion in section 4.6.

Except for the horizontal diffusion coefficient, the parameters are the same as used in chapter 3 and reflect the general regime in MacCready's 2004 paper [16]. The horizontal diffusion coefficient is, however, changed from 20 to 300 m^2/s. The value of 20 m^2/s has been found to generate boundary layers that are too small to fully resolve numerically. For a horizontal diffusion coefficient of 300 m^2/s, the boundary layers become numerically resolvable. Although the solutions for the different diffusivities are quantitatively different, the solutions are qualitatively similar. Throughout this chapter, when results are compared to solution from the EMM, they are compared to solutions from that model with a horizontal diffusion coefficient of 300 m^2/s.

The fixed salinity profile prescribed at the oceanic boundary (equation 2.47) is given as

$$s_0 = s_{\text{ocn}} + \frac{s_{\text{strat}}}{2}(\cos(\pi z/H) + 1) \tag{4.1}$$

This profile has the property that the salinity at the bottom is equal to the oceanic salinity, as required. The variable s_{strat} is the value of the top-to-bottom stratification, where a positive value of s_{strat} indicates unstable stratification.

4.1. Overview per wind speed

This section will provide an overview of the found solutions for four ranges of wind speeds. The first range of the four ranges of wind speeds covered is the range of offshore wind speeds and small onshore wind speeds, as defined in section 3.1. This range of wind speeds will be covered in section 4.1.1. These two ranges of wind speeds are grouped in this analysis, since in both ranges, only one solution was found in the EMM. These solutions were similar in terms of the $\Sigma_x - \Sigma$ characteristic. Sections 4.1.2 to 4.1.4 will cover medium, large and very large wind speeds respectively. These ranges of wind speeds correspond to the ranges of wind speeds identified in the previous chapter. The solutions found will only be introduced briefly in this section. A detailed analysis of each solution is found in sections 4.2 to 4.4.

parameter	value
β	$7.6 \cdot 10^{-4}$ psu^{-1}
s_{ocn}	30 psu
s_{strat}	4.8 psu
H	11 m
B	250 m
Q	40 m^3/s
A_v	$4 \cdot 10^{-4}$ m^2/s
K_H	300 m^2/s
C_D	10^{-3}
ρ_a	1.225 kg/m^3
ρ_0	1000 kg/m^3
N (number of grid points)	400
M	10

Table 4.1: List of parameters used in chapter 4

Throughout this section, the stratification used at the boundary is an unstable stratification of 4.8 psu. This stratification is chosen, since all solutions are possible for this stratification. Comments will be made on the influence of stratification on the solutions.

4.1.1. Offshore and small onshore wind speeds

For the range of offshore wind speeds and small onshore wind speeds, a unique solution was found in the EMM, which had stable stratification at the boundary. An overview of the solution in the EDM for one of these wind speeds is given in figure 4.1. The first panel shows the average salinity as a function of the along

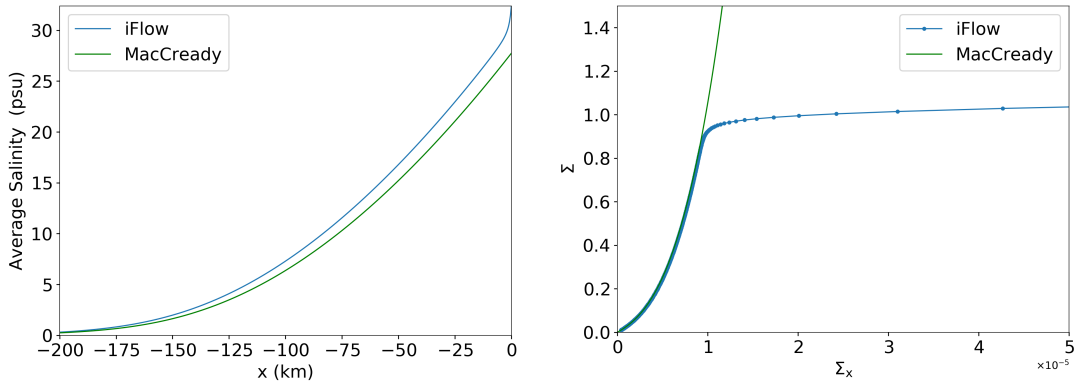

(a) $\bar{s}$ (psu)

(b) $\Sigma_x - \Sigma$ characteristic

Figure 4.1: Overview of the solutions in iFlow for a wind speed of 3 m/s and a prescribed boundary stratification of 4.8 psu

channel coordinate for the solution of the extended Dijkstra model (iFlow), and compares it to the solution of the extended MacCready model. The solution in the EDM has a higher salinity at the oceanic boundary than the solution of the EMM. This difference is caused by the fact that the stratification at the boundary is different for the two solutions. Since the boundary condition at the oceanic boundary for both models is that the salinity at the bottom of the estuary is equal to the oceanic salinity, the difference in stratification causes a difference in vertically averaged salinity. Near the oceanic boundary, a boundary layer and an interior layer can be seen in the solution of the EDM ($x > -5$ km), where the salinity gradient is particularly high. The fact that this region consists of both a boundary layer and an interior layer, rather than just a boundary layer, will be shown in the next paragraph. In the region beyond the boundary and interior layer, named the outer region, the gradients of the two solutions from the two models are similar. This solution can be found for any prescribed boundary stratification. The dynamics and salinity in the boundary and interior layer depend on the prescribed boundary stratification. The prescribed stratification determines the salinity at the oceanic boundary and in this way shifts the plot of the salinity in the outer region to or from the ocean, depending on

the prescribed stratification. Besides this shift, the prescribed stratification does not alter the outer solution.

The second panel compares the realized $\Sigma_x - \Sigma$ characteristic to the analytical characteristic from the EMM, in a similar manner as done in the bottom-left panels of the figures in chapter 3. Since the extended Dijkstra model is different from the extended MacCready model, the plotted $\Sigma_x - \Sigma$ pairs from the extended Dijkstra model will not necessarily be positioned exactly on the analytical curve from the extended MacCready model. If the two models do not agree in parts of the estuary, the analytical curve and the plot of the realized Σ_x and Σ values will not match. In this characteristic, three regions can be identified. For large salinities ($\Sigma > 0.95$) the salinity gradients for the solution to the extended Dijkstra solution are particularly high and tend towards the analytical characteristic from the EMM rapidly. This corresponds to the boundary layer. For salinities between $\Sigma = 0.9$ and $\Sigma = 0.95$, the salinity gradient is slightly larger than the analytical characteristic an tends to the analytical characteristic slowly, forming an interior layer. For lower salinities ($\Sigma < 0.9$), the two characteristics agree, which suggests that the outer solution in the EDM matches the solution of the EMM. Based on the first panel only, the two solutions look similar, but it is hard to conclude to what extent the solutions are fundamentally the same solution. However, based on the $\Sigma_x - \Sigma$ characteristic, it is unmistakable that the two solutions both describe the same solution. Similarity of two solutions is therefore best judged using the $\Sigma_x - \Sigma$ characteristic.

4.1.2. Medium onshore wind speeds

An infinite number of solutions was found in the EMM for medium onshore wind speeds, which all have stable stratification at the boundary.

Figure 4.2 provides an overview of the solutions for a wind speed within this range. Figure 4.2a shows the

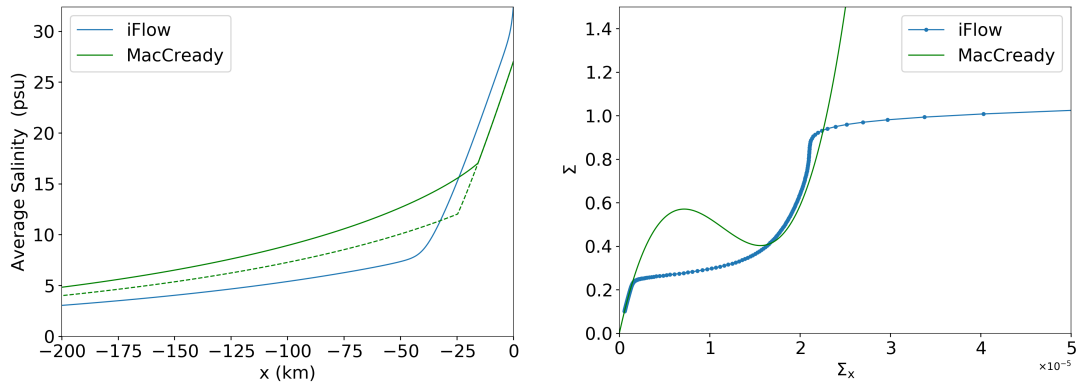

(a) $\bar{s}$ (psu)

(b) $\Sigma_x - \Sigma$ characteristic

Figure 4.2: Overview of the solutions in iFlow for a wind speed of -8.5 m/s and a prescribed boundary stratification of 4.8 psu

two solutions with the highest and lowest salinity from the infinite number of solutions from the EMM. While the EMM had an infinite number of solutions, the EDM has only one solution. The EMM has two sections with distinct gradients. The EDM solution also has these two sections, with the addition of an interior layer region where a smooth transition is made between the two gradients, as well as a boundary layer and an interior layer at the oceanic end. The fact that both a boundary layer and an interior layer are formed at the oceanic end, rather than just a boundary layer will be clear when the next panel is described. The solution obtains lower vertically averaged salinities than any solution in the EMM, for points 30 km or more from the oceanic boundary. Like for offshore and small onshore winds, the salinity at the boundary is larger for the solution of the EDM than for the EMM, due to the difference in stratification at the boundary. This difference becomes larger or smaller as s_{strat} is varied.

The $\Sigma_x - \Sigma$ characteristic is displayed in the second panel. Five regions can be identified in this characteristic. For large salinities ($\Sigma > 0.95$), the salinity gradient from the EDM is larger than the salinity gradient corresponding to the analytical characteristic and tends to the right branch of the analytical characteristic. This section is the boundary layer. An interior layer arises for salinities between $\Sigma = 0.7$ and $\Sigma = 0.95$, where it can be seen that Σ_x is slightly lower than the Σ_x corresponding to the analytical characteristic. For salinities between $\Sigma = 0.5$ and $\Sigma = 0.7$, the characteristic from the EDM roughly follows the analytical characteristic, forming an outer region. Here, the solution is expected to behave like solutions at the right branch in the EMM. For salinities between $\Sigma = 0.25$ and $\Sigma = 0.5$, the characteristic transitions from the right to the left

branch. This is interpreted as a second interior layer, and can be seen in figure 4.2a as the smooth transition from small to large salinity gradients that happens between $x = -40$ km and $x = -25$ km. A second outer layer is formed for the lowest salinities ($\Sigma < 0.25$), where the characteristic from the EDM follows the left branch of the analytical characteristic. Here, behaviour corresponding to the left branch of the characteristic in the EMM is expected. Since the transition from the right to the left branch is made at the lowest possible salinity, this solution corresponds to the solution with stable stratification at the boundary with the minimum possible salinity within the EMM. Note that the Σ values mentioned to in this paragraphs only apply to this specific example. These values will differ for different parameters.

4.1.3. Large onshore wind speeds

The third range of wind speeds that will be discussed is the range of large wind speeds. For large onshore wind speeds, an infinite number of solutions was found in the EMM, which had stable stratification at the boundary. Moreover in the EMM, an infinite number of solutions are found that are unstably stratified at the boundary.

Figure 4.3 displays the solutions found for these wind speeds. In the first panel, the maximum salinity

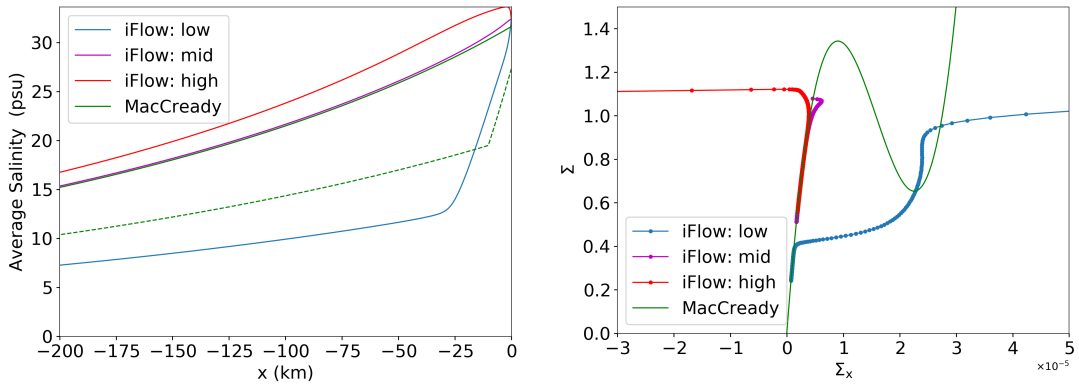

(a) $\bar{s}$ (psu) (b) $\Sigma_x - \Sigma$ characteristic

Figure 4.3: Overview of the solutions in iFlow for a wind speed of -10 m/s and a prescribed boundary stratification of 4.8 psu

and minimum salinity solution in the EMM are indicated using solid and dashed green lines respectively. The maximum salinity solution is partially obscured by the purple line. The plot shows that the EDM has three solutions for large onshore wind speeds. The three solutions are named the low, mid and high salinity solution, based on the order that exists between the solutions in the vertically averaged salinity throughout the estuary. The low salinity solution is the same solution branch as the solution found in the range of medium wind speeds; as a medium wind speed is increased to a large wind speed, the solution continuously moves from the solution in section 4.1.2 to the low salinity solution displayed in this figure. The mid and high salinity solution are two new solutions, which are both slightly higher in salinity than the maximum salinity solution with unstable stratification found in the EMM. Besides a small region near the boundary, the horizontal gradients of the vertically averaged salinity found in these solutions are comparable to the gradients found in the maximum salinity solution with unstable stratification in the EMM.

The second panel shows the analytical $\Sigma_x - \Sigma$ characteristic from the EMM in green, overlaid by a plot with blue markers of the realized $\Sigma_x - \Sigma$ characteristic for the three solutions found in the EDM. The low salinity in this case only has four of the five regions identified in the previous section. The first outer region, where the right branch is closely followed, is not featured for this wind speed, as the salinity gradients are slightly smaller than those of the analytical characteristic for every point between the boundary layer and the second interior layer. This solution therefore directly moves from the first to the second interior layer. The mid and high salinity solutions both predominantly use the left branch. At the points where the characteristics match the left branch of the analytical characteristic, behaviour typical of the left branch is expected to be found. For the mid salinity solution, the salinity gradient first rises quickly in the boundary layer, before it decreases towards the analytical characteristic, described as the interior layer. For the high salinity solution, a boundary layer and an interior layer can be identified as well. In the boundary layer, the salinity gradient rapidly increases from negative to positive values, while in the interior layer, the salinity gradient smoothly tends to the analytical characteristic. Since both the mid and the high salinity solution use the left branch of

the analytical characteristic for every point beyond the boundary and interior layer, the two solutions both correspond to the maximum salinity solution with unstable stratification at the boundary in the EMM, which is plotted using a solid green line in figure 4.3a.

In the range of large onshore wind speeds, the EDM has three solutions. The low salinity solution has been discussed before in section 4.1.2. While the EMM had an infinite number of solutions similar to this solution, the EDM only finds one. Moreover, an infinite amount of solutions that start on the left branch are found in the EMM, while the EDM only finds two of these solutions. The mid and high salinity solutions both correspond to the maximum salinity solution with unstable stratification at the boundary found in the EMM, and differ from each other in the way the interior dynamics are approached from the oceanic boundary. These two solutions are not found for prescribed stable stratification, while the low salinity solution is found for such stratification.

4.1.4. Very large onshore wind speeds

Finally, for very large wind speeds, the EMM has one solution. This solution is unstably stratified throughout the estuary.

The solutions found in this regime are displayed in the figure 4.4. Figure 4.4a, displaying the average

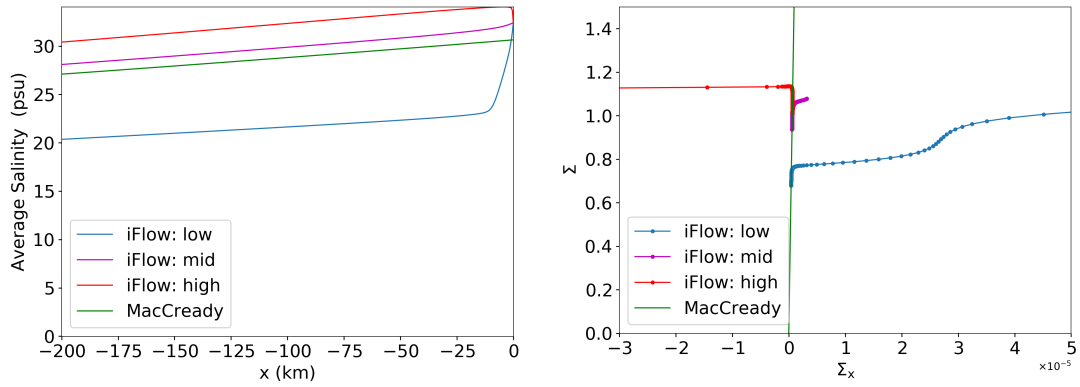

(a) $\bar{s}$ (psu)

(b) $\Sigma_x - \Sigma$ characteristic

Figure 4.4: Overview of the solutions in iFlow for a wind speed of 10.5 m/s and a stratification of 4.8 psu

salinity, shows that three solutions are found for this range of wind speeds in the EDM. These are the same three solutions that were found for large wind speeds. The mid and high salinity solution both correspond to the maximum salinity solution with unstable stratification at the boundary in the EMM. This is the only solution found for very large wind speeds in the EMM. The low salinity solution corresponds to the minimum salinity solution with stable stratification for medium and large wind speeds in the EMM. The low salinity solution in the EDM is feasible for very large wind speeds, while it is not feasible for this range of wind speeds in the EMM. The reason for the existence of this solution for very large wind speeds will be discussed in section 4.2.3.

The $\Sigma_x - \Sigma$ characteristics are visualized in the second panel. The characteristics of the mid and high salinity solution are similar to those in section 4.1.3: for the highest salinities ($\Sigma > 1$), the solutions tend to the characteristic from the EMM, which is followed for the rest of domain. The characteristic of the low salinity solution is visually similar to the characteristic displayed in figure 4.3b, featuring the same four regions: a boundary layer: $\Sigma > 0.95$; the first interior layer $0.85 < \Sigma < 0.95$, the second interior layer $0.8 < \Sigma < 0.85$ and the second outer region $\Sigma < 0.8$. Like the solution for large wind speeds, this solution does not have a first outer region. The main difference with the low salinity solution for large wind speeds is that the first interior layer ($0.85 < \Sigma < 0.95$), is not positioned near the right branch. This is because the right branch is not available for the salinities typically found in an estuary.

4.2. Low salinity solution

The low salinity solution found in the EDM will be studied in more detail in this section. For offshore winds and small onshore wind speeds, this solution contains a boundary layer, an interior layer and an outer solution, while for medium onshore wind speeds the solution features the same three layers with the addition of

a second interior layer and a second outer region. For large wind and very large wind speeds, all of these five regions are found except for the first outer region. Since the low salinity solution for medium wind speeds contains all five possible regions, the low salinity solution will be studied in detail for this range of wind speeds. It will be commented upon how the solutions for different ranges of wind speeds differ from the solutions for this range of wind speeds in section 4.2.3.

First, an overview of a sample solution will be given in section 4.2.1, followed by a decomposition of the horizontal velocity and salinity into contributions from different transport mechanisms in section 4.2.2. Section 4.2.3 will provide an overview of how the solution changes as the wind speed changes. The first goal of this section, is to verify that the parts of the domain which appear to be similar to solutions in the EMM are indeed governed by the same transport balances and have similar velocity and salinity structures as the corresponding solution in the EMM. The second goal is to determine the structure and relevant transport contributions in the boundary and interior layers, which are not described by the EMM.

As will be seen later in this section, the salinity stratification of this solution is stable in the first outer region. Yet, unstable stratification is imposed on the oceanic boundary in the solutions depicted in this chapter. This makes sure that the results are in line with the results displayed in section 4.1, where unstable stratification is used as well. Moreover, the boundary layer and the first interior layer become more pronounced for unstable stratification than for stable stratification at the boundary, since the deviation from the salinity profile of the interior is larger. This makes the boundary layers easier to identify visually.

For this solution, it is shown that the extent to which the results from this model are in accordance with the $\Sigma_x - \Sigma$ characteristic can be used to determine whether a solution is fully converged numerically. This analysis is included in appendix C.

4.2.1. Solution description

An example of the low salinity solution is presented in figure 4.5, for an unstable top-to-bottom stratification of 4.8 psu and a wind speed of -9 m/s. This solution is in the range of medium onshore wind speeds. For this example, five regions were identified: the boundary layer ($x > -5$ km), where the salinity gradient is larger than that of the analytical characteristic; the first interior layer (-10 km $< x <$ −5 km), where the salinity gradient is slightly lower than that of the analytical characteristic; the first outer region (-25 km $< x <$ −10 km), corresponding to the right branch of the $\Sigma_x - \Sigma$ characteristic; a second interior layer (-40 km $< x <$ −25 km); and finally the second outer region ($x <$-40 km), corresponding to the left branch of the $\Sigma_x - \Sigma$ characteristic.

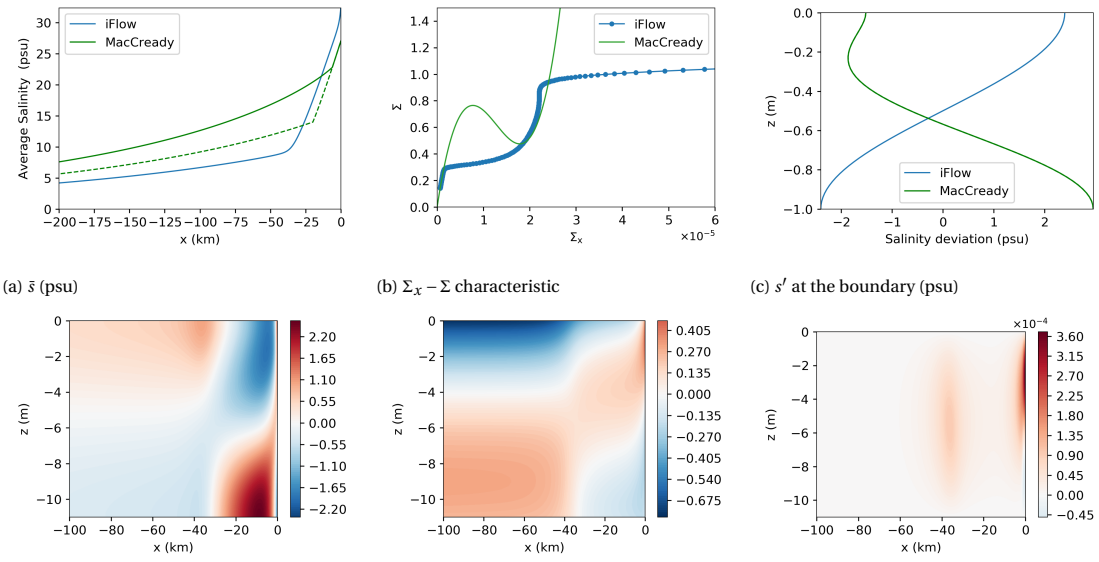

(a) $\bar{s}$ (psu) (b) $\Sigma_x - \Sigma$ characteristic (c) s' at the boundary (psu)

(d) s' (psu) (e) u (m/s) (f) w (m/s)

Figure 4.5: Overview of the low salinity solution for $u = -9$ m/s. The top left figure compares the vertically averaged salinity of the solution for the EDM (iFlow) to the solutions found using the EMM. The second figure for the $\Sigma_x - \Sigma$ characteristic features the analytical characteristic as a solid line, as well as a plot with markers of the realized characteristic. The top right figure compares the stratification at the boundary for these two solutions. The bottom row features heat maps of the variation in vertical salinity, the horizontal velocity and the vertical velocity

The first two panels show the vertically averaged salinity and the $\Sigma_x - \Sigma$ characteristic, which have already been discussed in section 4.1.2, but are included for reference. The third panel displays the vertical variation in salinity at the right-hand boundary for the extended Dijkstra solution and compares it to that of the solutions of the extended MacCready model. We see that unstable stratification is imposed on the boundary for the extended Dijkstra solution displayed, while the stratification obtained by the extended MacCready model is largely stable, with a small section of unstable stratification near the surface. The difference between the salinity at the bottom and the average salinity differs by about 5 psu between the two salinity profiles. The average salinity at the right-hand boundary is larger for the iFlow solution then for the solution of the EMM by the same amount. This confirms that the difference in average salinity at the boundary seen in the first panel can be explained by the difference in stratification at the boundary, as claimed in section 4.1.1.

Figure 4.5d shows a heat map of the vertical deviation in salinity s'. Starting at the right-hand side of the heat map, the boundary layer is observed ($x > -5$ km), where the stratification transitions from the prescribed unstable stratification to the stable stratification of the first interior layer and the first outer region. Between $x = -25$ km and $x = -5$ km, spanning the first interior layer and the first outer region, we find stable stratification. This type of stratification corresponds to the type of stratification that is typically found at the right branch. The right branch is followed strictly in the first outer region, and is followed roughly in the first interior layer. For -40 km $< x < -25$ km, the second interior layer, the stratification transitions from stable to unstable stratification. Finally, in the second outer region, we find unstable stratification. This is in line with the type of stratification expected for the left branch of the $\Sigma_x - \Sigma$ characteristic, based on the EMM.

The bottom center panel displays a heat map of the horizontal velocity. At the oceanic boundary, clockwise circulation is observed. In the boundary layer, this circulation transitions to counterclockwise circulation for approximately $z > -4$ m, and clockwise circulation for approximately $z < -4$ m. Across the first interior layer and the first outer region, the fraction of the water column with counterclockwise circulation becomes larger as the distance to the ocean becomes larger. In the second interior layer, this mixture of counterclockwise and clockwise circulation transitions to pure counterclockwise circulation. Finally, in the second outer region, circulation is counterclockwise throughout the water column. The modes of circulation in the outer regions are in line with the expectations based on the type of circulation found in the EMM for the branches these regions occupy in the $\Sigma_x - \Sigma$ characteristic.

Finally, figure 4.5f displays the vertical velocity. Vertical velocity is largest in the second interior layer and in the boundary layer. In order to meet continuity requirements, water flows upwards in the second interior layer between clockwise and counterclockwise flow.

4.2.2. Decomposition

In order to gain further understanding of the observed velocities and salinities, a decomposition of the horizontal velocity and salinity into contributions from different forcing mechanisms will be made, as discussed in section 2.4.8. The goal of this section is to verify whether the dominant transport phenomena are the same for the solutions of the EMM and the EDM in regions of the estuary where the $\Sigma_x - \Sigma$ characteristics match. Moreover, this section will study what transport mechanisms dominate the boundary and interior layers.

The velocity decomposition is given in figure 4.6. The contributions from gravitational circulation and advection are capped at a magnitude of 1 and 0.5 m/s respectively, in order to make sure that contributions beyond the boundary layer are visible, as these are typically lower in magnitude than those in the boundary layer.

The first panel shows the contribution from river flow. In line with section 1.2, this contribution is constant over the estuary, positive and largest near the surface. The second panel shows the wind contribution. This contribution is constant as well, and shows counterclockwise circulation as expected. The third panel displays the contribution from gravitational circulation, which is clockwise throughout. This contribution is largest in the boundary layer, where the salinity gradient is largest. In the first interior layer and the first outer region, the contribution is smaller, but still large enough to partially counter the counterclockwise circulation induced by wind. In the second interior layer, the magnitude of the contribution decreases as x decreases and in the second outer region, the contribution is negligible.

The fourth panel shows the contribution from the advection of momentum, which is neglected in MacCready's model. A large counterclockwise contribution can be found in the boundary layer. Moreover, clockwise contributions are found in the second interior layer and the second boundary layer. Contributions from momentum advection arise when horizontal gradients in the horizontal velocity are large. Considering that the velocity contributions from the wind stress and river discharge are constant in the horizontal direction, this decomposition shows that momentum advection reacts to the change in horizontal velocity caused by

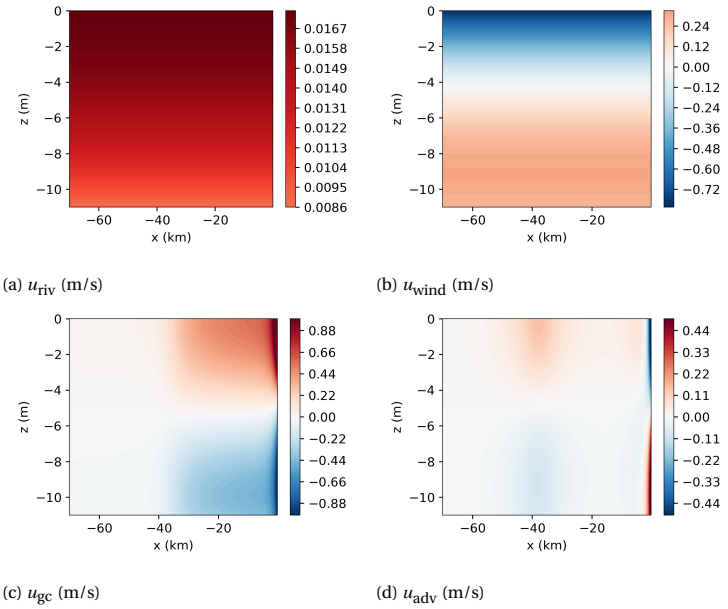

(a) u_{riv} (m/s) (b) u_{wind} (m/s)

(c) u_{gc} (m/s) (d) u_{adv} (m/s)

Figure 4.6: Decomposition of the low salinity solution for a wind speed of -9 m/s, into contributions from river discharge, wind stress, gravitational circulation and advection

the change in the contribution from gravitational circulation.

A similar decomposition is made for the vertical deviation in salinity as seen in figure 4.7. The first panel

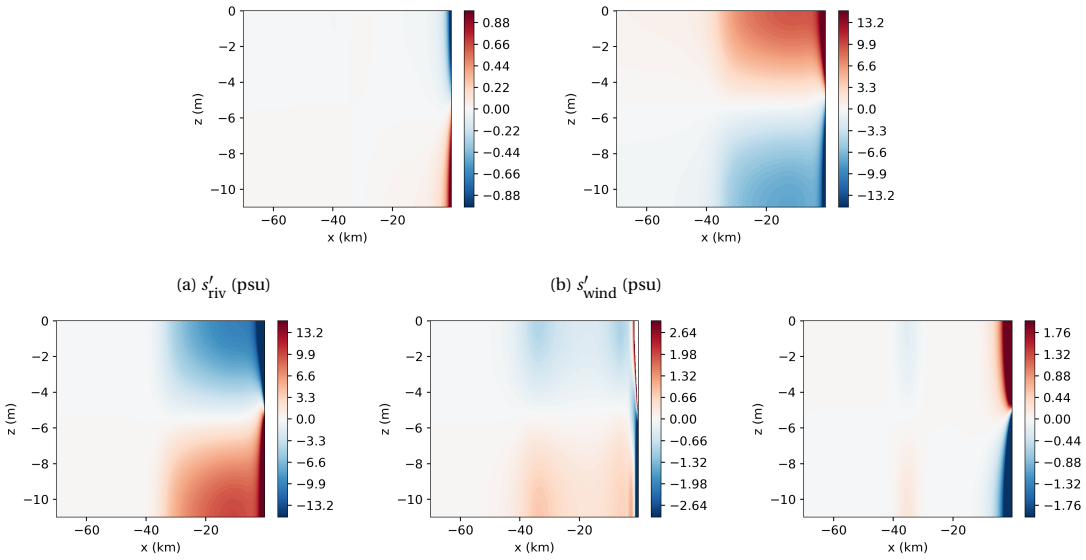

(a) s'_{riv} (psu) (b) s'_{wind} (psu)

(c) s'_{gc} (psu) (d) s'_{adv} (psu) (e) s'_{Kh} (psu)

Figure 4.7: Decomposition of the salinity of the low salinity solution for a wind speed of -9 m/s, into contributions from river discharge, wind stress, gravitational circulation, advection and horizontal diffusion.

shows the contribution from advection forced by the river discharge. This contribution is generally small, and is largest in the boundary layer, where the salinity gradient is largest. It promotes stable stratification.

The second panel shows the contribution from wind forced advection. In line with the results from chapter 3, wind promotes unstable stratification. This contribution is largest in the boundary layer, but is also significant in the first interior layer and the first outer region. In the second interior layer, the contribution decreases as the distance to the ocean increases, until in the second outer region, the contribution is small. In this way, the magnitude of the stratification mirrors the gradient of the vertically averaged salinity.

Figure 4.7c shows the contribution from gravitational circulation. As expected, gravitational circulation promotes stable stratification. The magnitude of the contribution develops similarly along the estuary as the magnitude of the contribution from wind stress.

The bottom center panel displays the contribution from salinity advection induced by momentum advection. This contribution spikes locally in the boundary layer. The first interior layer features a stably stratified contribution. In the second interior layer, a stable contribution can be found as well. This is in line with the velocity contribution in this region, which promotes clockwise circulation. A small contribution is observed in the first outer region, which appears to be the result of the fact that the contributions from the two interior layers are spread out into the first outer region. In the second outer region, the contribution is negligible. The final panel shows the contribution from horizontal diffusion. It is clear that diffusion is most significant in the boundary layer, and is also present in the interior layers.

The decomposition confirms that the domain can be split into five sections. In the boundary layer, contributions from river flow, wind advection, gravitational circulation, momentum advection and horizontal diffusion are all found. The exact dynamics in this section are beyond the scope of this thesis.

The first interior layer will be discussed after the first outer region. The first outer region, corresponding to the right branch of the $\Sigma_x - \Sigma$ characteristic shows major contributions from gravitational circulation and wind stress. In this region, the contribution from gravitational circulation is slightly larger than that from wind stress, leading to stable stratification and predominantly clockwise circulation. This is in line with the balance that is found on the right branch in the EMM.

In the first interior layer, the same dynamics are observed as in the first outer region, with the addition of a contribution from momentum advection. This momentum advection is the result of the difference in the velocity profile between the boundary layer and the first outer region. This contribution enhances the stratification and circulation found in this layer. As a result, smaller salinity gradients are required to achieve the stratification and circulation that are typical of the right branch. This explains why the salinity gradient is smaller than the salinity gradient for the analytical characteristic in this layer. As this interior layer takes up a considerable length, the vertically averaged salinity of the EDM solution becomes lower than that of the EMM solution, as the effective salinity at the point of the switch between branches become lower.

The second interior layer is mainly constituted of contributions from momentum advection and horizontal diffusion, and varying contributions from wind stress and gravitational circulation. Since momentum advection and horizontal diffusion of the vertical salinity profile are neglected from the EMM, this explains how the second interior layer can feature in a part of the $\Sigma_x - \Sigma$ plane which is not deemed feasible in the context of the EMM. Since the vertical profiles of horizontal velocity and salinity are different between the first and second outer region, it is logical that momentum advection and horizontal diffusion, which react to horizontal gradients of the velocity and salinity, feature prominently in the interior layer between these two regions.

In the second outer layer, positioned on the left branch, the only major velocity and salinity contribution is from wind stress. This is in line with the EMM, where wind dominates the velocity and salinity profiles of the left branch.

4.2.3. Solution for different wind speeds

A brief overview of the low salinity solution for different wind speeds is given in figure 4.8, using the $\Sigma_x - \Sigma$ characteristic. The top two panels show the characteristic for the wind speeds of 3 and -3 m/s respectively. Here, the EMM found only one solution. This solution corresponds to the solution found using the EDM for offshore winds and small onshore winds. As seen from the characteristic, the solution does not have the same five regions as discussed above, but three. The first region is a boundary layer, which like the solution for medium wind speeds, is constituted of an eclectic mix of different transport contributions, including diffusion. Here, the values of Σ_x are significantly larger than those for the analytical characteristic and rapidly tend to this characteristic. The second region is the interior layer, where the salinity gradients gradually tend to the $\Sigma_x - \Sigma$ characteristic. This region is characterised by significant contribution from momentum advection, and is caused by the horizontal velocity gradients between the outer region and the boundary layer. The third region is the outer region where the solution abides to the $\Sigma_x - \Sigma$ characteristic from the EMM. In this region, the salinity and velocity profiles are dominated by gravitational circulation for the majority of the domain, which gradually changes to a wind dominated domain as the salinity decreases. Similar to the solutions in the EMM, stratification remains stable and circulation clockwise over the entire domain for offshore wind, while stratification becomes unstable and circulation counterclockwise once wind dominates over gravitational circulation for small onshore wind speeds.

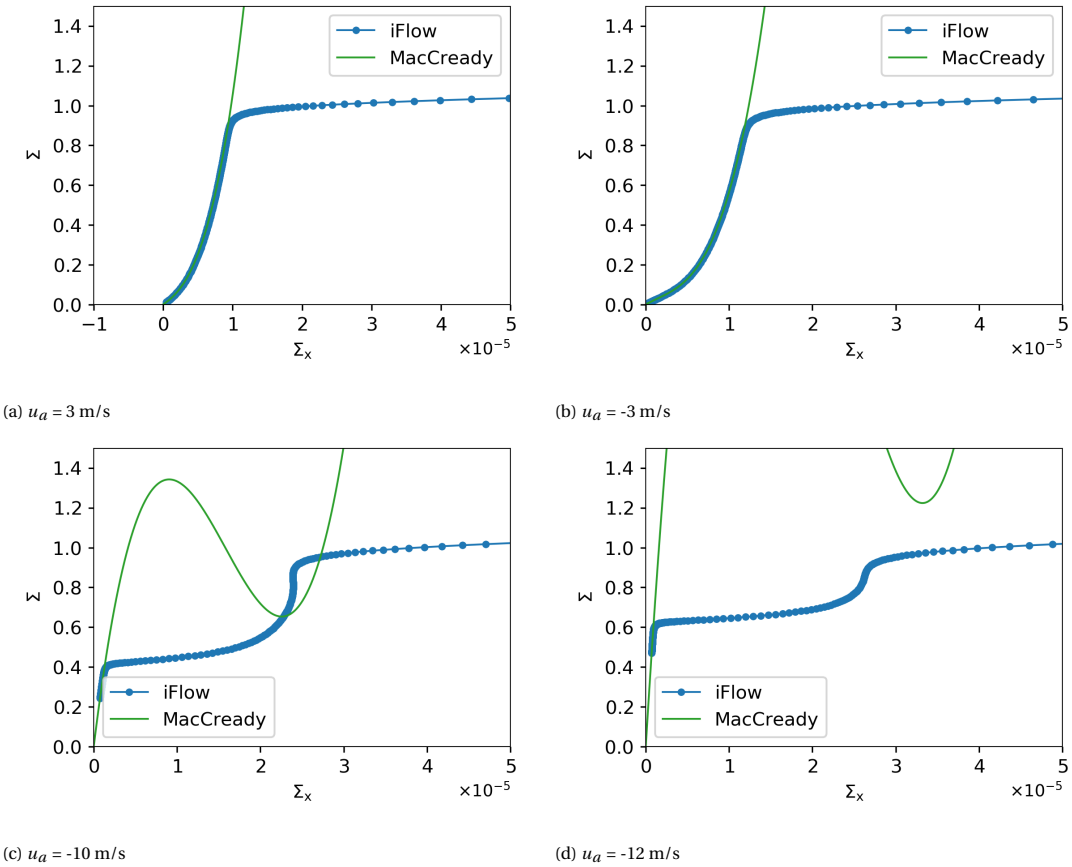

(a) u_a = 3 m/s

(b) u_a = -3 m/s

(c) u_a = -10 m/s

(d) u_a = -12 m/s

Figure 4.8: Close-up of the $\Sigma_x - \Sigma$ characteristic for the low salinity solution for a range of wind speeds

The bottom left panel shows the characteristic for a wind speed of -10 m/s, which is close to the wind speed of -9 m/s used in sections 4.2.1 and 4.2.2. For this wind speed, the first outer region does not exist. For every point between the boundary layer and the second interior layer, momentum advection is significant, such that the characteristic is positioned to the left of the right branch of the analytical characteristic.

The final panel shows that for a wind speed of -12 m/s, the right branch does not reach down far enough for solutions using the right branch of the $\Sigma_x - \Sigma$ characteristic at the boundary to be possible within the EMM. However, we see that a low salinity solution is still possible for this model. The realized characteristic resembles that in figure 4.8c, with the main difference that while the first interior layer was near the analytical $\Sigma_x - \Sigma$ characteristic in figure 4.8c, this layer is not near the analytical characteristic in figure 4.8d.

In order to verify whether the regions in the characteristic are correctly interpreted, a decomposition of horizontal velocity and salinity has been made for a wind speed of -12 m/s. This decomposition is not displayed in this thesis. The decomposition confirms that four of the five regions that were identified in section 4.2.1 are found in this solution. The first outer region is the region is not present for this solution, while the other four regions are retrieved. The contributions in these four regions are similar to those presented in section 4.2.2. For a wind speed of -12 m/s, gravitational circulation is not strong enough to counter the effects of wind stress. As a result, the right branch of the analytical is not available for the concerned salinities. In the first interior layer, momentum advection enhances the effects of gravitational circulation. In this solution, the sum of the effects of gravitational circulation and momentum advection is large enough to counter the effects of wind stress. As the onshore wind speed increases, the velocity gradients needed to force momentum advection that is large enough to counter the winds stress become increasingly large, such that the width of this region becomes increasingly smaller.

The stratification imposed at the boundary in this section is wildly different from the stratification obtained in the first outer region, which agrees with the stratification from the EMM. The more the prescribed stratification matches the stratification of the outer region, the less extreme the deviations from the $\Sigma_x - \Sigma$ characteristic in the boundary layer and first interior layer become. The salinity profile can be described in

such a manner that no boundary or interior layers are required. The required salinity profile closely matches the salinity profile obtained in the EMM at the boundary.

4.3. Mid salinity solution

This section will discuss the mid salinity solution. This section is similarly structured as section 4.2. Like in the previous section, the main goal is to understand how the boundary layer and interior layer are constituted, and to what extent the solution is in line with the EMM in the outer region.

4.3.1. Solution description

A typical example of this solution can be found in figure 4.9. This solution is generated for a wind speed of -10.5 m/s and an unstable top-to-bottom stratification of 4.8 psu at the entrance (see figure 4.9c). The heat maps on the bottom row feature only the first 20 or 40 km of the domain, in order to increase the visibility of boundary features. Three sections can be identified in this solution: the part near the boundary where the salinity gradient increases as the distance to the ocean increase(boundary layer, $x > -2$ km), the section near the boundary where the salinity gradient decreases (interior layer, -10 km $< x < -2$ km) and the outer solution. The first two plots have already been discussed in section 4.1.

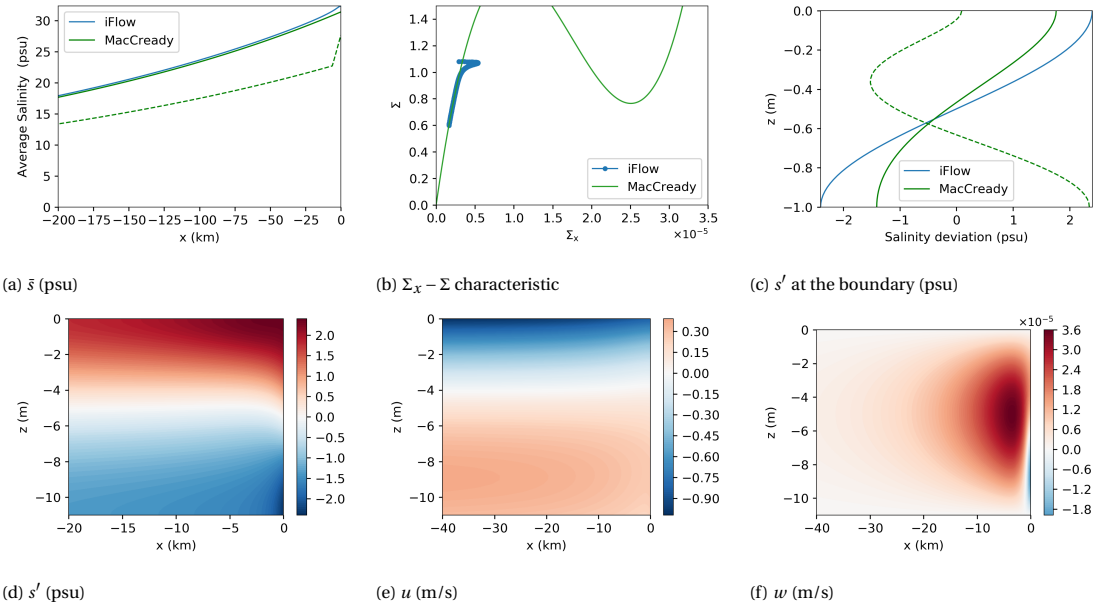

(a) $\bar{s}$ (psu) (b) $\Sigma_x - \Sigma$ characteristic (c) s' at the boundary (psu)

(d) s' (psu) (e) u (m/s) (f) w (m/s)

Figure 4.9: Overview of mid salinity solution for a wind speed of -10.5 m/s. The reader is referred to the caption to figure 4.5 for a full description of the individual panels.

Figure 4.9c shows the vertical salinity deviation at the boundary for the EDM, and compares it to the salinity deviation in the EMM. It can be seen that the prescribed salinity profile is similar to the salinity profile that arises in the EMM. As a result, the difference in vertically averaged salinity at the boundary is only minor.

Figures 4.9d shows that the estuary is unstably stratified throughout the domain. This corresponds to the type of stratification found for maximum salinity solution of the EMM for large and very large wind speeds. In the second boundary layer, the degree of stratification is larger than for the rest of the domain. This layer corresponds to the region where the salinity gradient is large, which is in line with equation 2.67, that states that stratification scales with vertically averaged salinity gradients. Close inspection reveals that in the boundary layer, the salinity stratification changes both in magnitude and in shape. Especially the salinity at the bottom rapidly changes in this layer.

The bottom center panel, displaying horizontal velocity, shows that the circulation is counterclockwise over the entire length of the estuary. This is in line the type of circulation found for the maximum salinity solution with unstable stratification at the boundary in the EMM. The magnitude of this circulation decreases slightly in the interior layer (-10 km $< x < -2$ km), this change is, however, small and is therefore not easily visible.

Finally, figure 4.9f shows that the vertical velocity is largest in the interior layer. The velocity is directed upwards. In the boundary layer, a small negative contribution can be seen at the bottom.

4.3.2. Decomposition

In order to be able to explain the figures presented in the previous section, the horizontal velocity and salinity will be decomposed into contributions from different forcings in this section. Similar to section 4.2.2, this will allow for the assessment of the similarities between the solutions from the two models in the outer region and give insight into the boundary layer and interior layer. The velocity decomposition is visualized in figure 4.10.

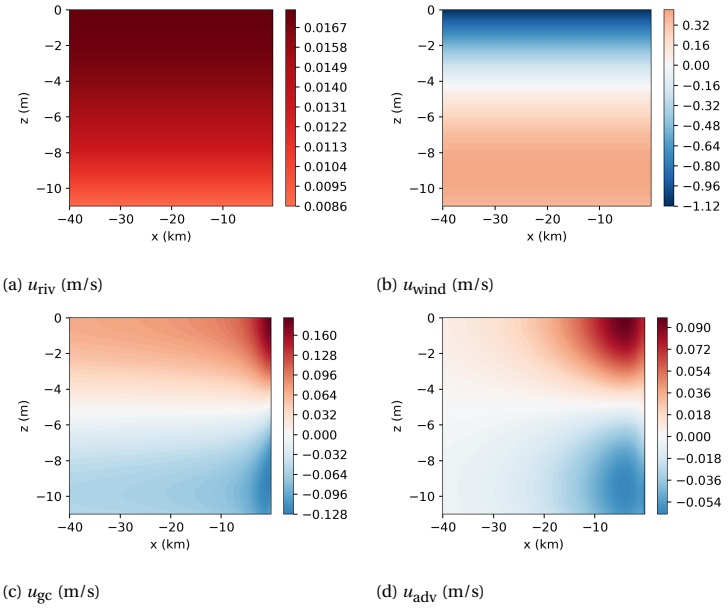

(a) u_{riv} (m/s) (b) u_{wind} (m/s)

(c) u_{gc} (m/s) (d) u_{adv} (m/s)

Figure 4.10: Decomposition of the mid salinity solution for a wind speed of -10.5 m/s, into contributions from river discharge, wind stress, gravitational circulation and advection

Figure 4.10a shows the velocity forced by the river discharge, while figure 4.10b displays the horizontal velocity forced by wind stress. Both these panels are identical to those shown in figure 4.6, except for the magnitude of the wind contribution, since the wind speed used for that figure is slightly smaller in magnitude than the wind speed used for figure 4.10.

The bottom left panel displays the contribution from gravitational circulation. For the majority of the domain, this contribution is near constant, since the salinity stratification and gradient are near constant in that region. In a small region near the boundary, between $x = -5$ km and $x = 0$, the contribution becomes significantly larger, reaching its maximum at or near the boundary.

Finally, the bottom right panel displays the contribution from momentum advection. This contribution is large in first 10 kilometers from the ocean. The region where the contribution from momentum advection is large coincides with the region where vertical velocity is large, as seen in figure 4.9f. It should be noted that this contribution is relatively small compared to the wind contribution, and is comparable in magnitude to the contribution from gravitational circulation. Momentum advection and vertical velocities arise as as consequence of horizontal gradients in vertical velocity. Gravitational circulation is the only contribution that varies along the length of the estuary, which means that the momentum advection is a reaction to the horizontal gradients of horizontal velocity caused by gravitational circulation. This is in line with the fact that the contribution from momentum advection is largest in the region where the contribution from gravitational circulation changes.

The decomposition of the vertical deviation in salinity is seen in figure 4.11. The top left panel displays the contribution from advection forced by the river discharge to the vertical deviation in salinity. The river discharge forces the estuary towards stable stratification. The contribution is generally small, while the contribution is signficantly larger in the boundary layer ($x > -2$ km). This is the region where the estuary experiences strong qualitative changes in salinity gradient. The salinity advection forced by river discharge strongly reacts to these changes.

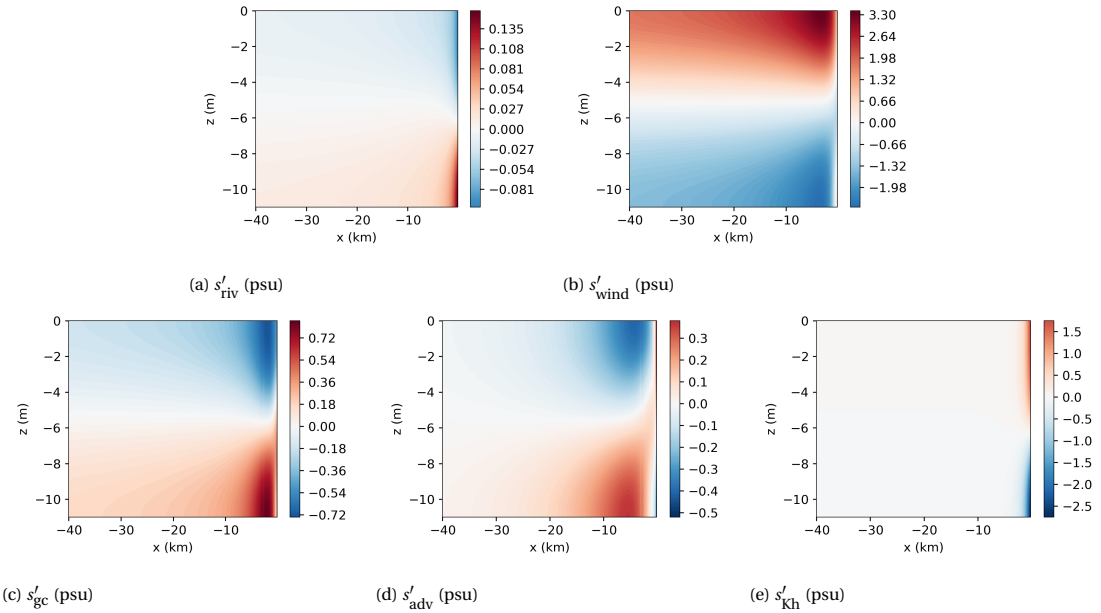

(a) s'_{riv} (psu) (b) s'_{wind} (psu)

(c) s'_{gc} (psu) (d) s'_{adv} (psu) (e) s'_{Kh} (psu)

Figure 4.11: Decomposition of the salinity of the mid salinity solution for a wind speed of -10.5 m/s, into contributions from river discharge, wind stress, gravitational circulation, advection and horizontal diffusion.

Figure 4.11b shows the contribution from wind stress. It is seen that wind stress promotes unstable stratification, in line with the results from chapter 3. The contribution is largest in the interior layer (-10 km $< x < -2$ km). The bottom left panel shows the contribution from gravitational circulation. It is clear that gravitational circulation promotes stable stratification, and that this effect is largest near the boundary ($x > -5$ km).

Figure 4.11d shows that the salinity advection forced by momentum advection promotes stable stratification, and that this forcing is largest for (-10 km $< x < -2$ km), the interior layer. This contribution smooths out the large horizontal gradient in the horizontal velocity caused by the contribution from gravitational circulation. Momentum advection reduces the counterclockwise circulation and unstable stratification caused by the wind stress. As a result, larger salinity gradients are required in order to increase the stratification and circulation to the magnitude where the transport from the average river flow is balanced. This explains why the salinity gradient is larger than the salinity gradient in the analytical characteristic in the interior layer.

Finally, the bottom right panel shows that diffusion is large in the boundary layer ($x > -2$ km). The contribution here is larger than that of the other contributions. It can thus be concluded that the small boundary layer is diffusive in nature.

It can be concluded that in the outer region, the vertical salinity and velocity profiles are dominated by wind stress. This is in line with the maximum salinity solution for unstable stratification for the EMM. This implies that the maximum salinity solution in the EMM and the mid salinity solution in the EDM are indeed determined by the same type of transport processes. Moreover, a boundary layer and an interior layer are identified. The first is a small, diffusive boundary layer with a depth of approximately 2 km. In this boundary layer, the salinity gradient increases as x decreases, as seen in the $\Sigma_x - \Sigma$ characteristic in figure 4.9b. The interior layer, reaching up to 10 km from the ocean, is determined by increased gravitational circulation and especially momentum advection. Here the contribution from gravitational circulation is largest near the ocean ($x >$-5 km), while the contribution from momentum advection peaks around $x = -5$ km. These two contributions reduce the unstable stratification and counterclockwise circulation that enable wind dominated transport. As a result, a larger salinity gradient than given by the analytical characteristic is required in order to satisfy the horizontal transport balance. The fact that the salinity gradient is larger than that of the analytical characteristic is what defines this region.

4.3.3. Solution for different wind speeds

Figure 4.12 displays the $\Sigma_x - \Sigma$ characteristic of the mid salinity solution for different wind speeds. These characteristic will be used to analyse how the solution changes with the wind speed.

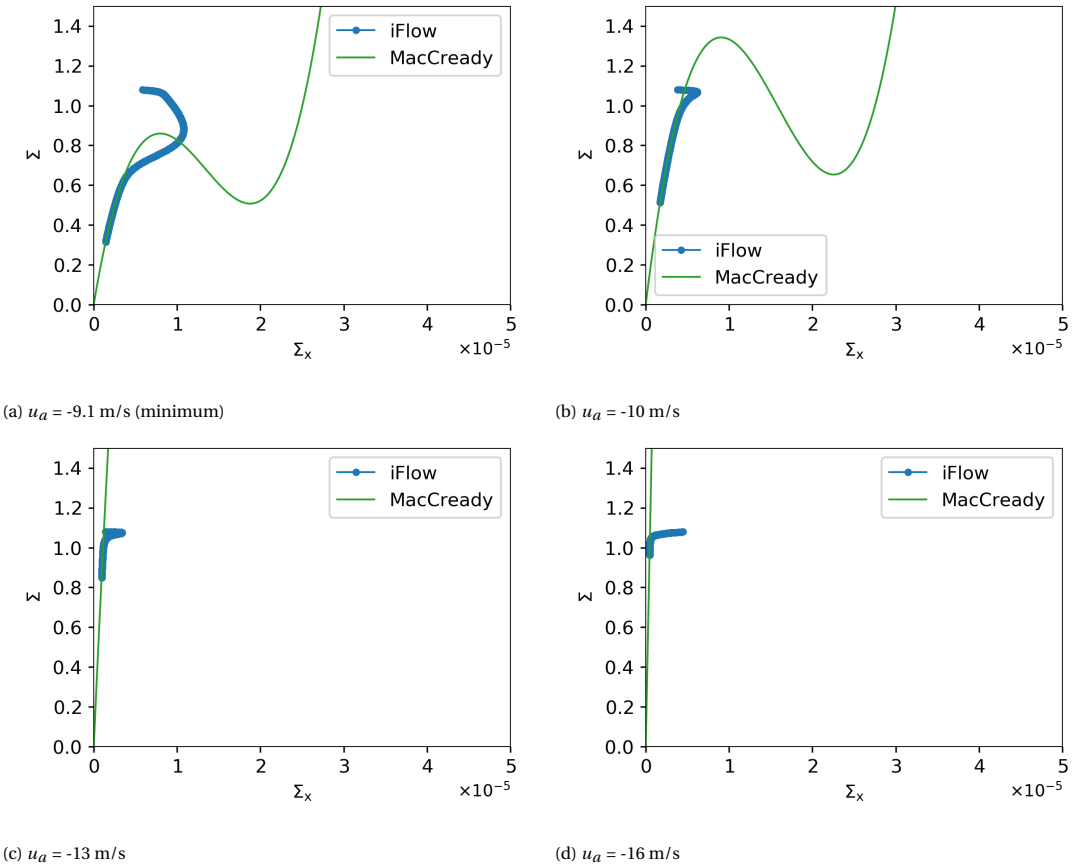

(a) u_a = -9.1 m/s (minimum)

(b) u_a = -10 m/s

(c) u_a = -13 m/s

(d) u_a = -16 m/s

Figure 4.12: Close-up of the $\Sigma_x - \Sigma$ characteristic for the mid salinity solution for a range of wind speeds

The predominant conclusion that can be drawn from the characteristics is that this solution type is always located on the left branch of the analytical characteristic. This means that the branch of the characteristic chosen is indeed a characterizing feature of the solution. Looking at the boundary layer, we note that for the first three panels the salinity gradient increases as the distance to the boundary increases, whereas for the final panel, the salinity gradient decreases as a function of the distance to the oceanic boundary in this boundary layer. The interior layer always has a larger salinity gradient than the analytical characteristic.

Figure 4.12a displays the $\Sigma_x - \Sigma$ characteristic for the minimum onshore wind speed (minimum in magnitude) for which this solution exists. It can be seen that the left branch of the analytical characteristic has a maximum value of about $\Sigma = 0.85$. Since the salinity at the boundary is approximately $\Sigma = 1.1$, the left branch cannot be used near the boundary. Considering that the solution is characterized by the fact that it solely uses the left branch, this implies that a mid salinity solution as portrayed in section 4.3.1 is not possible within the limitations of the EMM. However, in the context of the more extensive model formed by the EDM, a combination of boundary and an interior layer can be formed which enable the existence of a mid salinity solution. These two layers bridge the gap between the salinity at the oceanic boundary and the maximum salinity of the left branch. For onshore wind speeds smaller in magnitude than this critical wind speed, the maximum salinity of the left branch becomes even lower, and such layers are no longer feasible. Since the salinity decreases significantly within the boundary and interior layers, it can be concluded that those layers take up a significant portion of the estuary. Comparing this characteristic to the characteristic in figure 4.9b, we note that the boundary and interior layers in the two characteristics both consist of a section where the salinity gradient increases, followed by a section where this gradient decreases to the analytical characteristic from the EMM. We thus expect both boundary layers to be similarly structured.

The stratification that is imposed at the boundary is similar to the stratification that is obtained in the EMM solution. When stable stratification is prescribed, this solution is no longer feasible, since no combination of boundary and interior layers can be formed that connects the stable stratification at the boundary to the unstable stratification of the outer solution. For a specific salinity profile, no boundary and interior

layers are observed, while for salinity profiles that are very dissimilar, the boundary layer and interior layer will become more pronounced. The salinity profile that is required to obtain no boundary layer is similar to the salinity profile obtained at the boundary in the EMM solution. Similar to the low salinity solution, the imposed stratification determines the vertically averaged salinity at the oceanic boundary. Altering the stratification at the boundary thus alters the vertically averaged salinity troughout the estuary.

4.4. High salinity solution

This section will describe the solution found in the EDM that had the highest salinity. This solution is feasible for unstable stratification and onshore wind speeds that are large or very large. The structure of this section identical to the structure of the two previous sections. Similar to the previous sections, the primary goal is to study the boundary and interior layers, and to determine to what extent the solution is in line with the EMM in the outer region.

4.4.1. Solution description

An example of a typical high salinity solution is displayed in figure 4.13. This solution is generated for a wind velocity of 10.5 m/s and a boundary stratification of 4.8 psu. From the first two panels, three regions can be identified for this solution: the boundary layer ($x > -1$ km), where the salinity gradient is negative; the interior layer (-20 km $< x < -1$ km), where the salinity gradient tends to the left branch and an outer region ($x < -20$ km), where the left branch is followed. The first panel, displaying the average salinity, shows that

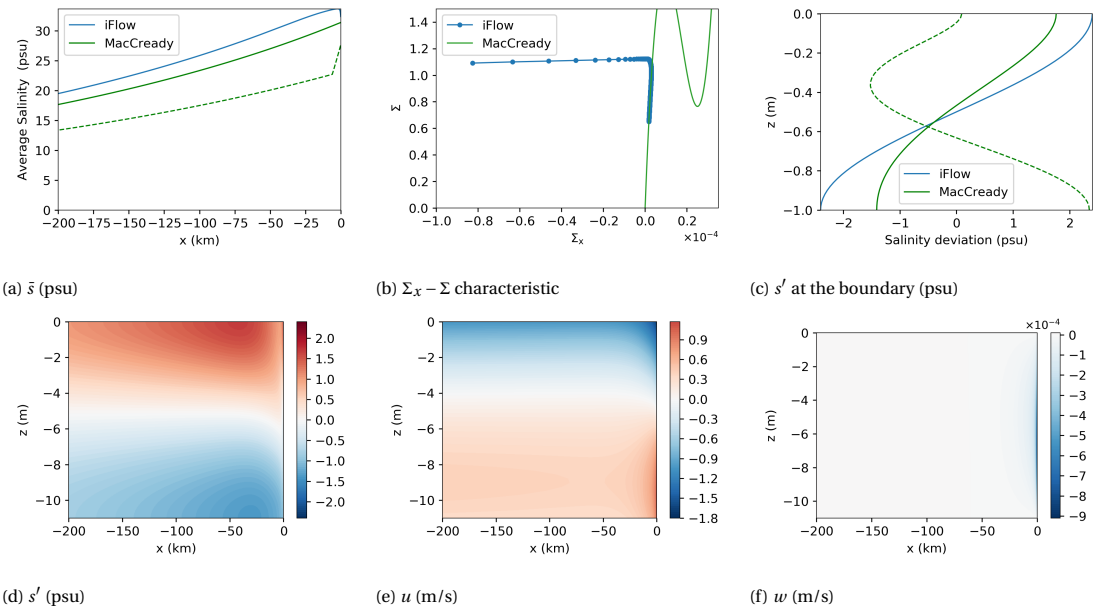

(a) $\bar{s}$ (psu) (b) $\Sigma_x - \Sigma$ characteristic (c) s' at the boundary (psu)

(d) s' (psu) (e) u (m/s) (f) w (m/s)

Figure 4.13: Overview of mid salinity solution for a wind speed of -10.5 cm/s. The reader is referred to the caption to figure 4.5 for a full description of the individual panels.

the salinity is larger close to the boundary, than at the boundary itself. A large negative gradient is present within the first km from the ocean. For points further away from the ocean, the gradient is similar to that of the maximum salinity solution for unstable stratification for the EMM, as determined by the fact that the $\Sigma_x - \Sigma$ characteristic overlaps with the analytical characteristic.

The local extremum in the vertical average of the salinity does not correspond to a local extremum in the salinity itself, as seen in figure 4.14. This figure shows a heat map of the salinity near the boundary. In contrast to earlier heat maps, red and blue do not correspond to positive and negative values respectively, but to relatively high or relatively low values. It is seen that the salinity has a local minimum on the bottom of the oceanic boundary. In transitioning from the large imposed stratification to the smaller stratification in the interior, the salinity at the bottom rapidly changes in the boundary layer, while the salinity at the surface does not show large horizontal gradients. This causes the vertically averaged salinity to decrease towards the ocean. Since the local maximum of the vertically averaged salinity in the interior of the domain does not correspond to a local maximum of the salinity, the maximum principle for elliptic equations is not violated

[34].

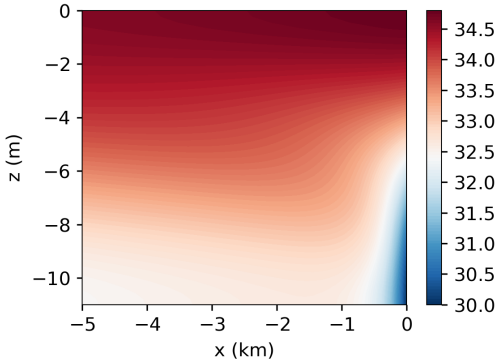

Figure 4.14: Close-up of the salinity for the high salinity solution near the boundary (psu)

Since both 4.13b and 4.13c have already been discussed in previous sections, we refer to sections 4.1.3 and 4.3.1, respectively, for a detailed discussion of these figures. A heat map for the vertical deviation in salinity s' can be seen in figure 4.13d. The estuary is unstably stratified throughout the estuary, which corresponds to the salinity structure of the maximum salinity solution for unstable stratification in the EMM. In the outer region, the degree of stratification slowly increases as x increases. In the boundary layer, the stratification is particularly small.

The bottom center panel shows the horizontal velocity. Circulation is counterclockwise throughout the estuary, the magnitude of which is constant apart from the boundary layer. Here, the degree of stratification increases towards the ocean. The final panel shows that vertical velocity is only significant in the boundary layer. In this region, appreciable downwards motion is observed.

4.4.2. Decomposition

In order to expand on the insight gained during the previous section, this section will present a decomposition of the horizontal velocity and salinity profile into contributions from different transport mechanisms. The aim of the decomposition is to check whether the transport balance for the interior of this solution matches the transport balance found on the left branch of the characteristic from the EMM. Moreover, this decomposition will inform about the transport mechanisms that are featured in the boundary and interior layers.

Figure 4.15 displays the decomposition of the horizontal velocity. In the boundary layer, gravitational circulation, wind stress and momentum advection have significant contributions. In the interior layer, the horizontal velocity is the superposition of a wind contribution and a contribution from momentum advection, with a small river discharge contribution. Both the contributions from wind stress and gravitational circulation are counterclockwise. Momentum advection reacts to the change in horizontal velocity that happens between the boundary layer and the outer solution, and makes sure that this change happens more gradually. In the outer region, the formation of the horizontal velocity is dominated by wind.

Figure 4.16 displays the contributions to the vertical salinity profile. Note that a number of transport contributions have been capped to a maximum magnitude in the boundary layer. In the boundary layer, wind stress, gravitational circulation, momentum advection and horizontal diffusion all have signi ficant contributions to the profile of the horizontal velocity. In the interior layer, the salinity profile is the sum of the contributions from momentum advection and wind stress. In this region, the wind contribution from wind stress decreases as the distance to the ocean decreases. This is caused by the fact that the contribution from momentum advection increases as the distance to the ocean decreases, mirroring the increase in the corresponding contribution in the velocity profile. In this way, the sum of the two contributions is relatively constant. Due to the fact that momentum advection enforces the type of stratification and circulation associated with wind stress in the interior layer, a smaller contribution from wind is required to satisfy the transport balance. This makes sure that the transport balance is satisfied for lower salinity gradients, which explains why the salinity gradient in this regime is lower than the gradient corresponding to the analytical characteristic. In the outer region, the contribution from momentum advection has become negligible, and wind stress dominates the salinity profile.

For the outer region, it can be concluded that the velocity and salinity profiles are dominated by wind,

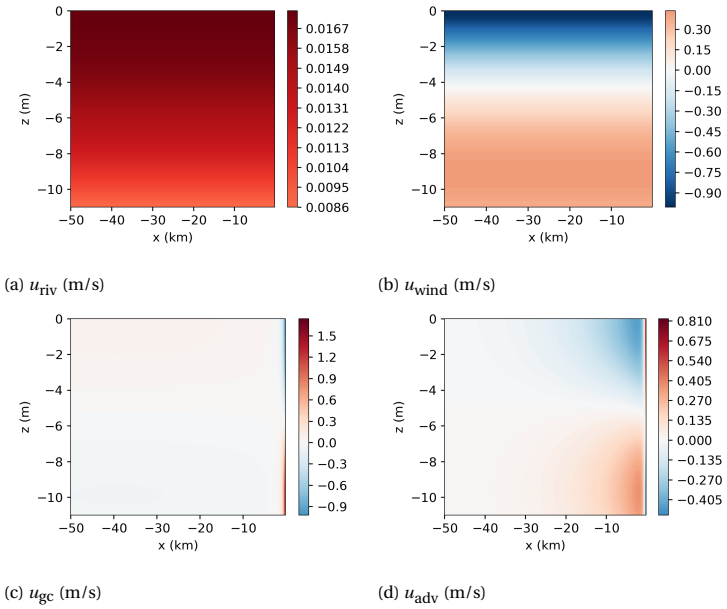

(a) u_{riv} (m/s) (b) u_{wind} (m/s)

(c) u_{gc} (m/s) (d) u_{adv} (m/s)

Figure 4.15: Decomposition of the high salinity solution for a wind speed of -10.5 m/s, into contributions from river discharge, wind stress, gravitational circulation and advection

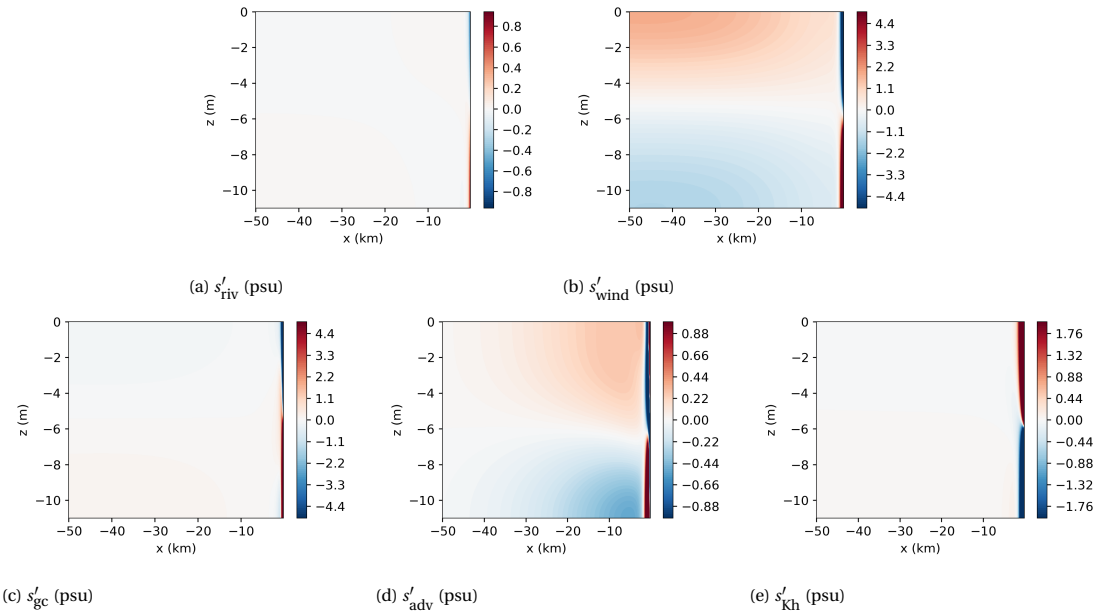

(a) s'_{riv} (psu) (b) s'_{wind} (psu)

(c) s'_{gc} (psu) (d) s'_{adv} (psu) (e) s'_{Kh} (psu)

Figure 4.16: Decomposition of the salinity of the high salinity solution for a wind speed of -10.5 m/s, into contributions from river discharge, wind stress, gravitational circulation, advection and horizontal diffusion.

which is expected behaviour for the left branch based on the results from the EMM. In the interior layer, momentum advection also has a significant contribution. Finally, in the boundary layer, the velocity and salinity profiles are shaped by a combination of contributions from wind stress, gravitational circulation, momentum advection and horizontal diffusion.

4.4.3. Solution for different wind speeds

This overview of the $\Sigma_x - \Sigma$ characteristics for different wind speeds in figure 4.17 confirms that being positioned on the left branch in the interior of the domain is a defining feature of this solution. In the bottom two panels, the onshore wind speed is of such magnitude that the right branch is not visible. However, outside of the visualized domain, local extrema are present in the analytical characteristic, such that clearly defined left

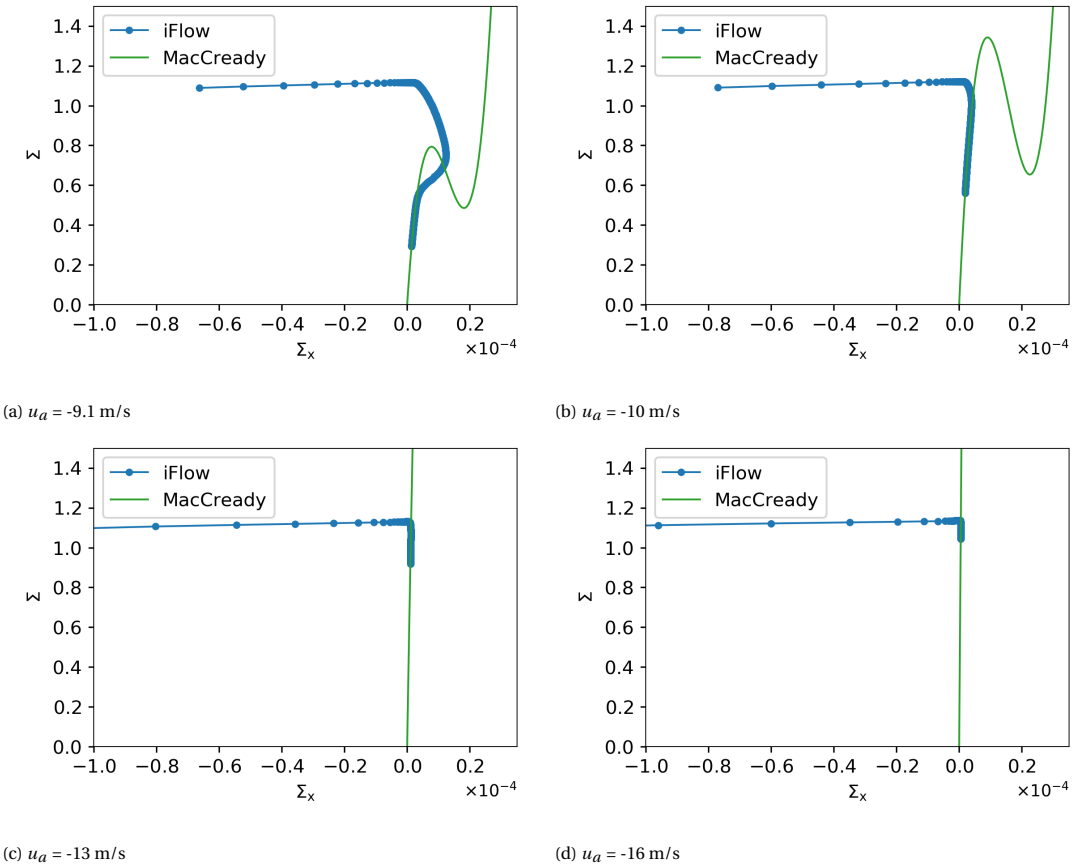

(a) u_a = -9.1 m/s

(b) u_a = -10 m/s

(c) u_a = -13 m/s

(d) u_a = -16 m/s

Figure 4.17: Close-up of the $\Sigma_x - \Sigma$ characteristic for the high salinity solution for a range of wind speeds

and right branches are present for any of the considered wind speeds.

Moreover, for any wind speed, the left branch is approached from the left. Every solution has a section with a negative salinity gradient, such that the vertical average of salinity has a local maximum. As the magnitude of the onshore wind speed increases, the gradients in the boundary layer become larger (more negative), meaning that the dynamics in the boundary layer become more extreme as the wind stress becomes more extreme.

Looking at the first panel, which displays the minimum feasible magnitude of the onshore wind speed for which this solution is valid, it can be seen that for this solution, the maximum salinity of the left branch in the analytical model, is significantly lower than the salinity at the oceanic end. This indicates that in a MacCready context, this solution would not be feasible. In a similar manner to the mid salinity solution, a combination of a boundary layer and an interior layer is formed that connects the high salinity of $\Sigma = 1.1$ to the lower salinities that are required for the left branch. This solution is similar to the solution for the minimum onshore wind speed for the mid salinity solution. A small difference is present between this plot and figure 4.12a, due to the fact that the found minimum onshore wind speed differs slightly between the two solution branches. This is due to the fact that solutions become hard to obtain for the Newton-Raphson algorithm.

Like the mid salinity solution, this solution is only feasible for unstable stratification at the boundary. Unlike the other two solutions, the boundary layer does not arise from differences between the stratification at the boundary and stratification in the outer region. As a result, no salinity profile can be prescribed at the boundary that eliminates the boundary layer entirely.

4.5. Topological structure

Three different solutions have been found within the extended Dijktra model. The feasible domain and stability properties of the low salinity solution will be discussed first, followed by a section covers these aspects for the mid and high salinity solutions simultaneously. Subsequently, an overview of the full topological struc-

ture will be given. The feasible domain is the set of all $s_{\text{strat}} - u_a$ pairs for which a solution exists, considering all other parameters fixed.

4.5.1. Low salinity solution

The low salinity solution is feasible for any stratification at the boundary and any wind speed. However, above a critical onshore wind speed and in a region around a wind speed of zero, the solution cannot be obtained numerically using the grid introduced in section 4.2. First, the critical onshore wind speed will be discussed, followed by a discussion of the infeasible region.

For onshore wind speeds that is larger in magnitude than the critical onshore wind speed, the boundary layer can become so small that the grid resolution is not sufficient to resolve the boundary layer. For the grid resolution used in the computations in this chapter, a maximum onshore wind speed is therefore encountered. This limit is eliminated by increasing the grid resolution. No limit is therefore expected for the analytical counterpart of this solution.

Secondly, we will go over the region located near wind speeds of 0 m/s, where the solution cannot be retrieved numerically. In this set of wind speeds, no solution can be found by the Newton-Raphson algorithm. The set of wind speeds depends on the stratification applied at the boundary. For stratification that is sufficiently negative, corresponding to stable stratification, the infeasible region does not exist. The solutions at the boundary of the infeasible region do not provide visible clues. The stability analysis in appendix D.1 reveals that analytical solutions are possible within the infeasible region, but that these are not numerically resolvable. It is unclear why this happens. Moreover, the stability analysis in appendix D.1 reveals that all eigenvalues for the low salinity solution are negative. This is therefore a stable solution.

4.5.2. Mid and high salinity solution

The mid and high salinity solutions have the same feasible domains. As has been suggested in sections 4.3.3 and 4.4.3, this domain features a minimum (in magnitude) onshore wind speed. The reason for this minimum onshore wind speed is that the maximum salinity of the left branch of the $\Sigma_x - \Sigma$ characteristic is too low with respect to the oceanic salinity. This is the same reason as to why there is a minimum onshore wind speed to solutions with unstable stratification at the boundary in the EMM. At this boundary, the solutions obtained by the high and mid salinity solutions are identical.

In addition, a minimum salinity stratification is required at the boundary. The minimum stratification at the oceanic boundary is highly dependent on the grid size in the region near the boundary. Based on the observed relation between grid size and minimum stratification, the expectation is that for analytical solutions to exist, unstable stratification is required.

Like the low salinity solution, the mid salinity solution cannot be obtained numerically above a critical onshore wind speed for coarse grids. This maximum onshore wind speed is eliminated by refining the grid.

The stability analyses performed in appendices D.2 and D.3 show that the mid salinity solution is unstable and that the high salinity solution is stable. If the mid salinity solution is perturbed with a perturbation that contains a non-zero component of the unstable eigenvector, it will either move towards the low salinity solution or towards the high salinity solution, depending on the sign of the component of the unstable eigenvalue. Moreover, the maximum eigenvalue of the mid and high salinity solutions are both shown to move towards zero as the minimum onshore wind speed is approached.

4.5.3. Dynamic structure

Using the analyses of the feasible domains and the stability properties of the three solutions, a three-dimensional bifurcation diagram can be created. This features the wind speed and the boundary stratification on the horizontal axes, and the vertically averaged salinity at a reference point in the estuary, in this case $x = -100$ km, on the vertical axis. This three-dimensional bifurcation diagram is plotted in figure 4.18. It can be seen that the low salinity solution is disjoint from the two other solutions, while the mid and high salinity solution are similar, and obtain the same salinity at the critical onshore wind speed. Moreover, the salinities of the two solutions move towards each other as the unstable stratification is decreased. The point where the two solutions meet is not numerically resolved, as explained above.

As the three-dimensional bifurcation diagram might be hard to read, two two-bifurcation diagrams have been made, as displayed in figure 4.19. These diagrams also show the stability of the different solutions. These diagrams are sketches of the relations between the wind speed and the vertically averaged salinity at a

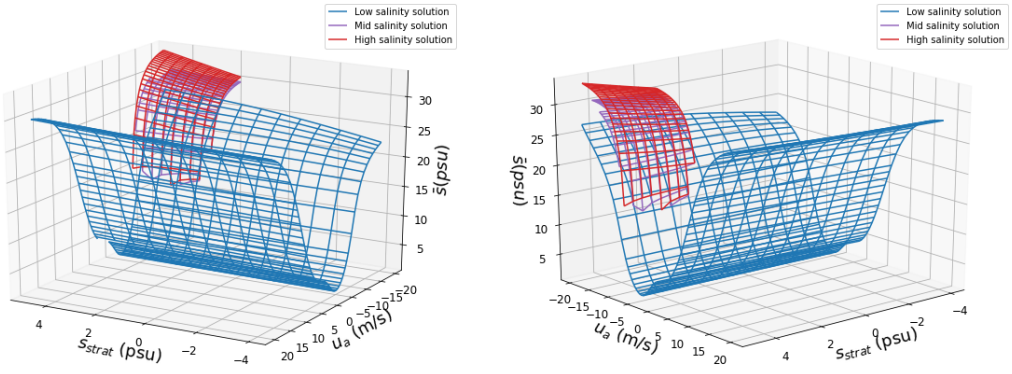

Figure 4.18: A three-dimensional bifurcation diagram from 2 different angles. The z axis represent the vertically averaged salinity at $x = -100$ km, while the horizontal axes represent boundary stratification and wind speed

reference point. Since the diagram is a sketch, rather than a quantitatively accurate figure, it should only be used conceptually, and so the axes lack ticks.

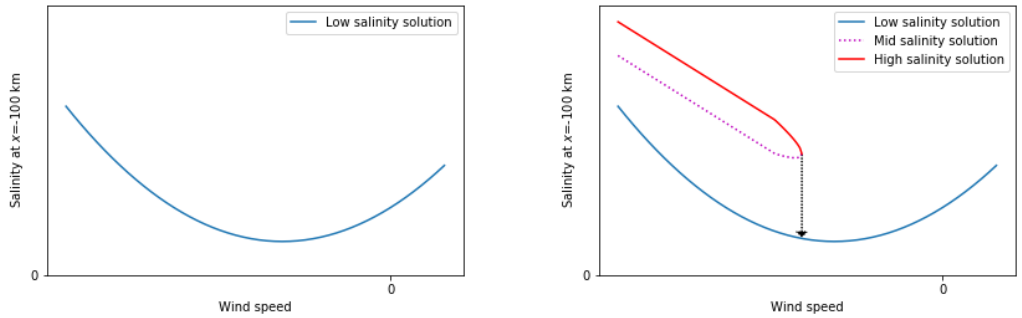

(a) Stable stratification

(b) Unstable stratification

Figure 4.19: Sketch of bifurcation diagram for imposed stable and unstable stratification at the oceanic boundary.

For stable stratification, only the low salinity solution is feasible. This solution is stable throughout the entire domain. The low salinity solution corresponds to the minimum salinity solution for stable stratification at the boundary in the EMM.

For unstable stratification, all three solutions are possible. The low salinity solution is feasible for any wind speed and is stable. The mid and high salinity solutions both only exist below a critical wind speed. At this maximum wind speed, the two solutions are equal, and a fold bifurcation occurs. As similar fold bifurcation occurs at the critical imposed stratification at the oceanic boundary. This fold bifurcation is not visualized in figure 4.19. The mid salinity solution is unstable, while the high salinity solution is stable.

4.6. Conclusion

First, an overview will be given of the solutions found in the EDM for the different wind speeds. Table 4.2 lists, for different sets of wind speeds: the relevant range of wind speeds, the type of salinity stratification typically found per solution and the number of solutions. This chapter has answered three of the six research questions formulated in section 1.5. Research questions 4 and 5 will be covered in this conclusion, for the answer to question 6, the reader is referred to figure 4.19.

Question 4 was which solutions from the EMM are valid in the EDM, and how these solutions differ between the two models. We will first answer which solutions from the EMM are valid in the EDM. For offshore or small onshore wind speeds the EMM found one solution, with stable stratification at the boundary. This solution is valid in the EDM. For medium and large wind speeds, infinitely many solutions with stable salinity stratification were found in the EMM. In the EDM, only one of these solutions was valid: the solution with stable stratification at the boundary with minimum salinity. In addition, for large wind speeds, an infinite

Wind speed	Wind speed (m/s)	Stratification in outer region(s)	# of solutions
Offshore	$u_a > 0$	Stable	1
Small Onshore	$-4.5 < u_a < 0$	Near sea: stable Far from sea: unstable	1
Medium Onshore	$-9.5 < u_a < -4.5$	Near sea: stable Far from sea: unstable	1
Large Onshore	$-13 < u_a < -9.3$	High salinity solution: unstable throughout Mid salinity solution: unstable throughout Low salinity solution: Near sea: stable Far from sea: unstable	1 ($s_{strat} \lesssim 0$) 3 ($s_{strat} \gtrsim 0$)
Very Large Onshore	$u_a < -13$	High salinity solution: unstable throughout Mid salinity solution: unstable throughout Low salinity solution: Near sea: stable Far from sea: unstable	1 ($s_{strat} \lesssim 0$) 3 ($s_{strat} \gtrsim 0$)

Table 4.2: Overview of the solutions for the different wind speeds, including the relevant range of wind speeds, the type of salinity stratification typically found in the outer region(s) per solution and the number of solutions

number of solutions with unstable stratification at the oceanic boundary was found in the EMM as well. Of these solutions, only the solution with maximum salinity was found to be feasible in the EDM. Two versions of this solution were found in the EDM. Both are equivalent to the maximum salinity solution in the EMM in the interior of the domain, but differ in the boundary and interior layers. For very large wind speeds, only one solution was found in the EMM, which is similar to the maximum salinity solution for large winds speeds. The two versions of this solution in the EDM were found for very large wind speeds as well. Moreover, a solution similar to the minimum salinity solution for unstable stratification at the boundary found for medium and large wind speeds in the EMM, was also found in the EDM for very large wind speeds.

The solutions found in the EDM typically start with a boundary layer at the oceanic end, in which a host of transport mechanisms, including horizontal diffusion of the vertical deviation in salinity, is relevant to the transport balance. Next, an interior layer arises, which has similar dynamics as the MacCready solution, with the addition of a contribution from momentum advection. This contribution from momentum advection is a reaction to the large horizontal gradient in the gravitationally induced horizontal velocity between the boundary layer and the outer region. After this interior layer, an outer region is typically found, where the solutions are accurately described by the EMM. The solutions equivalent to a solution in the EMM with a discontinuous horizontal salinity gradient then feature a second interior layer, with significant contributions from momentum advection and horizontal diffusion. This type of solution then features a second outer region, where the solution from both models are similar again. It should be noted that for large onshore wind speeds, the first outer region does not exist in these solutions. The outer regions are accurately described by the EMM, while the boundary layers and interior layer are not described by the EMM.

In chapter 3, it was wondered whether the solutions that had multiple transport regimes, separated by a discontinuous transition, had analogues in the EDM. It can be confirmed that such solutions are possible within this model

Finally, question 5 asks whether the EMM can be used to analyse the results from the EDM. The $\Sigma_x - \Sigma$ characteristic from the EMM has proven to be an indispensable tool in the analysis of the results of this model. It has, amongst others, been useful in characterizing solutions, identifying distinct regions within a solution, checking for numerical convergence (see appendix C) and understanding the sets of parameters for which solutions exist.

5
Conclusion

The main goal of this thesis was to develop and analyse a conceptual width averaged sub-tidal model on the effects of wind stress in partially mixed or well mixed estuaries. This conclusion will systemically answer the six questions raised in section 1.5, before providing suggestions for future research.

5.1. Research questions

Firstly, it has been found that MacCready's model can be extended to include wind stress, by using the exact same procedure to develop the model and obtain solutions to that model as was used by MacCready. The extension fits neatly in the existing framework. A major difficulty that did arise was that the applied method no longer gives rise to unique solutions. For certain onshore wind speeds, an infinite number of solutions is found to be possible. The fact that solutions cannot be determined unambiguously is a phenomenon that is not necessarily unique to this extension of the model. Extending the model to include other forcings could lead to similar situations.

The second question that was raised was what equilibrium solutions are found by this model. For offshore wind speeds, a unique solution was found that was stably stratified throughout the estuary and featured regular gravitational circulation. It was seen that wind stress enhances the circulation and stratification caused by gravitational circulation, increasing salt intrusion. For small onshore wind speeds, a similar unique solution was found. However, as the wind direction is flipped, wind stress partially counters the circulation and stratification caused by gravitational circulation, decreasing the salt intrusion length. For points far from the ocean, the absence of salinity caused wind stress to be dominant in the transport balance, resulting in unstable stratification. For medium onshore wind speeds, an infinite amount of equilibrium solutions is possible within the extended MacCready model. These solutions contain one or more regions where the contribution from gravitational circulation is slightly larger than the opposing contribution from wind stress, as well as one or more regions where the contribution from gravitational circulation is negligible compared to the contribution from wind stress. In the former region, stratification is stable and the circulation pattern typical of gravitational circulation, while in the latter region stratification is unstable and the mode of circulation is the reverse of typical gravitational circulation. In these solutions, discontinuous transitions between the two physical regimes were featured. The solution is always in the gravitational regime near the oceanic end, and in the wind dominated regime at points far from the ocean. For large wind speeds, the same solutions were possible, as well as solutions which are in the dominated regime at the oceanic boundary. As a result, solutions are possible that are unstably stratified throughout the entire estuary and feature circulation in the inverse direction of the typical direction caused by gravitational circulation. For even larger wind speeds, the latter solution is the only type of solution possible.

In light of question 3, it is clear that the solutions to the extended MacCready model are analysed best using the $\Sigma_x - \Sigma$ characteristic. The characteristic can be used to identify different types of solutions, and the physical regime at each point in the estuary can be determined from the characteristic. Moreover, the characteristic can be used to determine under what circumstances a transport balance is feasible, by determining when the corresponding branch of the $\Sigma_x - \Sigma$ characteristic is available.

Fourth, it was asked which of the solutions from the extended MacCready model are possible within the extended Dijkstra model. The unique solution that was present for offshore or small onshore winds in the first

model is also found in the extended Dijkstra model, and has similar properties. For medium wind speeds, where infinitely many solutions are found with stable stratification at the boundary, only the minimum salinity solution is feasible in the extended Dijkstra model. For large wind speeds, infinitely many solutions were possible in the extended MacCready model, of which both solutions with stable stratification and solutions with unstable stratification at the oceanic end are possible within Dijkstra's model. In the extended Dijkstra model, the minimum salinity solution with stable stratification at the ocean and the maximum salinity solution with unstable stratification at the ocean were the only solutions possible solutions. Two versions of the latter solution were found, adding up to a total of three solutions. Finally, for very large wind speeds, a unique solution was found in the EMM, whereas in the EDM the same solutions were obtained as those found for large wind speeds. In the outer regions of the solutions, the solutions from the EDM and the EMM typically agree on the salinity and velocity, as well as on the dominant transport balance. The solutions from the EDM feature boundary layers and interior layers, in addition to these outer regions. These boundary layers have large contributions from diffusion and momentum advection, which are both neglected in the EMM. All in all, the only major difference between the two models is that whenever the EMM finds an infinite amount of solutions, the EDM reduces this to one or three solutions.

In the analysis of the solutions from the extended Dijkstra model, it was seen that the $\Sigma_x - \Sigma$ characteristic from the EMM is of great value. The characteristic has been succesfully used to characterize solutions, to identify equivalent solutions in the extended MacCready model, to identify distinct regions which are described by different physical processes within a solution, to check for numerical convergence and to understand why some solutions are only possible for certain parameter regimes. Studying how a parameter affects the characteristic provides direct insight into how a parameter affects the solutions that are possible within the model.

Finally, the stability properties of the solutions in Dijkstra's model have been assessed. In the EDM, three different solutions were found. The first solution, corresponding to the minimum salinity solution in the extended MacCready model, was found to be stable throughout the entire domain. The other two solutions are similar to each other and both correspond to the maximum salinity solution for unstable stratification at the boundary in the extended MacCready model. Of these two solutions, one was found to be stable, while the other was unstable. Moreover, these solutions were both only possible for a sufficiently large onshore wind speed. At this minimum wind speed, a fold bifurcation occurs.

5.2. Future research

We will proceed by making four recommendations for further research. These recommendations primarily serve to verify whether the conclusions from this thesis can be expected to hold true in physical cases. It is especially wondered whether estuaries that are (partially) dominated by onshore wind and feature unstable stratification and counterclockwise circulation are physically possible. For conclusions that do not hold true physically, it is of interest which assumptions made in the derivation of the models used has enabled these conclusions to be obtained. The conclusions from this thesis can only be used as leads for future research, since without further research, it is unclear which conclusions from this thesis are applicable in physical cases.

In the models used, the viscosity and diffusivity are assumed constant in space and time, and independent of wind speed. Physically, we would expect the eddy viscosity and eddy diffusivity to increase with increased wind speed as a result of the larger velocities obtained in the estuaries. It has been shown that beyond a certain wind speed, the turbulence caused by the increased wind speed has a larger effect than the added wind stress [19]. As shown in 3.7, this could cause unstable stratification and reverse circulation to become infeasible. As a recommendation for further research, it is therefore suggested to incorporate parametrisations for the viscosity and diffusivity that depend on the wind speed or the dynamics in the estuary, in order to determine whether the conclusion drawn for this model still holds.

A second suggestion is to use simulations like done by Lange and Burchard in 2020, to study the effect of onshore wind for prolonged periods of time. In that study, reverse circulation caused by onshore wind is found. Since the study considers transient behaviour on a time scale that is too fast for the salinity to fully adjust, it is unclear whether unstable stratification is not found because the estuary has not had the chance to fully adjust to the onshore wind speed, or whether no steady-state solutions with stable stratification exist. The models studied in this thesis assume that the horizontal and vertical mixing coefficients are constant over the tidal period and constant over the width of the estuary. If as a result of varying mixing coefficients, stratification is reduced in magnitude at points in time or space where stratification is unstable, and increased

in magnitude at places where stratification is stable, the width-averaged sub-tidal salinity profile will tend to stable stratification. Since the model by Lange and Burchard allows for varying turbulence, a study as just described could determine whether the fact the turbulence is non-constant causes unstable stratification to become infeasible, or whether unstable stratification is actually obtained within the context of that model.

Thirdly, it was found in both models that stable stratification was reduced by offshore wind and increased by onshore wind, which is the opposite of the conclusions drawn by Chen and Sanford. It is hypothesized that the results for Chen and Sanford are obtained for a parameter regime that is more diffusive than the regime studied for the majority of this thesis. It has been shown that the results from Chen and Sanford are recovered in the models when diffusivity is increased. It is worth studying whether the relation found between stratification and wind speed in this thesis can also be found by Chen and Sanford, if a less diffusive regime is studied.

Finally, it is recommended to apply the $\Sigma_x - \Sigma$ characteristic to results from different models or empirical studies in order to determine how broadly applicable the tool is. In the extended Dijkstra model, which has a great number of similarities to the extended MacCready model, the $\Sigma_x - \Sigma$ characteristic was a valuable tool. If the characteristic can also be used successfully for empirical studies or models that differ more from the extended MacCready model, this provides a powerful tool for the analysis of these results. Case studies for the $\Sigma_x - \Sigma$ characteristic are not required to include the effects of wind stress, as the $\Sigma_x - \Sigma$ characteristic can also be applied when this effect is not taken into account. An example of a study that can possibly be analysed with the use of the $\Sigma_x - \Sigma$ characteristic is the mentioned study by Chen and Sanford.

A

Derivation of salinity equation for the extended MacCready model

In this appendix, the salinity equation for the extended MacCready model will be derived from equation 2.44, using the assumptions listed in section 2.3.1. For the salinity equation, the time derivative of s can be eliminated, since equilibria are sought. This leaves

$$us_x + ws_z = K_s s_{zz} + K_H s_{xx}. \tag{A.1}$$

Using the continuity equation, we can write the advective terms as

$$us_x + ws_z = (\bar{u}\bar{s})_x - \bar{u}_x\bar{s} + \bar{u}_x s' + \bar{u}s'_x + u'\bar{s}_x + (u's')_x + (ws')_z. \tag{A.2}$$

Since $s'_x \ll \bar{s}_x$, $\bar{u}s'_x$ is dominated by $\bar{u}\bar{s}_x$ and can hence be dropped. In section 2.3.1. It is assumed that $(ws')_z$, the vertical advection of s', is negligible. This term is dropped. Moreover, it is assumed that the vertically varying contribution of $(u's')_x$ is negligible, but that the vertically averaged contribution is significant. The term $(u's')_x$ is therefore replaced by $(\overline{u's'})_x$. Here, $\overline{u's'}$ indicates the vertical average of $u's'$, rather than the product of their individual averages, which is zero. After these assumptions, the advective term becomes as in equation A.3.

Additionally, $s'_{xx} \ll \bar{s}_{xx}$ is assumed in order to reduce $K_H s_{xx}$ to $K_H\bar{s}_{xx}$. In order to simplify the expressions, the assumption that $A_v = K_v$ is used. Applying these assumptions lead to the following salinity equation:

$$(\bar{u}\bar{s})_x - \bar{u}_x\bar{s} + \bar{u}_x s' + u'\bar{s}_x + (\overline{u's'})_x = K_H\bar{s}_{xx} + A_v s'_{zz}. \tag{A.3}$$

B

Galerkin coefficients for the extended Dijkstra model

This appendix will list the Galerkin coefficients introduced in section 2.4.3.

$$G^b_{1,k} = \int_{-1}^{0} c_k^2 d\sigma, \tag{B.1}$$

$$G^b_{2,km} = \int_{-1}^{0} c_m c_k (\sigma + 1 + R) d\sigma, \tag{B.2}$$

$$G^b_{3,km} = \frac{1}{\lambda_m} \int_{-1}^{0} c_k (s_m + \sin(\lambda_m)) d\sigma, \tag{B.3}$$

$$G^b_{7,km} = \int_{-1}^{0} \bar{c}_m (\sigma + \frac{3}{2}) \bar{c}_k d\sigma, \tag{B.4}$$

$$G^b_{8,km} = m\pi \int_{-1}^{0} \bar{s}_m \bar{c}_k d\sigma, \tag{B.5}$$

$$G^b_9 = 1. \tag{B.6}$$

Here

$$c_m = \cos(\lambda_m \sigma), \tag{B.7}$$

$$s_m = \sin(\lambda_m \sigma), \tag{B.8}$$

$$\bar{c}_m = \cos(m\pi\sigma), \tag{B.9}$$

$$\bar{s}_m = \sin(m\pi\sigma). \tag{B.10}$$

The coefficients not listed in this appendix are found in the supplement to Dijkstra's paper [22].

C

Grid convergence for the extended Dijkstra model

In order to validate whether the solution is fully converged, the low salinity solution has been computed for a range of grid sizes. Figure C.1 depicts the $\Sigma_x - \Sigma$ characteristic for each of the solutions. The panels only show the left branch, so that small deviations in the $\Sigma_x - \Sigma$ can be seen more easily. It can be seen that for 50

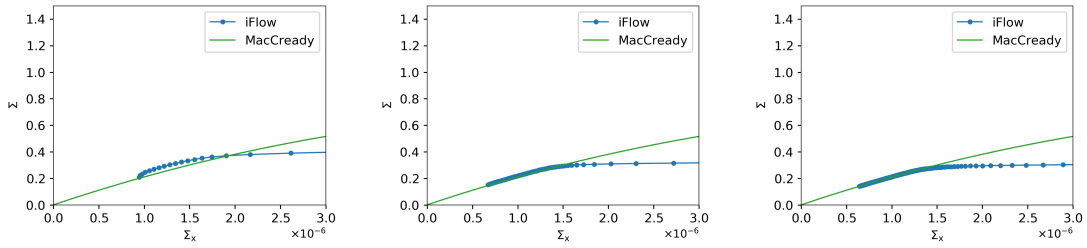

(a) 50 grid points (b) 150 grid points (c) 400 grid points

Figure C.1: Close-up of the $\Sigma_x - \Sigma$ characteristic for a wind speed of -9 m/s, a stratification of 4.8 psu and a range of grid sizes

grid points, a slight discrepancy is present between the $\Sigma_x - \Sigma$ characteristics for the extensions of Dijkstra's and MacCready's models. As the number of grid points increases, the characteristics of the solutions become closer to the analytical characteristic. For the used grid of 400 grid points, the characteristic is well converged. This shows that the $\Sigma_x - \Sigma$ characteristic can be used to check whether the grid used is fine enough on the parts of the solution that described by the extended MacCready model, bearing in mind that other factors besides grid size can cause a discrepancy between the analytical and realized characteristics. If the two characteristics do not match, it should be tested whether increasing the grid resolution brings these closer together. A similar analysis will not be presented for the other two solutions, since these yield identical results.

D

Stability of the solutions in the extended Dijkstra model

D.1. Low salinity solution

The eigenfunctions and eigenvalues of this solution have been determined according to section 2.4.7. These will be studied in this section. A plot of the maximum eigenvalues as a function of wind speed for two different prescribed levels of stratification can be found in figure D.1.

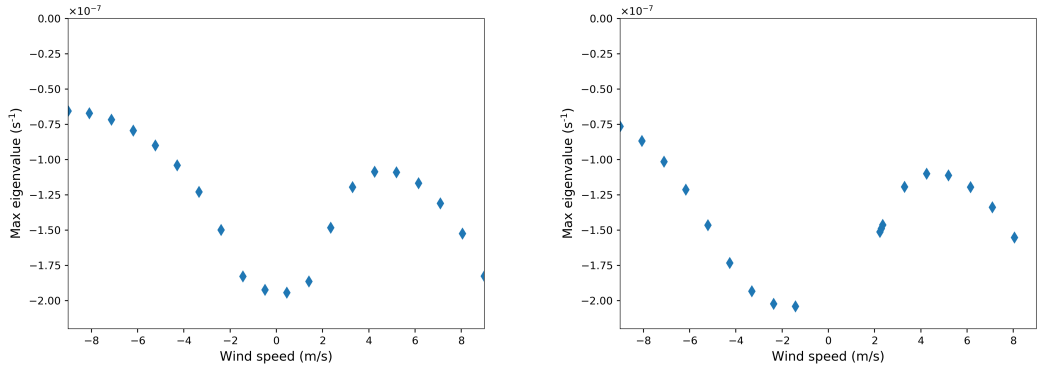

(a) s_{strat} = -8 psu (stable)

(b) s_{strat} = 4.8 psu (unstable)

Figure D.1: Maxium eigenvalue vs wind speed for the low salinity solution for two different stratifications at the boundary.

The first panel displays the largest eigenvalues for a stratification of -8 psu at the boundary, which corresponds to stable stratification. For this stratification, the low salinity solution has no infeasible region. It can be seen that all eigenvalues are negative, and that the eigenvalues are a continuous function of wind speed.

The second panel shows the largest eigenvalues for an unstable stratification of 4.8 psu. For this stratification, an unfeasible region is present, as described in section 4.5.1. Like in the first panel, all eigenvalues are negative. Moreover, the curve is similar to the curve of the first panel, except from the fact that the eigenvalues in the infeasible region are missing. The eigenvalues do not show aberrant behaviour as the infeasible region is approached, but continue to follow a smooth curve similar to that in displayed in figure D.1a. This suggests that analytical solutions are available in the infeasible set, but that these cannot be recovered numerically.

D.2. Mid salinity solution

The maximum eigenvalues for this solution are plotted against the wind speed in figure D.2. For this solution, one eigenvalue had a positive real part. This implies that the solution is unstable. In this figure, the eigenvalues do not go to zero, as the minimum onshore wind speed on the right-hand side of the figure is reached. In section 4.4.3, it is shown that the high salinity solution moves to the mid salinity solution as the

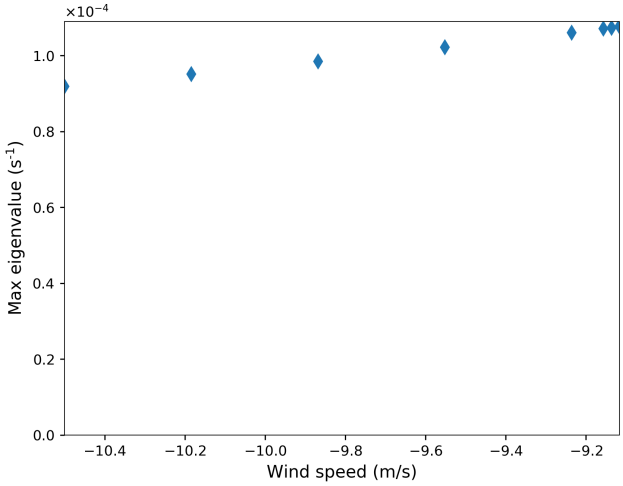

Figure D.2: Characteristics of the eigenvalues of the mid salinity solution versus wind speed for a stratification of 4.8 psu

minimum onshore wind speed is approached. Moreover, section D.3 shows that the eigenvalues of the high salinity solution go to zero as the minimum wind speed is approached. The minimum wind onshore speed (least negative) obtained for the high salinity solution is slightly lower than the minimum wind speed found for the mid salinity solution. It is therefore argued that the eigenvalues of the mid salinity go to zero as the minimum wind speed is approached, but that the wind speeds for which this can be seen are not reached by the continuation procedure used.

As said above, the mid salinity solution has one positive eigenvalue. Figure D.3 depicts the eigenvector corresponding to this eigenvalue. Perturbing the mid salinity solution according to this eigenvector will cause the perturbation to increase. The first panel shows the perturbation in the vertically averaged salinity. It is

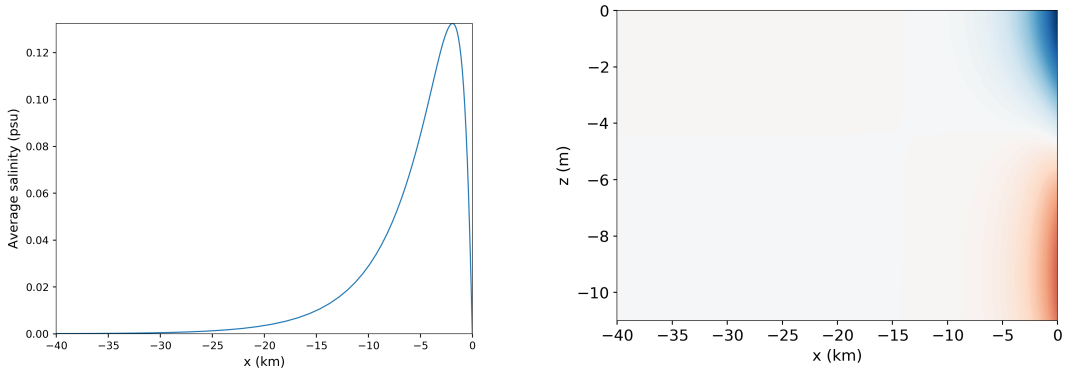

(a) Vertically averaged salinity

(b) Horizontal velocity

Figure D.3: A few characteristics of the eigenvector belonging to the largest eigenvalue for a wind speed of 10.5 m/s and a stratification of 4.8 psu

seen that the perturbation increases the vertically averaged salinity in the first kilometers near the boundary. The second panel shows a heat map of the perturbation if horizontal velocity. Here, it can be seen that the perturbation enhances the counterclockwise circulation related to wind drive circulation, or decreases the clockwise circulation related to gravitational circulation.

As will be identified in section 4.4.1, the high salinity solution has a distinctly higher average salinity near the oceanic boundary than the mid salinity solution. Moreover, the counterclockwise circulation near the boundary is stronger for the high salinity solution than for the mid salinity solution. A positive perturbation of the type displayed in D.3 is therefore expected to causes the mid salinity solution to move to the high salinity solution.

Moreover, the vertically averaged salinity near the boundary is lower for the low salinity solution than for the mid salinity solution. Furthermore, the circulation near the boundary is clockwise for the low salinity solution, while it is counterclockwise for the mid salinity solution. A negative perturbation of the type displayed in figure D.3 causes a decrease in the salinity near the boundary, and forces the circulation near the boundary from counterclockwise circulation towards clockwise circulation. Negative perturbations of the mid salinity solution of this type are therefore expected to force the mid salinity solution towards the low salinity solution.

D.3. High salinity solution

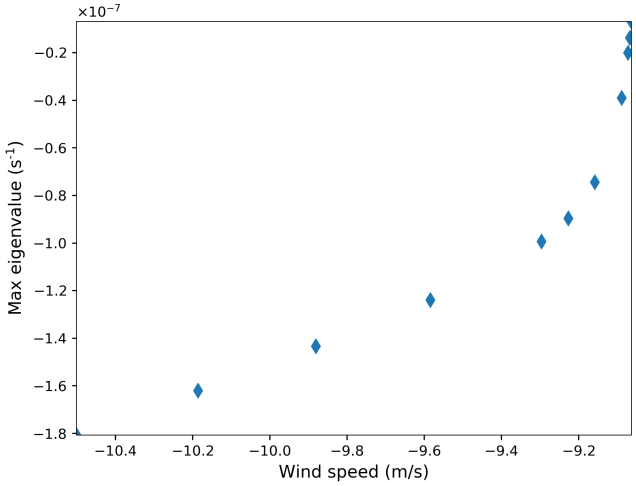

Figure D.4: Characteristics of the eigenvalues of the high salinity solution versus wind speed for a stratification of 4.8 psu

Finally, the stability of the high salinity solution will be analysed. An overview of the largest eigenvalue as a function of the wind speed can be found in figure D.4. It is clear that the solution is stable throughout, and that the eigenvalues move to zero as the wind speed decreases towards the maximum wind speed (smallest magnitude).

Bibliography

[1] A. de Brauwere, B. de Brye, S. Blaise, and E. Deleersnijder, "Residence time, exposure time and connectivity in the Scheldt Estuary," *Journal of Marine Systems*, vol. 84, pp. 85–95, Feb. 2011.

[2] H. Liu, N. Yoshikawa, S. Miyazu, and K. Watanabe, "Influence of saltwater wedges on irrigation water near a river estuary," *Paddy and Water Environment*, vol. 13, pp. 179–189, Apr. 2015.

[3] J. H. Sharp, L. A. Cifuentes, R. B. Coffin, J. R. Pennock, and K.-C. Wong, "The influence of river variability on the circulation, chemistry, and microbiology of the Delaware Estuary," *Estuaries*, vol. 9, pp. 261–269, Dec. 1986.

[4] R. Zhao, Z. Yang, T. Sun, B. Chen, and G. Chen, "Freshwater inflow requirements for the protection of the critical habitat and the drinking water sources in the Yangtze River Estuary, China," *Communications in Nonlinear Science and Numerical Simulation*, vol. 14, pp. 2507–2518, May 2009.

[5] P. MacCready and W. R. Geyer, "Advances in Estuarine Physics," *Annual Review of Marine Science*, vol. 2, pp. 35–58, Jan. 2010.

[6] E. Ruiz-Castillo, J. Sharples, and J. Hopkins, "Wind-Driven Strain Extends Seasonal Stratification," *Geophysical Research Letters*, vol. 46, no. 22, pp. 13244–13252, 2019.

[7] F. Martinho, R. Leitão, J. M. Neto, H. N. Cabral, J. C. Marques, and M. A. Pardal, "The use of nursery areas by juvenile fish in a temperate estuary, Portugal," *Hydrobiologia*, vol. 587, pp. 281–290, Aug. 2007.

[8] H. N. Cabral, "Comparative feeding ecology of sympatric Solea solea and S. senegalensis, within the nursery areas of the Tagus estuary, Portugal," *Journal of Fish Biology*, vol. 57, no. 6, pp. 1550–1562, 2000.

[9] M. Elliott, M. G. O'Reilly, and C. J. L. Taylor, "The forth estuary: a nursery and overwintering area for North Sea fishes," *Hydrobiologia*, vol. 195, pp. 89–103, 1990.

[10] M. D. E. Haywood, D. J. Vance, and N. R. Loneragan, "Seagrass and algal beds as nursery habitats for tiger prawns (Penaeus semisulcatusand P. esculentus)in a tropical Australian estuary," *Marine Biology*, vol. 122, pp. 212–223, 1995.

[11] D. Pritchard, "Estuarine circulation patterns," *Proceedings of the American Society of Civil Engineers*, vol. 81, pp. 1–11, 1955.

[12] D. Pritchard, "Salinity Distribution and Circulation in the Chesapeake Bay Estuarine System," *Journal of Marine Research*, vol. 11, pp. 106–123, 1952.

[13] D. Hansen, M. Rattray, and U. o. W. D. o. Oceanography, *Gravitational Circulation in Straits and Estuaries*. Technical report (University of Washington. Department of Oceanography), Sears Foundation for Marine Research, 1965.

[14] R. H. Weisberg, "The Nontidal Flow in the Providence River of Narragansett Bay: A Stochastic Approach to Estuarine Circulation," *Journal of Physical Oceanography*, vol. 6, no. 5, pp. 721–734, 1976.

[15] P. C. Chatwin, "Some remarks on the maintenance of the salinity distribution in estuaries," *Estuarine and Coastal Marine Science*, vol. 4, no. 5, pp. 555 – 566, 1976.

[16] P. MacCready, "Toward a unified theory of tidally-averaged estuarine salinity structure," *Estuaries*, vol. 27, pp. 561–570, Aug. 2004.

[17] P. MacCready, "Estuarine Adjustment," *Journal of Physical Oceanography*, vol. 37, pp. 2133–2145, Aug. 2007.

[18] D. K. Ralston, W. R. Geyer, and J. A. Lerczak, "Subtidal Salinity and Velocity in the Hudson River Estuary: Observations and Modeling," *Journal of Physical Oceanography*, vol. 38, pp. 753–770, Apr. 2008.

[19] S.-N. Chen and L. P. Sanford, "Axial Wind Effects on Stratification and Longitudinal Salt Transport in an Idealized, Partially Mixed Estuary," *Journal of Physical Oceanography*, vol. 39, pp. 1905–1920, Aug. 2009.

[20] X. Lange and H. Burchard, "The Relative Importance of Wind Straining and Gravitational Forcing in Driving Exchange Flows in Tidally Energetic Estuaries," *Journal of Physical Oceanography*, vol. 49, pp. 723–736, Mar. 2019.

[21] X. Lange, K. Klingbeil, and H. Burchard, "Inversions of estuarine circulation are frequent in a weakly tidal estuary with variable wind forcing and seaward salinity fluctuations," *Journal of Geophysical Research: Oceans*, June 2020.

[22] Y. M. Dijkstra and H. M. Schuttelaars, "A unifying approach to subtidal salt intrusion modelling in tidal estuaries," *submitted to Journal of Physical Oceanography*, p. 21.

[23] Dijkstra, Y.M., Brouwer, R.L., Schuttelaars, H.M., and Schramkowski, G.P., "The iFlow modelling framework v2.4," *Geoscientific Model Development*, vol. 10, July 2017.

[24] E. A. Spiegel and G. Veronis, "On the Boussinesq Approximation for a Compressible Fluid.," *The Astrophysical Journal*, vol. 131, p. 442, Mar. 1960.

[25] J. Pedlosky, *Geophysical Fluid Dynamics*. Springer-Verlag, 1987.

[26] K. Bryan, "A Numerical Method for the Study of the Circulation of the World Ocean," *Journal of Computational Physics*, p. 16, 1969.

[27] A. B. Kara, A. J. Wallcraft, E. J. Metzger, H. E. Hurlburt, and C. W. Fairall, "Wind Stress Drag Coefficient over the Global Ocean," *Journal of Climate*, vol. 20, pp. 5856–5864, Dec. 2007.

[28] J. Wu, "Wind stress and surface roughness at air-sea interface," *Journal of Geophysical Research (1896-1977)*, vol. 74, no. 2, pp. 444–455, 1969.

[29] S. D. Smith, "Coefficients for sea surface wind stress, heat flux, and wind profiles as a function of wind speed and temperature," *Journal of Geophysical Research: Oceans*, vol. 93, no. C12, pp. 15467–15472, 1988.

[30] V. Zhurbas, G. Väli, M. Golenko, and V. Paka, "Variability of bottom friction velocity along the inflow water pathway in the Baltic Sea," *Journal of Marine Systems*, vol. 184, pp. 50–58, Aug. 2018.

[31] A. Guha and G. A. Lawrence, "Estuary Classification Revisited," *Journal of Physical Oceanography*, vol. 43, pp. 1566–1571, Aug. 2013.

[32] W. R. Geyer and P. MacCready, "The Estuarine Circulation," *Annual Review of Fluid Mechanics*, vol. 46, no. 1, pp. 175–197, 2014.

[33] H. Kato and O. M. Phillips, "On the penetration of a turbulent layer into stratified fluid," *Journal of Fluid Mechanics*, vol. 37, pp. 643–655, July 1969.

[34] Q. Han and F. Lin, *Elliptic Partial Differential Equations*. Courant lecture notes in mathematics, Courant Institute of Mathematical Sciences, New York University, 2011.